Universidade do Minho
Escola de Ciências

Carla Sofia da Cunha Ferreira

An environmental approach using niobium supported on zeolites for the catalytic acetalization of glycerol

julho de 2014

An environmental approach using niobium supported on zeolites for the catalytic acetalization of glycerol
Carla Sofia da Cunha Ferreira
UMinho | 2014

Universidade do Minho
Escola de Ciências

Carla Sofia da Cunha Ferreira

An environmental approach using niobium supported on zeolites for the catalytic acetalization of glycerol

Dissertação de Mestrado
Mestrado em Técnicas de Caracterização e Análise Química

Trabalho realizado sob a orientação da
Professora Doutora Isabel Correia Neves
do
Professor Doutor António Maurício Fonseca
e do
Professor Doutor Miguel Bañares

julho de 2014

Nome: Carla Sofia da Cunha Ferreira

Endereço eletrónico: pg21302@alunos.uminho.pt

Título: An environmental approach using niobium supported on zeolites for the catalytic acetalization of glycerol

Orientador(es): Professora Doutora Isabel Correia Neves**,** Professor Doutor António Maurício Fonseca e Professor Doutor Miguel Bañares

Instituições de Acolhimento:

Instituto de Catálisis y Petroleoquímica, CSIC, Madrid

Departamento de Química, DQ, Universidade do Minho

Ano de conclusão: 2014

Designação do Mestrado: Mestrado em Técnicas de Caracterização e Análise Química

Universidade do Minho, ___/___/_____

Assinatura: _____

ACKNOWLEDMENTS

The completion of this work would not be possible without the contribution of the following people or institutions, to which I'm mostly happy to express my sincere thankfulness:

- to my supervisors, Prof. Isabel Correia Neves and Prof. Maurício Fonseca, for the indispensable guidance and support throughout the execution of this work;

- to Prof. Miguel Bañares from the Catalytic Spectroscopy Laboratory, *Instituto de Catálisis y Petroleoquímica*, Madrid, for welcoming me in his workgroup and for the most useful stay provided. From the same institute, special thanks to Vanesa Calvino Casilda for her assistance and contribution to this work;

- A special thanks to all workers I met in *Instituto de Catálisis y Petroleoquímica*, Raquel, Ana, Alba, Maria José, Diego, Arturo, Mario, Chen Hao, Manuel, Nati, Patri, by the way they received and helped me during my stay, and by all the good moments proportionated by this amazing people.

- to Cátia, the best laboratory colleague at the Chemistry Department, University of Minho, for her assistance and collaboration throughout my academic progression;

- to all my friends for their support;

- to my parents, without which my academic raising could not have been possible. My kindest thanks for them for the support and understanding through the good and less good times;

- To my sisters, Inês e Beatriz, by they patience, affection and encouragement provided throughout this journey;

- to Mr Rogério, Mrs Emília, Ana and Pedro by they support, affection and encouragement during my academic raising, without them it couldn't be possible;

- to Tiago, for welcoming me as part of his life, believe in my abilities, his unconditional support, good advices, understanding, patience, help, joy, love and all that he means in my lifetime.

ABSTRACT

Glycerol is produced at a large amount as a by-product or waste stream from biodiesel production. Due to the high growth of biodiesel production, the oversupply of glycerol has become an economic drawback for the development of biofuel itself. Despite of the wide applications of pure glycerol, it is imperative its conversion into value added chemicals.

This work reports the results of the acetalization of glycerol with acetone to give *solketal*, an oxygenated compound useful as chemical and fuel additive for gasoline, diesel and biodiesel over a series of niobium-containing zeolites. NaY, HY, HUSY and HZSM5 were used as the parent zeolites with different amounts of Nb_2O_5 (Nb_x-ZEO, x=5, 10 and 15 wt%), prepared by impregnation method. Selected catalysts were characterized by morphological and structural analyzes: N_2 adsorption isotherms, chemical analysis (ICP-OES), Fourier transform infrared spectroscopy (FTIR), X-ray photoelectron spectroscopy (XPS), X-ray diffraction (XRD), scanning electron microscopy (SEM) and thermogravimetric analysis (TGA). The results obtained in the characterization of the heterogeneous catalysts show that the impregnation of the Nb(V) improve the catalytic properties of the materials. The hydrophilic behavior of the parent zeolites: NaY > HY > HUSY > HZSM5 was verified during the reaction.

The catalysts were evaluated on the acetalization of glycerol with acetone in a batch reactor using a molar ratio 1:2. The influence of type of catalyst, different reaction temperatures (70 ºC, 40 ºC and room temperature) and catalyst amount were investigated in the selected heterogeneous catalysts. The progress of the reaction was monitored following the variation in intensity of characteristic Raman bands and the quantification was performed by gas chromatography analysis. All parent zeolites and series of Nb_x-NaY and Nb_x-HY were not active in the conditions tested. When the reaction is performed with Nb_x-HUSY and Nb_x-HZSM5 catalysts, the results showed good conversion of glycerol into *solketal*. The best results were obtained with 2 wt% of Nb_{15}-HZSM5 catalyst at 70 ºC with 74 % conversion and 98 % selectivity. However, highly efficient conversion of glycerol to *solketal* over the Nbx-HUSY/HZSM5 catalysts could be achieved with 10 % of Nb at 40 ºC with highest selectivity (98 %) with 2 wt% of catalyst, showing that our catalysts can be used in moderate temperatures.

RESUMO

O glicerol é produzido em grande quantidade como subproduto ou resíduo da produção do biodiesel. O elevado aumento da produção de biodiesel, resulta no excesso da oferta de glicerol tornando-se uma desvantagem económica para o desenvolvimento do próprio biocombustível. Apesar das amplas aplicações do glicerol puro, é importante a sua transformação em produtos químicos de valor acrescentado.

Este trabalho apresenta os resultados da acetalização do glicerol com acetona na transformação do *solketal*, um composto oxigenado muito utilizado aditivo para gasolina, diesel e biodiesel, através da utilização de catalisadores funcionalizados com nióbio. NaY, HY, HUSY HZSM5 foram utilizados como suportes para os catalisadores heterogéneos com diferentes quantidades de Nb_2O_5 (Nb_x-ZEO, x = 5, 10 e 15% em peso), preparados pelo método de impregnação. Os catalisadores heterogéneos selecionados foram caracterizados por diferentes análises morfológicas e estruturais: isotérmicas de adsorção de N_2, análise química (ICP-OES), espectroscopia no infravermelho com transformada de Fourier (FTIR), espectroscopia fotoelectrónica de raios-X (XPS), difração de raios-X (XRD), microscopia eletrónica de varrimento (SEM) e análise termogravimétrica (TGA). Os resultados obtidos na caracterização dos catalisadores heterogéneos mostram que a impregnação de Nb(V) melhora as propriedades catalíticas dos suportes. O comportamento hidrofílico dos zeólitos foi estudado durante a reação: NaY> HY> HUSY> HZSM5.

A acetalização de glicerol com acetona, usando uma proporção molar de 1:2, foi realizada num reactor fechado. Os parâmetros reacionais, tipo de catalisador, temperaturas de reação (70 ºC, 40 ºC e temperatura ambiente) e quantidade de catalisador, foram estudados nos catalisadores heterogéneos selecionados. O progresso da reacção foi monitorizado seguindo a variação na intensidade das bandas de Raman características e a quantificação foi realizada por análise de cromatografia em fase gasosa. Os zeólitos NaY, HY e as séries de Nb_x-NaY e Nb_x-HY não apresentaram actividade nas condições testadas. Quando a reação é realizada com os catalisadores Nb_x-HUSY e Nb_x-HZSM5, os resultados apresentaram uma boa conversão do glicerol em *solketal*. Os melhores resultados foram obtidos com o catalisador Nb_{15}-HZSM5 a 70 ºC, com 2% em peso, verificando-se uma conversão de 74 % e 98 % de selectividade. No entanto, a 40 ºC os catalisadores Nb_{10}-HUSY/HZSM5 apresentaram boas conversões do glicerol com alta selectividade (98 %) em *solketal*, demostrando que estes catalisadores podem ser utilizados em condições suaves.

INDEX

ABBREVIATIONS

A – Acetone

BE – Binding energies

BET – Brunauer, Emmet and Teller

BSE – Backscattered electrons

DSC – Differential scanning calorimetry

DTG – Differential thermogravimetry

EDX – Energy dispersive X-ray

EFAL – Extra-framework alumina species

FAU – Three letter code for a faujasite structure

FID – Flame ionization detector

FTIR – Fourier transform infrared spectroscopy

G – Glycerol

G-A – Glycerol-acetone interaction

GC – Gas chromatography

G-G – Glycerol-glycerol interaction

ICP-OES – Inductively coupled plasma optical emission spectroscopy

ICP-OES – Inductively coupled plasma optical emission spectroscopy

IUPAC – International union of pure and applied chemistry

IZA – International zeolite association

MFI – Three letter code for the pentasil family framework

nd – Not defined

S – Solketal

S (%) = S*olketal* selectivity in percentage

SE – Secondary electrons

SEM – Scanning electronic microscopy

STP - Standard temperature and pressure

SUB – Secondary building unit

TGA – Thermogravimetric analysis

USY – Ultrastable Y zeolite

W – Water

X (%) – Conversion of glycerol in percentage

XAS – X-ray absorption spectroscopy

XPS – X-ray Photoelectron Spectroscopy

XRD – X-Ray diffraction

XRF – X-ray fluorescence spectroscopy

Y (%) – S*olketal* yield in percentage

ZEO – Zeolite

ZSM5 – Zeolite socony mobil-five

LIST OF FIGURES

LIST OF TABLES

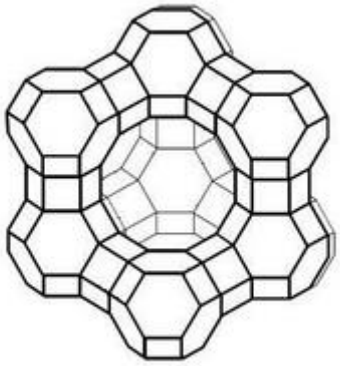

CHAPTER I - INTRODUCTION

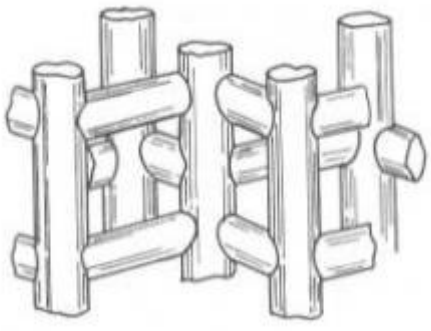

CHAPTER I – INTRODUCTION

Biodiesel production has steadily grown over the past decade. It is a renewable, biodegradable, non-toxic and clean-burning diesel replacement that is reducing the dependence on fossil fuels and improving the environment. This fuel provides more usable energy than the fossil energy needed for its production, reduces greenhouse gases (GHGs) and several major air pollutants, and has minimal impact on human and environmental health [1]. Today, biodiesel is sold in commercial-scale across all countries and actually reache**s** billion gallons of annual production. This production results in the generation of large amounts of glycerol as a byproduct. The use of glycerol as a feedstock for the production of value added chemicals can be attractive to valorize different sources of biomass energy. Condensation of glycerol with aldehydes and ketones to cyclic acetals and ketals, respectively, is often considered one of the most promising glycerol applications for fuels/chemical intermediates [2, 3].

In order to make the ketalization environmentally friendly, many studies were undertaken mostly in batch reactors using heterogeneous catalysts such as zeolites [4], montmorillonite [5] silica [6], amberlyst [7], and nafion [8]. In recent studies, zeolites have gained much interest as catalysts for glycerol acetalization into *solketal* and have been referred as a low-cost and environmental friendly solid acid catalysts [3]. *Solketal* is a ketal obtained from glycerol and acetone reaction, used as a solvent and plasticizer or as suspension agent in pharmaceutical preparations [9]. It can be also used as a fuel additive, surfactant and flavoring agent. Thus, the transformation of glycerol by acetalization into *solketal* is an important and developing area of research.

The main objective of this work is the development of efficient and stable catalysts for glycerol acetalization using zeolites as supports. The work started with the assessment of different zeolite structures modified with niobium pentoxide by the impregnation method. Niobium pentoxide is an interesting compound used in the modification of solid materials due to its high acidity and water tolerant properties which makes it useful in the processes of acid catalysis and adsorption where activity, stability, and selectivity depend on the characteristics of both acidic and metallic sites, and pore size. Subsequently, the preparation method and the catalysts formulation were optimized. Y and ZSM5 zeolites were assessed as supports. Several niobium metal oxide catalysts supported on zeolites with 5, 10 and 15 % of metal were studied and characterized. Different techniques of

characterization as N_2 adsorption isotherms, chemical analysis (ICP-OES), Fourier transform infrared spectroscopy (FTIR), X-ray photoelectron spectroscopy (XPS), X-ray diffraction (XRD), scanning electron microscopy (SEM) and thermogravimetric analysis (TGA) were used in order to select the best catalysts. The practical feasibility of the process was addressed, evaluating glycerol acetalization by studying the reaction temperature and catalyst amount.

1.1 Outline

The presentation of the different aspects related to the development of this work was divided in five chapters, Figure 1. Chapters I and II will be devoted to the presentation of the fundamental aspects that will enable a better understanding of the work and it will cover all aspects related to the development of experimental work. Chapters III and IV will approach both material characterization and catalytic results, respectively, with discussion of the obtained results. Chapter V will close this thesis and summarizes and integrates the main conclusions withdraw from the work.

Figure 1 presents the division and themes covered in the different chapters.

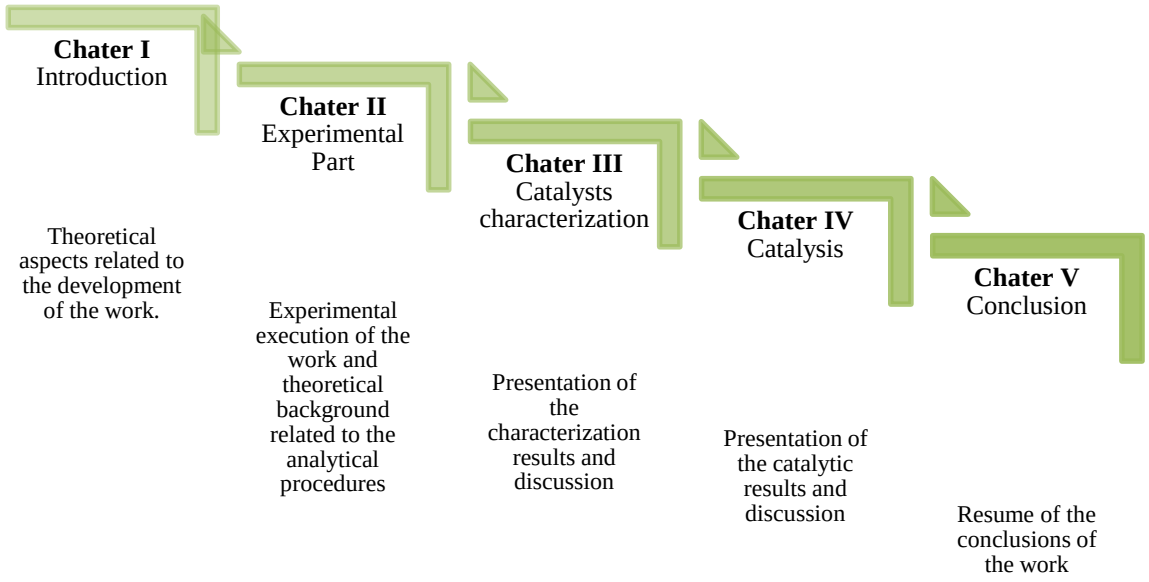

Figure 1: Outline of the thesis.

1.2. Theory and Fundamentals

The first chapter of this thesis presents general considerations about *Biodiesel production*, focusing on the presence of *Glycerol* and its conversion into value added chemicals such as *solketal* by acid catalysts. An overview of the results reported in the literature of the glycerol acetalization is provided. Zeolites FAU (Y) and MFI (ZSM5) were selected as supports in order to obtain selectivity catalysts for glycerol acetalization. A summary of the zeolite structures, properties and methods of preparation as well as their catalytic activity was included. Finally, it is discussed the role of niobium catalyst in glycerol acetalization.

1.2.1. Biodiesel production

Biodiesel became attractive due to its environmental benefits. It is a synthetic diesel-like fuel, chemically defined as a mixture of methyl esters of long-chain fatty acids, produced from a broad variety of biologic resources including recycled cooking oil, vegetable oils and animal fats [10, 11]. With some engine modifications biodiesel can be used directly as a fuel or mixed with petroleum diesel and used in diesel engines with few or no modifications [12-16]. There are also more three main ways for oils and fats have suitable properties for be used as fuel: micro-emulsions, thermal cracking (pyrolysis) and transesterification [17-19]. The most usually method used for converting oil to biodiesel is the transesterification, which can be processed in the presence or absence of a catalyst by using primary or secondary aliphatic monohydric alcohols containing from 1 to 8 carbons [17], Figure 1.1.

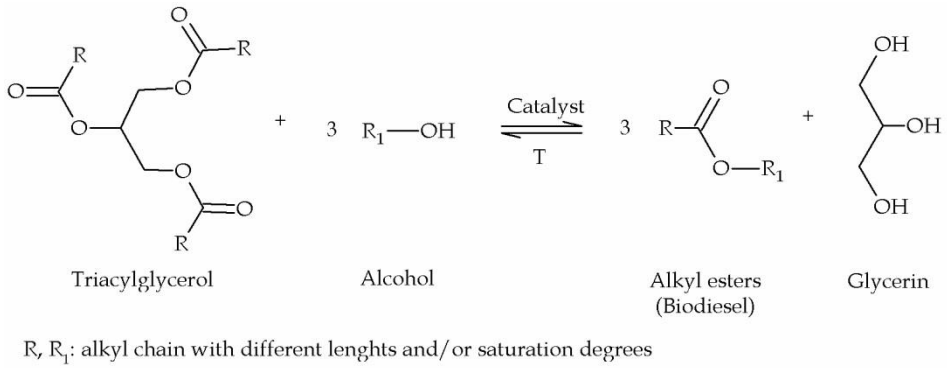

Figure 1.1: Transesterification reaction of biodiesel [17].

Although in theory the reaction is an equilibrium, a bigger amount of monohydric alcohol may be added to displace the equilibrium reaction to the right and consequently produce more methyl esters as a by-product [17]. The monohydric alcohols most commonly used are ethanol, because it comes from agricultural products and is renewable and biologically less polluting to the environment, and methanol because of its low cost and its physical and chemical advantages (polar and short chain alcohol) [20]. Normally, is also used an acid, basic or enzymatic catalyst, to improve the yield rate of the reaction [21-23].

To complete the transesterification stereochemically, it is required a molar ratio of 3 moles of triglycerides to 1 mole of alcohol. Triglyceride is then gradually converted to diglyceride, monoglyceride, and finally to glycerol by releasing one mole of alkyl ester at each step [24], Figure 1.2. In practice, the ratio should be higher to take the equilibrium to a maximum yield of the ester [20].

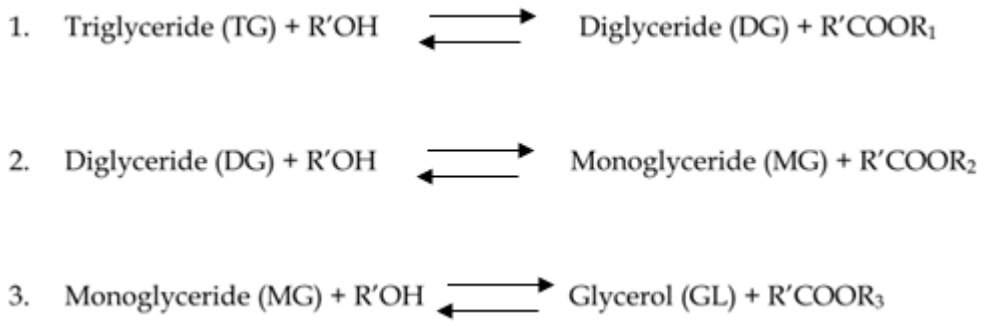

Figure 1.2: Mechanism of transesterification reactions of vegetable oil with alcohol to esters and glycerol [25].

After transesterification step, either biodiesel or glycerol is contaminated with unreacted catalyst, alcohol, oil and other substances that may possibly form during this process. So, as biodiesel is a commercial fuel, it is essential to refine the crude biodiesel and analyze it through sophisticated analytical equipment to ensure that it follows to the international standards [26].

The main disadvantage of biodiesel is its cost, which can be lowered by increasing feedstock yields, developing new technologies, and increasing economic return on glycerol production by finding other uses for this by-product, which, due to oversupply is sold for little value [27]. To have an idea, per 100 Kg of biodiesel are produced 10 Kg of glycerol and is predicted that by 2020 the global production of biodiesel will be 41.9 billion liters,

which means 4.19 billion liters of glycerol produced [28]. So, it is imperative that the glycerol needs to be converted into value added chemicals; otherwise the economic viability of biodiesel is compromised.

1.2.2. Glycerol

Glycerol (propano-1,2,3-triol) is a clear, colorless, viscous and sweet-tasting liquid that belongs to the alcohol family of organic compounds. Derivatives have resulted in a numerous options for use as a sweetening and preserving food, in the manufacture of cosmetics, perfumes, inks, certain glues and cements, as a solvent and it is also present in some medicines [29]. Figure 1.3 illustrates the innumerous traditional and industrial applications of glycerol in percentage. The conversion of glycerol into this value-added chemicals can be done by oxidation processes [30], etherification [31], esterification [32, 33], polymerization [34], transesterification [35], acetylation, etc.

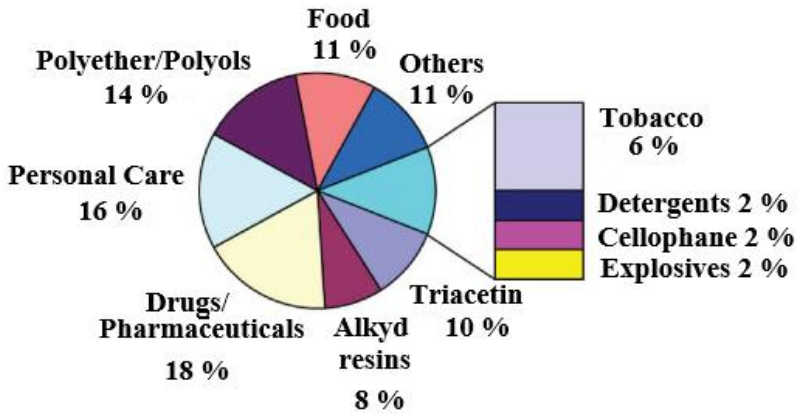

Figure 1.3: Market for glycerol (volumes and industrial uses) [29].

Recently, there has been interest in converting glycerol into *solketal*, an attractive product, useful as an additive for the formulation of gasoline, diesel and biodiesel, which can be also used as a surfactant, a flavoring agent, pharmaceutical intermediate, rapid hemostat and even as a histo-agglutinant [36-42].

1.2.3. Solketal

Glycerol can be acetalized with acetone to yield two structural isomers, (2,2-dimethyl-1,3-dioxolan-4-yl) methanol, usually known as *solketal*, and 2,2-dimethyl-1,3-dioxan-5-ol, producing also water as by-product (Figure 1.4). Theoretical calculations

suggest that the five member ring (*solketal*) is thermodynamically more stable than 2,2-dimethyl-1,3-dioxan-5-ol isomer due to steric repulsions provoked by the presence of the methyl group in axial position of the six member ring [43]. However, other studies suggested that five-membered ring compounds are kinetically favorable and the six-membered ring compounds are favored by thermodynamics [44]. As the equilibrium constant of this reaction is unfavorable, it is required a large amount of acetone to drive the equilibrium to the right [45].

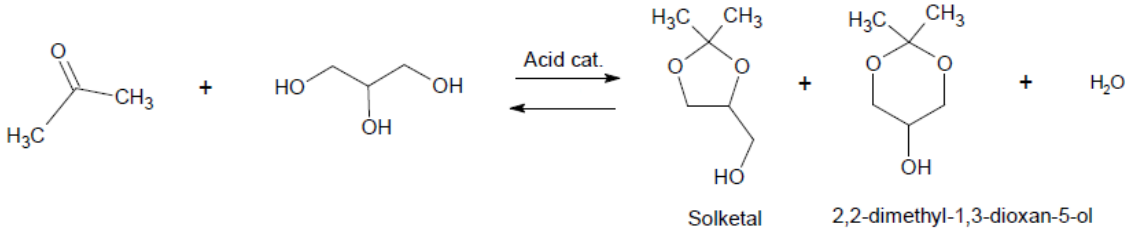

Figure 1.4: Ketalization reaction of glycerol and acetone over acid catalysts [38, 46].

Acetone is widely produced from biomass conversion as well as from the chemical process of cumene cracking, which makes the reaction between two biomass derived products, glycerol and acetone, be advantageous due to its excess and economic value. The main challenges involved in this reaction is the production of water, which has to be removed in order to hinder the reversibility of the reaction, since it weakens the acid strength of the catalyst and favors the reversibility of the reaction [3, 47]. Another difficulty is the reduced miscibility of glycerol with acetone.

Generally, ketalization of glycerol with acetone is performed under batch reactors and catalyzed by strong Brønsted acids such as sulphuric acid, hydrochloric acid, phosphoric acid, hydrofluoric acid or p-toluene sulphonic acid [45, 48-50]. Nevertheless, these processes brought serious problems such as corrosion and catalyst separation from the product stream, hence raising environmental and economic concerns [2]. Some solid acid catalysts also have been reported in the literature, such as amberlyst, heteropolyacids, and others; but they exhibited disadvantages like poor thermal stability, poor regeneration ability, low specific surface area, limited accessibility, inactivity [3, 6, 8, 51-54].

In order to make the ketalization environmentally friendly, it is crucial the development of an effective heterogeneous catalysts and therefore, zeolites may be an excellent choice. Also, the incorporation of metal oxides in zeolite structures can offer several advantages like stability, regenerability and activity. In this work, ketalization of

glycerol with acetone was performed at mild reaction conditions using niobium oxide supported on different zeolites structures as catalysts.

1.3. Catalysts

Catalysts probably provide one of the largest chemical contributions to economic growth and environmental protection. They are substances capable of directing and accelerating thermodynamically possible reactions, without changing its thermodynamic equilibrium and without itself being affected [55, 56]. According to their physical state, catalysts can be divided in heterogeneous and homogeneous catalysts. The type of catalysis reaction which they participate is also divided in the same two categories. In heterogeneous catalysis, the catalyst is in a different phase from the reactants and because of that, it is susceptible to diffusion limitations between bulk reactants and the catalytic active sites on the catalyst surface, requiring efficient mass transfer in order to be comparatively active as the homogeneous counterparts [57]. Its greatest advantages are the easy and inexpensive separation of the products from the catalyst and they are rarely corrosive [56, 58]. In homogeneous catalysis, the catalysts are usually more active, since the limitation of mass transfer by diffusion is favorable for catalysts and reactants that are dispersed on the same phase [57].

During a catalysis reaction, the catalyst combines with the reactants to generate intermediate compounds, facilitating its transformation into products. Usually, the intermediary is highly reactive and therefore, is difficult to detect. At the end of the reaction, occurs the catalyst regeneration, which remained chemically unchanged and with exactly the same amount of catalyst as in the beginning. The catalyst can be reused in a new catalytic cycle [55].

This catalyst effect is purely kinetic since the catalysts lower the activation energy barrier between reactants and products without affecting the Gibbs free energy of the total reaction [59]. Thus, less free energy is required to reach the transition state and form the intended product. However, some catalysts may act as inhibitors or poisons, reducing the reactions speed.

Apart from accelerating reactions, catalysts also have the ability to affect the selectivity of chemical reactions, reacting with only one substance or a small set of substances to enhance the creation of its product [51]. When more than one reaction is possible, different products can be obtained from a given starting material using different

catalytic systems [55]. Therefore, it is necessary, for example, modify the catalyst structure and make it selectivity to a particular substance that will lead the reaction to the desired product. For be a suitable catalyst for an industrial process, it needs to be also stable in the current conditions because the chemical, thermal, and mechanical stability may be affected by many factors (decomposition, coking, poisoning, etc.) during the reaction. The deactivation of a catalyst shall be followed by measuring its activity or selectivity as a function of time [55]. The total catalyst lifetime is essential for the economics of a process [55].

Different zeolite structures present these necessary catalyst features and the possibility to be modified in order to improve them.

1.3.1. Zeolites

The zeolites, are an aluminosilicate classes of heterogeneous catalysts that have been the subject of remarkable interest for the chemical and petrochemical industries, because they exhibit unique characteristics such as high adsorption capacity, intrinsic acidity, high surface area, high stability (hydro) thermal and high selectivity, which allows control over the type of molecules that can diffuse through the crystal framework and reach the active sites of the zeolite [43-45]. Besides, zeolites are also well known as environmentally friendly catalysts and are not expensive as material.

The history of zeolite started in 1756 by a Swedish mineralogist named Axel Fredrick Crønsted, the first scientist to describe the peculiar frothing characteristic of zeolites when heated in a blow-pipe flame [60]. When he heated a mineral ‘stilbite’ (natural zeolite), he observed that it released water so vigorously that it appears being boiling. That way, it was used the combination of the Greek words *Zeo* ("boiling") and *Lithos* (stone or rock) to give the designation of zeolite [61].

Others natural zeolites such as analcime, clinoptilolite, erionite, heulandite, laumontite and mordenite having valuable properties as sorbents and catalysts were then discovered. However, they often had faults and irregularities in their structures that limit their application [62]. So, it began the era of the synthetic zeolites, which allowed an adjustment of their properties, such as size and composition.

These facts led to discover of zeolites A, X and Y and its applications in three domains: adsorption, catalysis and ion exchange. Later, it was also found that organic “templates” could be used to make new zeolite structures, such as ZSM-5 (from

tetrapropylammonum ion), among others [62]. In this contest, over 200 different framework structures have been synthesized number that may increase within a nearly future.

Zeolites are crystalline solids which have a well-defined structure, as well as pores and channels of molecular dimensions that allow hosting selectively active compounds. Its elemental units, SiO_4 and AlO_4, are linked to each other by sharing an oxygen atom at their vertices, resulting in a inorganic macromolecule structure with a three dimensional tetrahedral framework [63], Figure 1.5. Each atom of Si and Al, are generally referred to as T-atoms.

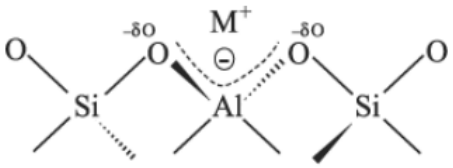

Figure 1.5: Three dimensional tetrahedral framework in crystalline structure of zeolites [64].

Löwenstein rules avoids adjacent aluminum atoms (prohibiting Al-O-Al bonds), so primary building units of zeolites can be arranged to yield Si-O-Si and Si-O-Al moieties [65]. For all zeolite topologies these primary arrangements of T atoms are the same, being possible construct different zeolite topologies by assembling different geometric arrangements of SiO_4 and AlO_4 tetrahedra, the so called 'Secundary Building Units' (SBU). In Figure 1.6, a group of SBU's which are common to various types of zeolite structures is presented.

The junction of these SBU's, gives rise to different zeolites that can have entrances to the cavities formed by 6-, 8-, 10-, and 12-ring apertures (small-, medium-, and wide pore zeolites). The International Zeolite Association (IZA), is the association responsible for listing these arrangements and regulates and assigns a classification for known zeolitic structures, whose authority is recognized by International Union of Pure and Applied Chemistry (IUPAC).

The presence of AlO_4 tetrahedra in the zeolite framework, leads to the formations of a negative charge on the oxygen atoms surrounding the lattice Al ion (Figure 1.5). As zeolites framework contains micropores with dimensions between 0.2 to 1.0 nm, allow the

passage of water molecules and small cations to compensate the negative charge [63, 66]. This water presented in the zeolites porous, can be removed by heating treatment [67].

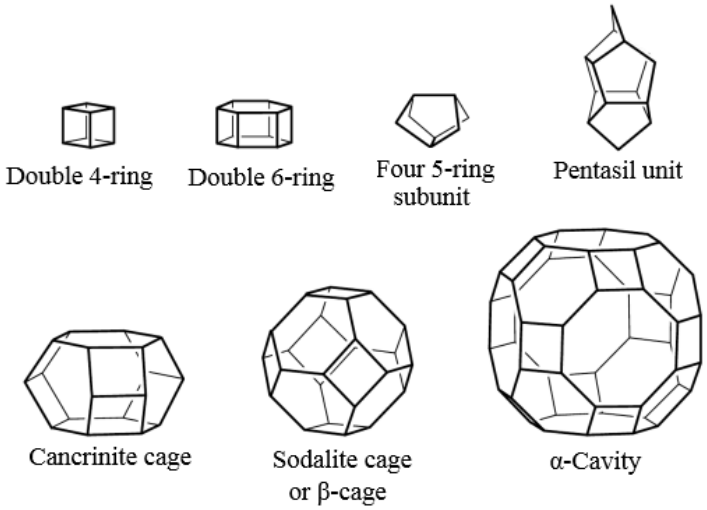

Figure 1.6: Structures of some SBU's [68].

Once the empty space left by the molecules of water is available, the adsorption of other molecules can occur [69]. Alkaline metals, alkaline-earth or transition metals are the cations which can be introduced to compensate the charge deficit. Regards the size of the micropores, it not only limits the diffusion of compounds within those pores, but also limit the size of molecules that can be catalyzed [66].

The typical chemical composition of the zeolite crystal framework has the empirical formula, equation 1:

$$A_{y/m}^{m+}\left[(SiO_2)_x \,.\, (AlO_2^-)_y\right] . zH_2O \qquad (1)$$

where ***y*** varies from 2 to ∞, ***m*** represents the cation valence of **A** cation and ***z*** corresponds to the number of water molecules confined in the voids of the zeolite per structural unit. (x + y) is the tetrahedra number per unit crystallographic cell and x/y ratio is called silicon/aluminum proportion. The minimum ratio value of Si/Al is 1, i.e., this is the limiting case in which all the SiO_4 tetrahedra are individually connected to the AlO_4-tetrahedra, don't existing a maximum limit for the Si/Al value [67, 70, 71]. The higher this ratio (Si/Al), the higher is the strength of the acid sites on zeolite.

1.3.2. Zeolites properties

Zeolites are constituted by tridimensional networks of well-defined micropores that can act as reaction channels whose activity and selectivity will be enhanced by introducing active sites [72]. The existence of strong electric fields and controllable adsorption properties within the pores will produce an exceptional type of catalyst, which can be considered as a catalytic micro-reactor [72]. Summarizing, zeolites are solid catalysts with the following peculiar properties [72]:

(i) High surface area.
(ii) Molecular dimensions of the pores.
(iii) High adsorption capacity.
(iv) Partitioning of reactant/products.
(v) Possibility of the creation of active sites, whose strength and concentration can be controlled according to the desired application, *i.e*. it is possible modulate the electronic properties of the active sites.
(vi) Possibility for pre-activating the molecules when in the pores by strong electric fields and molecular confinement.

Moreover, zeolites are 'molecular sieves', allowing the selective adsorption of molecules and ions with equal or smaller in size than the pore opening (shape selectivity) [61]. The accessibility of the pores for molecules is also subject to certain geometric or steric restrictions [55]. In addition to selectivity, the pores shape of the zeolites also determines both speed and stability of the reactions [61, 73].

1.3.3. Zeolites acidity

Zeolites may be used in many reactions as acid, basic, acid-basic, redox and bifunctional catalysts. To describe the acidity of zeolites in an adequate manner, it is essential to clearly distinguish the nature of the acid site, *i. e*., Brönsted or Lewis acid sites [63]. Brønsted acid sites are generated on the surfaces of zeolites when a negative charge is created in the framework (due to Si^{4+} replacement by a trivalent metal cation such as, for instance, Al^{3+}), which can be compensated by positively charged ions (Figure 1.7).

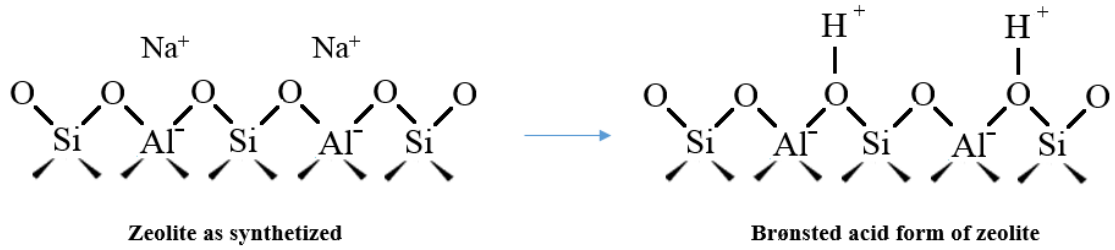

Figure 1.7: Representation of a Brønsted acid site [56].

Usually, synthesized zeolites have Na^+ ions balancing the framework charges, but these can be readily exchanged for protons. An easy way to obtain the zeolite in acid form is realizing a treatment with ammonium salts followed by calcination at higher temperatures to decompose the NH_4^+ ions in NH_3 and H^+, without changing the zeolitic structure. The protons are attached to the oxygen atoms forming OH^- groups. Thus, the active sites formed are known as Brønsted acid sites, and the zeolite has the ability to donate protons to an adsorbed reactant.

Further heating, above approximately 500 ºC, water is removed from the Brønsted acid site, converting it into Lewis acid site by exposing a threefold coordinated Al ion, which has electron-pair acceptor properties [56] (Figure 1.8).

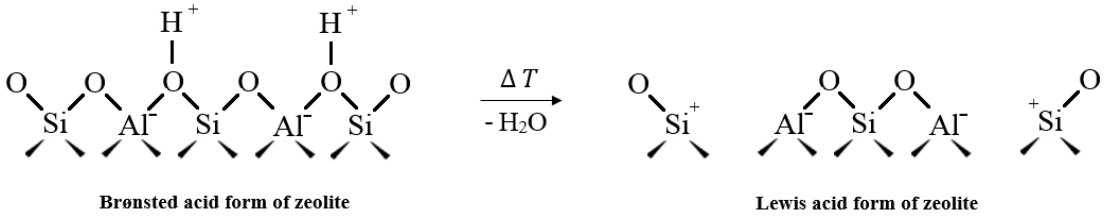

Figure 1.8: Formation of a Lewis acid site via dehydroxylation of two Brønsted acid sites by heating [56].

Depending on the method of zeolite preparation, the surfaces of zeolites can exhibit either Brønsted or Lewis acid sites but also the combination of the two forms. Under specific conditions, Lewis acid sites might enhance the strength of nearby Brønsted acid sites, thereby exerting an indirect influence on the catalytic activity [74]. The strength of the acid sites is directly related to the framework composition of the zeolite, since the strongest acid sites are exhibited by zeolites with the higher Si/Al ratio, *i.e.*, by high-silica zeolites such as ZSM5, for example [56]. It was discovered that the acid strength depends on the number of Al atoms that are adjacent to a silanol group (Si–O–H). So, as the Al

distribution is nonuniform, a wide range of acid strengths results [55]. However, as the ion-exchange capacity is related with the Al^{3+} content of the zeolites, those with lower Si/Al ratios have higher concentrations of active centers and consequently, high concentrations of protons [55]. Zeolites with high content of protons are hydrophilic and have great affinity for small molecules that can enter within the pores [55].

Thus, two different zeolitic structures with different Al^{3+} content, one that belongs to faujasite family (FAU), the zeolite Y, and another from pentasil family (MFI), the zeolite socony mobil-five (ZSM-5), were used and study in the acetalization reaction.

1.3.4. Zeolite Y

Zeolite Y is an aluminosilicate with a FAU framework structure type ($|Ca, Mg, Na_2)_{29}\,(H_2O)_{240}|[Al_{58}\,Si_{134}\,O_{384}]$) with 192 T-atoms per cell unit, that presents pores of 0.74 nm diameter with a well-defined topology (Figure 1.9). In the following figure is also possible to identify two different SUB's interconnected by hydrogen bridges: sodalite cages, which are arranged to form 8 supercages large enough to accommodate guest molecules with 1.30 nm diameter, and hexagonal prisms (Double 6-ring). The resulting cavity is a 12-ring aperture.

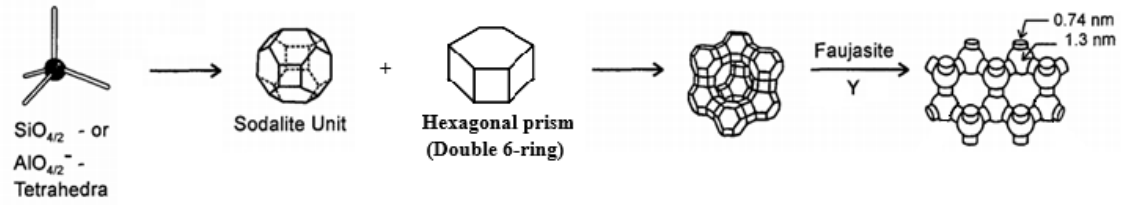

Figure 1.9: The structure of faujasite or Y zeolite showing the sodalite cages and the hexagonal prism interconnection and it micropore system and dimension [63].

To compensate the negative charge carried by Si-O-Al units, exchangeable cations such as Na^+, K^+ and Mg^{2+} can be introduced. These positive ions are rather loosely fixed at their cationic positions located in three discrete positions of zeolite framework: in the hexagonal prism faces between the sodalite units (site I), in the sodalite cages in the open of hexagonal faces (site II)) and on the walls of the supercage (site III) [75, 76], Figure 1.10. This location is dependent not only on the type of cation, as well as on the loading and the hydration state [76]. The charge compensation can also be provide by protons rendering the zeolite strongly acidic [76]. This cations can then readily be displaced via

contact solution or via other chemical treatments, making this structure useful in catalytic applications.

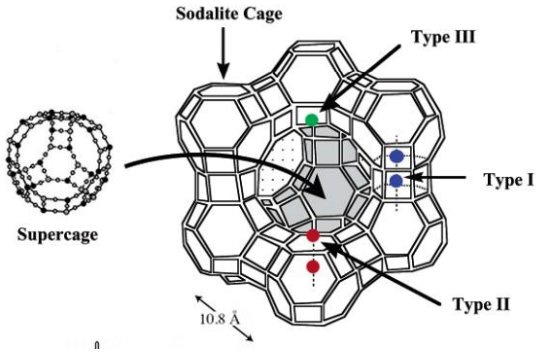

Figure 1.10: The cations positions identified as Types I, II, and III in the zeolite supercage [77].

Si/Al ratio of this zeolite framework is between 2.4 and 3, which makes this structure an ideal system for adsorption applications, ion exchange and catalysis. However, this low ratio confers weak acidity and low hydrothermal stability since a high density of Al substitutions at next-nearest neighbor positions leads to a strong increase of the negative zeolite charge, which results in strong binding of the protons (lower acidity) and greater susceptibility of the zeolite framework to hydrolysis [78, 79]. This acidity, can be strengthen by the introduction of H^+ protons in Y framework or by its transformation in ultrastable Y (USY) zeolites, which usually exhibit much higher acidity compared to the parent low-silica zeolite as well as higher thermal and chemical stability [76, 80].

In catalytic applications it is also advantageous to incorporate metal cations into the zeolite framework, to modify the number and nature of the acid sites and also to affect the diffusion of reactants and products [81].

1.3.5. Zeolite ZSM-5

ZSM-5 is a medium-pore zeolite that belongs to the silicon-rich zeolites. Its empirical formula is $Na_nAl_nSi_{96-n}O_{192}.16H_2O$. The substitution of an aluminum ion (charge 3^+) for a silicon ion (charge 4^+) requires the additional presence of a proton, which gives the zeolite a high level of acidity enhancing its activity.

ZSM-5 and its all-silica analogue silicalite-1 ($n_{Si}/n_{Al} = \infty$) are a highly porous material composed of 5-rings as secondary building units and throughout its structure it has an intersecting two-dimensional pore structure. ZSM-5 has two types of pores, both formed

by 10-membered oxygen rings (Figure 1.11). The first of these pores is straight and elliptical in cross section (0.55 x 0.51 nm), the second pores intersect the straight pores at right angles, in a zig-zag pattern and are circular in cross section (0.56 x 0.53 Å) [82, 83]. This unique two-dimensional pore structure allows a molecule to move from one point in the catalyst to another in the particle.

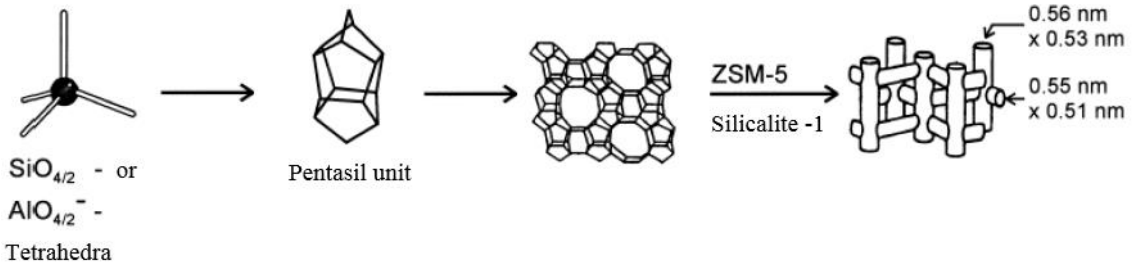

Figure 1.11: The structure of ZSM-5 zeolite showing the pentasil units and its micropore system and dimension [63].

ZSM-5 is another example of a zeolite which has gained enormous importance in heterogeneous catalysis due to its pore structure, high stability and high acid strength that derive from the high Si/Al ratio, which makes ZSM-5 a highly active and shape selective catalyst very useful in chemical industry [84].

The behavior and properties of zeolites as catalysts can also be improved by inclusion of metal species in their structure by modifications.

1.3.6. Zeolite modifications

In order to enhance the catalytic activity and selectivity of zeolites, different metals can be incorporate into the structure. In those cases, the zeolite support works as an active phase dispersed on a carrier [85-88]. The most common preparation methods are ion-exchange, adsorption, deposition-precipitation and impregnation [87, 89-93].

Ion exchange - This method consists of replacing ion in an electrostatic interaction with the surface of a support by another ion species [87, 91]. The support containing ions A is plunged into an excess volume (compared to the pore volume) of a solution containing ions B [94]. Ions B gradually penetrate into the pore space of the support, while ions A pass into the solution, until equilibrium is established corresponding to a given distribution of the two ions between the solid and the solution [91, 94].

In case of zeolites, they are low cost ion exchangers with particular properties that result from the presence of positively charged exchangeable ions, and using a proper salt solution, for example, it is possible to prepare the acid form of zeolite by exchanging NH_4^+ for Na^+ [95]. Due to its net negative charge, zeolites have a strong affinity for transition metal cations and might be easily replaced by them, however it presents much lower affinity for anions.

Adsorption **–** Process that allows the controlled anchorage of a precursor (in an aqueous solution) on the support, where ionic species from aqueous solutions are attracted electrostatically by charged sites on a solid surface [91, 92]. This process is ideal for most of oxide supports, since when they are placed in an aqueous solution, develop a pH-dependent surface charge. Its surface charge will depend on its isoelectric point, pH and ionic strength of the solution [94].

Deposition–precipitation **–** It is a relatively easy method that presents as advantage the fact of an insoluble metal salt that is deposited on the support can no longer move during a drying step [96]. Deposition-precipitation involves two processes: precipitation from bulk solutions or from pore fluids, and interaction with the support surface [94]. The first process consists in dissolve a metal salt with a good solubility in a well-mixed vessel, together with the catalyst support, and then to slowly add a second salt, which causes the precipitation of the first salt [96]. The precipitate is then deposited exclusively (adsorbed) onto the support [97]. To obtain an uniform precipitation, it should be use the hydrolysis of urea as a source of OH^-, since the urea dissolves in water and decomposes slowly at *ca*. 90 ºC, giving a uniform concentration of OH^- in both the bulk and pore solutions [94]. Thus the precipitation occurs evenly over the support surface.

Impregnation - The simplest way to deposit a metal ion on a support is by impregnation, whereby a certain volume of solution containing the precursor of the active phase is contacted with the solid support, which, in a subsequent step, is dried to remove the imbibed solvent [87, 94, 97]. After this process the activation of the catalyst is done by calcination, reduction or other appropriate treatment [87].

Two methods of contacting may be distinguished, depending on the volume of solution, wet impregnation and incipient wetness impregnation. In wet impregnation an

excess of solution is used for a certain time, then the solid is recovered by filtration and the excess solvent is removed by drying [87, 94, 98]. Although the mixing is improved in this method, the metal which does not strongly interact with support is wasted and because of that, the metal loading must be measured. In incipient wetness impregnation, the volume of the solution was added to the support contains a precise metal loading and is equal or slightly less than the pore volume of the support [94, 98]. The metal concentration might be adjusted for the desired weight loading, which is only limited by the solubility of the precursor in the solution. The disadvantages from the incipient wetness impregnation arise when metal precursors do not interact strongly with the support surface because metal ions that remain in solution can migrate significantly during drying, resulting in a poorer distribution of the precursor [98]. However, the simple way of catalysts preparation by this method and the success reported by many authors, make the incipient wetness impregnation method an excellent choice to prepare the selected zeolite structures with different amount of niobium oxide studied in the current work.

Recent studies show the applications of niobium-based systems as a catalyst in the transformation of the glycerol in different reactions: acetalization [99], dehydration [100], etherification [101], esterification [102], hydrogenolysis [103], condensation [104] and oxidation [105]. All these reactions aims to convert the glycerol into different value-added chemicals such as polyglycerols and polyglycerol-esters that can be used as new materials for surfactants, lubricants, cosmetics and food additives [106]; acrolein used in a wide range of chemical materials such as acrylic acid, methionine, high absorbable polymers and detergents [100, 107]; acrylic acid used in polymer dispersions, adhesives, fibers, plastics, and other chemical intermediates [105] and *solketal* used as a solvent and plasticizer or as suspension agent in pharmaceutical preparations [108].

Therefore, Nb_2O_5 was impregnated in zeolite structures to improve its catalytic activity and it was tested in glycerol conversion into *solketal*.

1.3.7. Modified zeolites with Niobium

Niobium is estimated to be one of the most common elements in the Earth's crust, with 20 ppm, what makes it an optimum metal to be used in diverse applications due to its greater availability and its lower price [109]. Its most characteristic and stable oxidation state is +5, although it presents more oxidation states in an extension that goes from +5 to -1 [110]. Therefore, materials containing niobium have broad relevance in heterogeneous

catalysis, where they are used as catalyst components or are added in small amounts to catalysts [109].

These catalysts exhibit special properties not revealed by others transition metal catalysts, even by those compounds of neighboring elements of niobium in the periodic table (V, Zr, Mo). Some of these properties, such as stability and strong metal support interaction are of utmost importance for a good quality catalyst [111]. Others characteristic features of niobium compounds are the promoter effect, the support effect and its acidic property. Niobium oxides extraordinarily enhance catalytic activity and prolong catalyst life when the small amounts are added to known catalysts [112, 113]. When it is used hydrated niobium pentoxide, $Nb_2O_5 \cdot nH_2O$, which is usually entitled niobic acid, its surface acid strength, corresponds to the acid strength (H_o ~< -5.6) of 70% sulfuric acid and exhibits high catalytic activity, selectivity and stability for acid-catalyzed reactions in which water molecules participate or are liberated [113].

The selected solid support for proper dispersion of the active species of Nb used in this study, were the zeolites Y-type and ZSM-5, which can combine with those properties due to the high surface area and pore (size and distribution) system extremely needed for this type of material reach an acceptable activity [87]. To provide more acidity to the selected support, it was used an aqueous impregnation of ammonium niobium oxalate, with Nb^{5+} as charge compensation cations, to be impregnated on the zeolites.

In the present work, we have evaluated the catalytic properties of Nb_x-NaY, Nb_x-HY, Nb_x-HUSY and Nb_x-HZSM5 catalysts, where x represents the different amount of Nb in the zeolites.

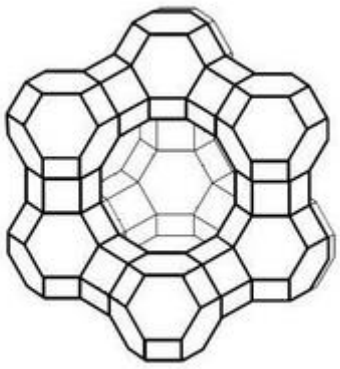

CHAPTER II –EXPERIMENTAL PART

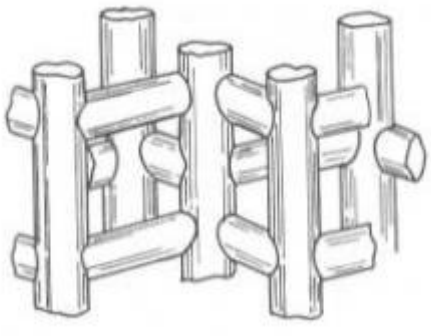

CHAPTER II – EXPERIMENTAL PART

This chapter covers all aspects and details related to the execution of the experimental work. Especially emphasis will be done in the description of the techniques used in the studies for the catalyst characterization and the evaluation of the catalytic behavior of the catalysts based in zeolites.

2.1. Materials and reagents

The zeolites were obtained from Zeolyst International in powder form. The zeolites (NH_4)USY (ultrastabilized Y, CBV 500) and (NH_4)ZSM5 (CBV 3024E) were available in the ammonium form. The other zeolites were available in the proton form for HY (CBV 400) and sodium form for NaY (CBV 100). These zeolites were used on the impregnation of niobium metal. The other reagents used in the experimental work, the ammonium niobate (V) oxalate hydrate ($C_4H_2NNbO_9.H_2O$), glycerol ($C_3H_8O_3$), acetone (C_3H_6O) and *solketal* ($C_6H_{12}O_3$, [(S-) (+) 1, 2-isopropylideneglycerol, 99 wt.%]) were supplier by Sigma Aldrich. All reagents were used without any additional purification method. *Solketal* was used as a calibration standard for GC and Raman analysis.

2.2. Catalysts preparation

A series of niobium-containing zeolites were synthesized by impregnation method as described in detail elsewhere [114]. The impregnation and subsequent calcinations were repeated on time for each parent zeolite using the same experimental conditions. Aqueous solutions of ammonium oxalate complex of niobium(V) with a ratio 10 mL/g_{zeo} were used to incorporate the different amounts of Nb_2O_5 on the support (5, 10 and 15 wt%). The resulting suspensions were stirred during 3 h at room temperature. The suspensions were dried in air at 60 ºC and then calcined at 500 ºC during 4 h under a dry air stream (50 mL/min). In the samples with (NH_4)USY and (NH_4)ZSM5 after calcination, the ammonium present was transformed in NH_3 and H^+. NH_3 desorbs and the presence of the protons increases the number of acid sites. The obtained samples were identified as Nb_x-ZEO, where x represent the amount of Nb in the zeolites. Table 2.1 presents the experimental conditions and the nomenclature used for the Nb_x-ZEO samples prepared.

Table 2.1: Nb_x-ZEO samples prepared by impregnation method.

Zeolite	$mMoles_{complex}$[a]	Nb_2O_5 (%)	Nomenclature
NaY	2.83	5	Nb_5-NaY
HY			Nb_5-HY
(NH_4)USY			Nb_5-HUSY
(NH_4)ZSM5			Nb_5-HZSM5
NaY	5.98	10	Nb_{10}-NaY
HY			Nb_{10}-HY
(NH_4)USY			Nb_{10}-HUSY
(NH_4)ZSM5			Nb_{10}-HZSM5
NaY	9.71	15	Nb_{15}-NaY
HY			Nb_{15}-HY
(NH_4)USY			Nb_{15}-HUSY
(NH_4)ZSM5			Nb_{15}-HZSM5

[a]mmoles of ammonium oxalate complex of niobium(V)

2.3. Catalytic reaction

The catalysts were evaluated by the ketalization of glycerol with acetone in liquid phase. The reaction was carried out in a 10 mL round-bottom flask as semi-batch reactor with magnetic stirring. The temperature was measured with a thermometer (±1 ^oC) inserted in the reactor. Before each catalytic run, the catalyst was placed in an oven (SELECTA P) at 220 ºC for 2 h in order to remove the water and activate their catalytic centers. In all catalytic runs, predetermined amounts of reactants (0.08 moles, 4.68 g of acetone and 0.04 moles, 3.64 g of glycerol) were loaded into the reactor using an acetone/glycerol molar ratio 2.1 before the addition of the catalyst. The experimental conditions as reaction temperature and amount of the catalyst were adjusted throughout the work. The reactor was heated under stirring at 1250 rpm in an oil bath to do the desired reaction at 70 ºC, 40 ºC and room temperature. The amount of catalyst used was 1, 2 and 5 % of the initial amount of glycerol. The reactions were allowed to run for 3, 4 and 6 h, depending on which temperature the reaction was tested, and always continuously monitored by Raman spectroscopy. Samples of the reaction mixture were also withdrawn at fixed time intervals

and analyzed by gas chromatography. Figure 2.1 present the batch reactor used in the catalytic studies.

Figure 2.1: Equipment used for the catalytic studies.

2.4. Analytical techniques

The catalysts were characterized by N_2 adsorption isotherms, elemental chemical analyses (ICP-OES), Fourier transform infrared spectroscopy (FTIR), X-ray photoelectron spectroscopy (XPS), X-ray diffraction (XRD), scanning electron microscopy (SEM) and thermogravimetric analysis (TGA). The catalytic behaviour of the catalysts tested was monitored by Raman spectroscopy and analyzed by gas chromatography (GC).

2.4.1. N_2 adsorption isotherms

- **General description**

The specific surface area is determined by physical adsorption of a gas molecules on the surface of the solid, calculating the amount of the adsorbate gas bound by relatively weak forces (van der Waals forces) to a monomolecular layer on the surface [115]. As the adsorbate gas usually used is the nitrogen, the analysis is carried out at the temperature of

liquid nitrogen. The amount of nitrogen adsorbed can be then measured by volumetric or continuous flow procedure.

BET analysis, based on BET model proposed by Brunauer, Emmet and Teller in 1938, provides external area and pore area evaluations in order to determine the total specific surface area (m^2/g) of the material. This data is important information in studying the effects of surface porosity and particle size in many applications [116].

However, this method shows an inability to accurately measure the true surface area of microporous materials but it is easy to apply and is widely accepted [115]. The data obtained are treated according to the BET adsorption isotherm equation (2):

$$\frac{1}{\left[Va\left(\frac{P_0}{P}-1\right)\right]} = \frac{C-1}{V_m C} \times \frac{P}{P_0} + \frac{1}{V_m C} \qquad (2)$$

where P and P_0 are the equilibrium and the saturation pressure of adsorbate gas at the temperature of adsorption, Va is the volume of gas adsorbed at standard temperature and pressure (STP) [0 ºC and atmospheric pressure (1.013 × 105 Pa)] and V_m is the volume of gas adsorbed at STP needed to produce an apparent monolayer on the sample surface. C is the BET constant describe by the equation 3:

$$C = \frac{E_1 - E_L}{RT} \qquad (3)$$

where E_1 is the heat of adsorption for the first layer, and E_L is for the second and higher layers and is equal to the heat of condensation of the vapor.

The BET equation requires a linear relation, which is represented by $\frac{1}{\left[Va\left(\frac{P_0}{P}-1\right)\right]}$ in function of $\frac{P_0}{P}$. The range of linearity is, however, restricted to a limited part of the isotherm, usually between a $\frac{P_0}{P}$ range of 0.05-0.30. From the resulting linear plot is obtained a slope **α** equal to $\frac{C-1}{V_m C}$ and a constant **i** equal to $\frac{1}{V_m C}$. From these values, V_m is calculated as 1/(α + i), while C is calculated as (α / i) + 1. From the value of V_m so determined, the specific surface area, S_{BET}, in $m^2 \cdot g^{-1}$, is calculated by the equation 4:

$$S_{BET} = \frac{V_m \times N_A \times a}{V \times m} \qquad (4)$$

where N_A, is the Avogadro constant (6,02 x 10^{23}mol^{-1}), a is the area occupied by one nitrogen molecule adsorbed on the monolayer at STP, V is the molar volume of the adsorbate gas and m is the mass of the adsorbent.

The external surface area (S_{ext}) of samples can be obtain by the *t*-method, which takes in account the statistical adsorbed film thickness, t. This method of isotherm data analysis, introduced by de Boer, it assumes that in a certain isotherm region, the micropores are already filled-up and because of that cannot contribute further to the adsorption process [117, 118]. That way, Va, volume of gas adsorbed by mesoporous, is plotted against *t* values. To calculate the *t* parameter is used the equation of Harkins-Jura:

$$t = \left[\frac{13,99}{0,034 - \log(P - P_0)}\right]^{0,5} \quad (5)$$

The intercept of the curve *t* obtained is 0 and the slope V_a/t is equal to the external surface area of the system. It generally gives very good agreement with the surface area deduced from the BET model.

Total and specific pore volume can also be determine using adsorption and desorption techniques and by applying the respective equations. In case of total pore volume, it is derived from the amount of vapour adsorbed at a relative temperature close to unity (assuming pores are filled with liquid adsorbate) and it is given by the following equation:

$$V_{total} = \frac{P_a \times V_a \times V_m}{RT} \quad (6)$$

where V_{total} is the total volume of liquid N_2 in pore, V_a is the volume of gas adsorbed, V_m is the molar volume of liquid adsorbate, P_a is the ambient pressure, T is the ambient temperature and R is the gas constant. The volume of micropores can be also calculated from the *t*-plot method introduced by de Boer and the mesoporous volume by the difference between the total pore volume and microporous volume, equation 7:

$$V_{meso} = V_{total} - V_{micro} \quad (7)$$

❖ **Conditions of analysis**

The surface area of the catalysts and the adsorption/desorption isotherm were determined with a Micromeritics ASAP-2000 analyzer using nitrogen (N_2) as the adsorbate at −196 ˚C. The samples were pre-treated under vacuum at 200 ˚C for 16 h. The surface areas were calculated by applying the BET equation, while external surface areas (S_{ext}) and micropore volume (V_{micro}) were calculated by the *t*-method.

2.4.2. Inductively coupled plasma optical emission spectroscopy (ICP-OES)

❖ **General description**

ICP-OES is one of the most powerful and popular analytical tools for identify and reliably quantify trace elements in a numerous sample types. The technique is based on three general steps: atom formation, excitation, and emission. So, it is applied an electrical energy in the form of spark generated between an electrode and a metal sample, converting the sample solution to an aerosol and directing it into the central channel of the plasma [119]. At its core the inductively coupled plasma (ICP), which promotes an electrically neutral and ionized ambient, sustains a temperature of approximately 10 000 K, vaporizing the aerosol into atoms very quickly and bringing them to a high energy state, the excited state [120]. Once excited, both the atomic and ionic excited state species may then relax to the ground state via the emission of a photon [119, 120]. These photons emit an electromagnetic radiation at characteristic wavelengths of a particular element, creating a unique emission spectrum that allows the identification from which element they were originated. The total number of photons is directly proportional to the concentration of the originating element in the sample [120]. To extract the emission spectrum for the target elements, the emitted light is split by a diffraction grating. Then, equipment detectors (photomultiplier tubes) measure the presence or absence of the spectrum extracted for each element and the intensity of the spectrum to perform qualitative and quantitative analysis of the elements.

In this study, this technique was essential to quantify the amount of Si, Al and Nb present in each catalyst.

❖ **Conditions of analysis**

Metal ion concentrations were determined by Varian Vista ICP-OES and measured with a Perkin Elmer inductively coupled plasma optical emission spectrometer (model Optima 3300 DV), using plasma as the atomization and excitation source. The samples were previously digested, by microwave (ANTON PAAR Multiwave 3000) using a mixture of acids and alcaline fusion (CLAISSE FLUXY).

2.4.3. Fourier Transform Infrared Spectroscopy (FTIR)

❖ **General description**

Infrared spectroscopy is a technique that used the absorption energy in the infrared region of the electromagnetic spectrum which gives information about both rotation and vibration of the molecule. In the middle region ($4000 > \nu > 200$ cm^{-1}) the energies of vibrations and rotations of the molecules provide information for molecular characterization or identification of compounds. Infrared radiation hasn't enough energy to cause electronic transitions, so, when it is absorbed by a material, occurs vibrational transitions followed by a certain number of rotational transitions. As all vibrations of a chemical bond occur at a characteristic frequency, when a compound is irradiated with a radiation of frequency equal to a certain vibration, it will absorb this radiation. This absorption gives raise infrared spectrum characteristic of each molecule since the energy at which any peak appears in spectrum corresponds to the frequency of a vibration of a part of a sample molecule [121].

The structural information obtained from FTIR analysis is useful in case of zeolites characterization because provides information of framework structure, location of sites and cations vibrations, identification of compounds that are introduced or react inside the structure and also about catalytic properties of zeolites [122].

❖ **Conditions of analysis**

Room temperature FTIR spectra of the solid samples were collected on a ABB-FLTA 2000 spectrometer in the range 4000-500 cm^{-1}. In an agate mortar were added 2 mg of material for analysis and 100 mg of dry KBr powder. The mixture was homogenized and the resulting powder was pressed using a press Manfrendi with a weight of 10 tons for

5 min. Spectra were collected by averaging 16 scans at a rate of 41 scans/min with a resolution of 8 cm^{-1}.

2.4.4. X-ray photoelectron spectroscopy (XPS)

❖ General description

X-ray based spectroscopies are useful in determining the chemical composition and the oxidation state of the elements present in the solid materials. These techniques include X-ray absorption spectroscopy (XAS), X-ray fluorescence spectroscopy (XRF), energy dispersive X-ray spectroscopy (EDX), and X-ray photoelectron spectroscopy (XPS). They are mostly based on detecting and analyzing radiation absorbed or emitted from a sample after excitation with X-rays, with the exception that electrons are analyzed in XPS [123].

The technique used a monochromatic X-ray radiation source to focus on the sample and cause the ejection of electrons from atoms. As X-ray radiation is highly energetic, occurs the ejection of electrons from the innermost atomic layers to a higher energy orbital. Additionally, occur the relaxation through displacement of those electrons to fill the vacancy left after ejection, which results in an X-ray fluorescence emission. Ejection of additional electrons from outer orbital may also arise during relaxation, generating the so called Auger effect [124].

Since the binding energy of the electrons from atomic inner layers depend on the environment of the atom and on its chemical state, the ejected electrons possess the binding energy specific to the elements from which they were removed. That way, for each and every element, there will be a characteristic binding energy associated with each core atomic orbital and because of that, each element will give rise to a characteristic set of peaks in the photoelectron spectrum at kinetic energies determined by the photon energy and the respective binding energies. The intensity of the peaks is related to the concentration of the element within the sampled region.

XPS is a powerful technique which provides an elemental analysis of a shallow layer (approx. 20 nm depths for soft X-rays) of the zeolite grain. The information is useful to discover the chemical composition and the different oxidation states of the atoms present on the top layers on a zeolite surface, once the charge of an atom also affects the electronic energy levels.

❖ **Conditions of analysis**

XPS spectra were recorded on a SPECS GmbH spectrometer equipped with a UHV system with a Phoibos 150 9MCD detector. The source X-ray source (Al Monochrome) had a power of 200 W and energy of 12 kV. The samples were previously pressed into a small disc. Casa software has been used for quantification and spectra treatment.

2.4.5. X-ray diffraction (XRD)

❖ **General description**

X-ray diffraction (XRD) is a powerful technique used for the characterization of crystalline materials such as zeolites. When a crystal solid is hit with X-ray radiation, the X-ray beam is diffracted in specific directions with specific angles. In order to measure those angles and intensities, the equipment makes use of a crystallographer to produce a three dimensional image of the electrons within the crystal. The diffraction occurs due to the interference phenomena between the X-ray photons with wavelength comparable to inter-atomic planes on a crystal lattice, and the electrons from the atoms in the crystal lattice. Since a crystalline material presents well-defined planes with a high density of atoms, electronic density will be therefore high. This increases the chance of a merely elastic collision between the X-ray photons and electrons, giving rise to a high density of diffracted photons. From this electron density, it is possible determine the average positions of the atoms in the crystal, their chemical bonds, their disorder, their phase purity and characterize the unit cell geometry [125].

❖ **Conditions of analysis**

X-ray diffraction patterns were recorded by a PANalytical X´Pert Pro diffractometer using a Ni-filtered Cu Kα radiation (I=1.540598 Å). The measurement was carried out at room temperature, in the 2θ angle range from 4º to 90º and a step size 0.0335 º/s.

2.4.6. Scanning electron microscopy (SEM)

❖ **General description**

Scanning Electron Microscopy (SEM) is characterized by its ability to obtain three-dimensional images of the surface of a wide variety of heterogeneous materials in a

nanometer (nm) and micrometer (mM) range. During SEM analysis, a beam of high-energy electrons is focused on a spot volume of the specimen, resulting in an emission of various types of radiation and electrons such as*: backscattered electrons (BSE)*, high-energy electrons that are ejected by an elastic collision of an incident electron, usually with a sample atom's nucleus, that allow distinguish regions with light atoms from regions with heavy atoms in the sample test, thus achieving a topographic contrast and *secondary electrons (SE)*, which result from inelastic collisions between the electrons present in electron clouds of sample atoms and are scattered at lower energies than backscattered electrons, what makes them the main source of detectable electrons in SEM [126, 127].

Through simultaneous analysis of the signals collected by the detectors, the SEM technique allows the characterization of samples in terms of topography (SE and BSE), atomic number (BSE) crystalline properties (BSE), chemical composition (BSE) magnetic field (BSE) and local crystal orientation of the sample (BSE). When the electron beam interact with the sample and removes electrons from the inner orbitals, it occurs the relaxation of the atom with emission of radiation in the X-ray region. The photon wavelength is specific to the element from which the electron is removed, and this is useful for qualitative analysis of a sample. Therefore, the SEM is typically equipped with detectors of energy dispersive (EDX) allowing the three-dimensional images and mapping to determine the distribution of elements on the surface and characterizing the sample in visual and elemental terms [128].

- **Conditions of analysis**

Scanning electron micrographs (SEM) of parent zeolites and catalysts were collected on a Jeol JSM-6010LV Scanning Microscope equipped with an EDX system. In order to avoid surface charging, the samples were previously placed in a carbon tape and coated with a thin layer of gold (5 nm) for 15 min at a pressure of 10^{-5} Tor by using a Polaron SC502 sputter coated. The magnification of 5000x and 15000x were used with an energy beam of 15 kV.

2.4.7. Thermogravimetric analysis (TGA)

- **General description**

Thermogravimetric analysis (TGA) is a thermal technique which allows the evaluation of changes in sample mass in function of temperature, giving information about

material thermal stability and composition. This happens due to the exposure of a sample to high temperatures may cause, for example, a change in its chemical structure and consequently change its physical properties [129].

In addition to weight changes, two auxiliary tools for the thermogravimetric characterization of a material may be used: differential thermogravimetry (DTG) and differential scanning calorimetry (DSC). The first one, DTG, is simply the derivative of sample mass variation in function of temperature and it is very useful for the exact determination of the temperatures at which the maximum rate of mass variation takes place, providing more detailed information about the behavior of the degradation process. The second tool, DSC, can be used to monitor the energy released or absorbed via chemical reactions during the heating process [130].

- **Conditions of analysis**

The thermal stability of the zeolite samples were carried out using a thermal analyzer STA 6000 from PerkinElmer under nitrogen supplied at a constant flow rate of 20 mL/min. All samples were subjected to a 10 °C/min heating rate and were characterized between 25 and 800 °C on aluminum sample cell.

2.4.8. Raman spectroscopy

- **General description**

Raman spectroscopy has proved to be a very powerful characterization technique for obtaining detailed information about molecular structures, since each molecular state possesses a unique vibrational spectrum that is related with the structure [131]. Furthermore, Raman spectroscopy has been also increasingly applied under *in situ* conditions and relevant reaction conditions (operando methodology), creating a new revolution in catalysis science important for accurate molecular understanding of catalytic structure-activity/selectivity relationships [132].

When a sample is hit by monochromatic radiation from the visible to infrared region, it occur absorption and reflection and light-scattering processes. In Rayleigh scattering, the incoming photon excites the scattering matter from its electronic ground state into a virtual state, from which it relaxes under the emission of a Raman scattered photon of smaller or higher energy (Stokes or anti-Stokes scattering) depending on the initial and final vibrational levels [133]. If the emitted energy is lower than incident

radiation energy, is referred as Stokes-scattering. If the emitted energy is higher than the incident energy is referred as Anti-Stokes-Raman scattering. Since the amount of photons scattered by Raman effect is very small, modern Raman spectrometers have employed lasers as light source, which comply the requirements for a monochromatic and highly energetic excitation source, to create an intense excitation light and consequently generate a significant Raman signal. Moreover, lasers can be applied to liquid, gas or solid samples or even suspensions or solutions.

In the present work, Raman spectroscopy was used to follow the reaction between glycerol and acetone in the presence of a catalyst. The study of reactions catalyzed by zeolitic structures using Raman spectroscopy can meet technical difficulties, such as strong background noise which mask Raman signals due to the strong zeolite fluorescence, mainly caused by the presence of organic fluorescent molecules that could be formed inside the framework or the presence of iron (Fe) impurities [134].

- **Conditions of analysis**

All reactions were continuously monitored by Raman spectroscopy with an immersion probe fitted to a Perkin-Elmer Raman Station 400F system using 100 mW of near-infrared 785 nm excitation line. Spectra were acquired continuously; each spectrum consisted of 6 accumulations of 10 s.

2.4.9. Gas chromatography (GC)

- **General description**

Gas-phase chromatography (GC) is a separation technique based on the partition between a mobile gaseous phase carrying the analyte and a stationary phase, which may be solid (gas-solid chromatography) or immobilized liquid (gas-liquid chromatography). Like the others chromatographic techniques, the basic principle in GC is the separation of the components of a sample by their different affinity for the stationary phase.

In gas chromatography, a sample is quickly heated and vaporized at the injection port. Then, it is transported through the column by a chemically inert gas (mobile phase) such as helium or an unreactive gas like nitrogen, which should be chosen depending on type of detector which is used. One of the most frequently employed detectors in GC analysis is the flame ionization detector (FID), which consists of a H_2/air burner fitted with

a collector electrode over the flame, and it is responsible for measure the conductivity of the sample. When organic compounds are pyrolized by the flame, ions are produced, which decreases electrical resistance, allowing electric current to flow through the plasma. This current is detected by the electrode and the amount of ionized species (which in turn is related to their concentration) promotes a linear response.

The signals acquired by the detector are presented as a chromatogram with depicted as detector signal in function of elution time. Owing to the fact that various compounds diffuse through the column at different rates, each component of the mixture shows up as a separate peak and, from the time taken for it to appear, identification can be made and from the size of the peak, concentration can be measure, ensuring both qualitative and quantitative analysis of the sample [135].

❖ Conditions of analysis

The reactions were analyzed by gas chromatography using a Bruker 430-GC equipped with a capillary column (BR-5ms Wcot fused silica, 30 mx0.25 mm) and a flame ionization detector (FID) in order to evaluate the conversion of glycerol and the selectivity of the catalyst, which were calculated using the following equations:

$$\text{Conversion (\%)} = \frac{\text{Moles of glycerol consumed}}{\text{Initial moles of glycerol}} \times 100\% \quad (8)$$

$$\text{Selectivity (\%)} = \frac{\text{Moles of solketal formed}}{\text{Moles of glycerol consumed}} \times 100\% \quad (9)$$

$$\text{Yield (\%)} = \frac{\text{Conversion (\%)} \times \text{Selectivity (\%)}}{100} \quad (10)$$

The oven temperature was maintained at 60 ºC for 1 min, then increased to 250 ºC at a ramp rate of 5 ºC/min and finally the oven temperature was maintained at 250 ºC for 10 minutes. Injector and detector block temperature were maintained at 230 and 300 ºC respectively.

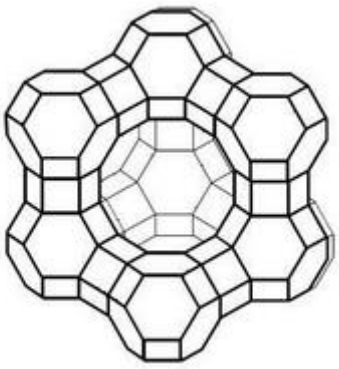

CHAPTER III – CATALYSTS CHARACTERIZATION

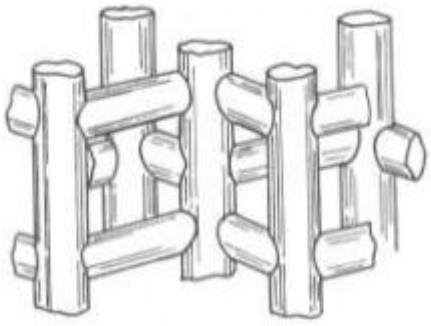

CHAPTER III – CATALYSTS CHARACTERIZATION

This chapter presents the experimental results and related discussion of the preparation and characterization of niobium supported catalysts, obtained through morphological and structural analyzes using different techniques: N_2 adsorption isotherms, X-ray diffraction (XRD), chemical analysis (ICP-OES), Fourier transform infrared spectroscopy (FTIR), X-ray photoelectron spectroscopy (XPS), scanning electron microscopy (SEM) and thermogravimetric analysis (TGA).

3.1. N_2 adsorption isotherms

In order to evaluate the changes induced in the structure of the parent zeolites due to the impregnation of niobium, the porosity volume and surface area were determined by nitrogen adsorption isotherms. The nitrogen adsorption-desorption equilibrium isotherms at -196 ºC for the parent zeolites NaY, HY and HUSY (a) and HZSM5 (b) are illustrated in Figure 3.1. These isotherms represent the relationship between the volumes of adsorbed/desorbed measured with pressure from the surface at constant temperature.

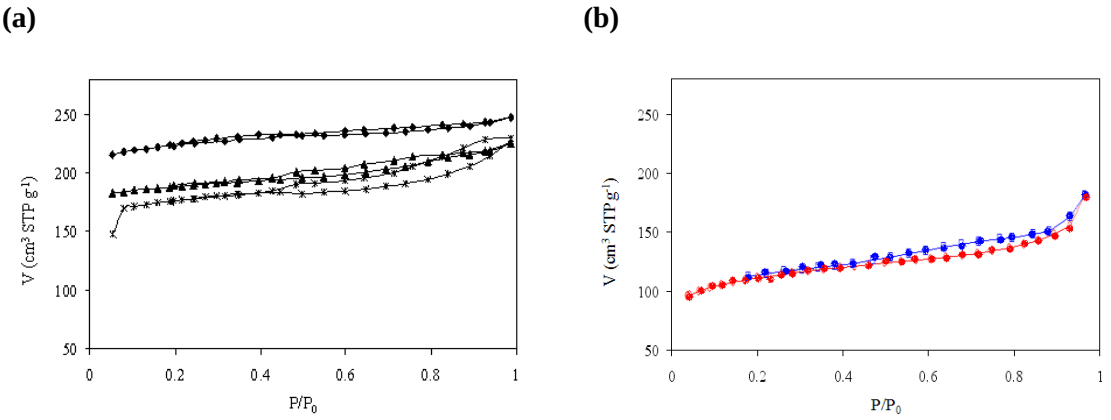

Figure 3.1: Nitrogen adsorption-desorption equilibrium isotherms of the different zeolites at – 196 ºC: (a) (♦) NaY, (▲) HY and (∗) HUSY [136] and (b) HZSM5 [137].

The N_2 adsorption isotherms for all parent zeolites are of type-I isotherm, according to IUPAC classification, which is typical of solids with microporous structure [138]. This type of isotherm is followed by microporous solids having relatively small external surfaces, which the limiting uptake is governed by the accessible micropore volume rather

than by the internal surface area [138]. The shape of both adsorption and desorption isotherms of the zeolites is very similar with each other. However, the existence of an hysteresis loop observed in the isotherms of the zeolites HUSY and HZSM5 suggest that these zeolites has an extended degree of mesoporosity.

The shape of the isotherms was retained after Nb impregnation on all parent zeolites. Figure 3.2 shows the nitrogen adsorption-desorption isotherms of Nb_x-ZEO catalysts.

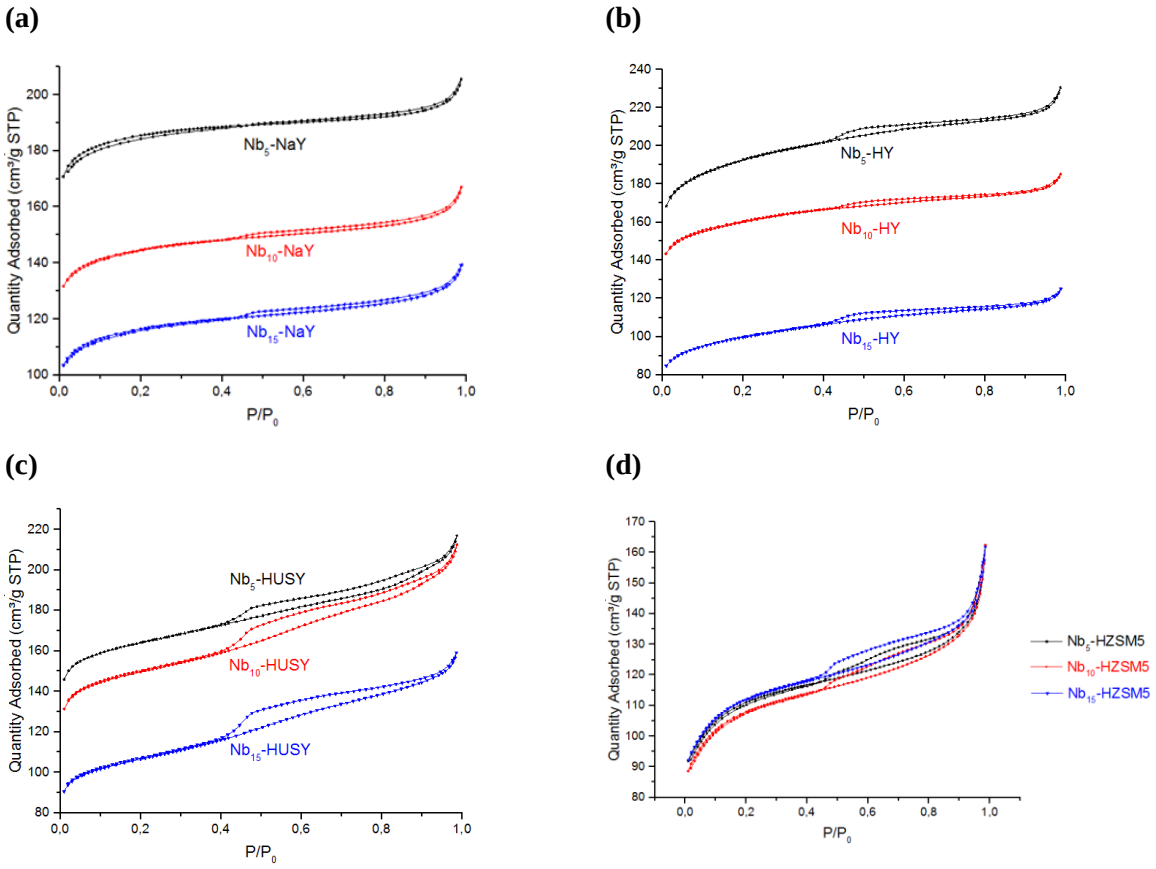

Figure 3.2: N_2 adsorption isotherms of Nb_x-ZEO catalysts, a) NaY, b) HY, c) HUSY and d) HZSM5.

The data from Figure 3.2 confirms that all isotherms are typical of type I isotherm of the original Brunauer classification. Even with higher concentrations of Nb_2O_5, all zeolites retained their porosity. The impregnation method practically no affects the structure of the zeolite.

The micropore volumes (V_{micro}) and mesopore surface areas (S_{ext}) were calculated by the *t*-method and the total surface areas were calculated by applying the BET equation (S_{BET}). The mesopore volume (V_{meso}) was calculated as the difference between the total

pore volume for P/P_0=0.986 ($V_{P/Po=0.986}$) and the micropore volume. These values are summarized in Table 3.1.

Table 3.1: Textural properties of catalysts and supports.

Zeolite	S_{BET} (m^2/g)[a]	S_{ext} (m^2/g)[b]	V_{total} (cm^3/g)[c]	V_{micro} (cm^3/g)	V_{meso} (cm^3/g)[d]
NaY	787	19	0.382	0.347	0.035
Nb_5-NaY	565	68	0.312	0.257	0.055
Nb_{10}-NaY	443	67	0.252	0.194	0.058
Nb_{15}-NaY	358	69	0.210	0.149	0.061
HY	665	25	0.349	0.302	0.047
Nb_5-HY	599	102	0.348	0.303	0.045
Nb_{10}-HY	495	103	0.281	0.231	0.050
Nb_{15}-HY	313	100	0.189	0.110	0.079
HUSY	750	24	0.355	0.269	0.086
Nb_5-HUSY	508	111	0.327	0.205	0.122
Nb_{10}-HUSY	465	114	0.319	0.181	0.138
Nb_{15}-HUSY	335	109	0.239	0.117	0.122
HZSM5	383	43	0.231	0.155	0.076
Nb_5-HZSM5	348	118	0.235	0.119	0.116
Nb_{10}-HZSM5	339	117	0.234	0.115	0.119
Nb_{15}-HZSM5	351	119	0.237	0.120	0.117

[a] Surface area calculated from BET equation

[b] External surface area and micropore volume calculated by the *t*-method

[c] Total pore volume determined from the amount adsorbed at P/P_0 = 0.99

[d] Mesopore volume calculated by the difference $V_{total}-V_{micro}$

As expected a significant decrease of specific surface area was observed while the external surface increase after Nb impregnation on zeolites. These results reveal that the degree of reduction observed in surface area is the same for all Y zeolites. In presence of lower amounts of Nb, 10% (HY) to 32% (HUSY) is lost in the surface while with higher amounts of Nb the loss is about 55%. However, independent of the Nb amount, the

decrease in surface area is the same for Nb_x-ZSM5 catalysts. For the external surface, the increase was 3 to 5 times for all zeolites. Nevertheless, HUSY and HZSM5 zeolites show higher mesoporous volume than the other Y zeolites.

The pores distribution of parent zeolites can be also determine by this analysis. Table 3.2 presents the porous distribution in micro and mesoporous size for the parent zeolites.

Table 3.2: Porous distribution of the parent zeolites.

Porous Radius, dV(r) (Å)	NaY (%)	HY (%)	HUSY (%)	HZSM5 (%)
0-20	76	71	59	59
20-50	22	28	29	38
> 50	2	2	12	3

In fact, the mesoporous size distribution confirms that the HUSY and HZSM5 zeolites present larger pores than the others zeolites. Contrary to the other zeolites, HUSY shows a significant amount of mesoporous with a radius larger than 50 Å. Thus, the impregnation of different amounts of Nb in these two zeolites (HUSY and HZSM5) affects more the mesoporous volume, which may enhance the catalytic properties of these catalysts.

In general, for higher amounts of Nb_2O_5, the decrease of these textural parameters is more pronounced. These results are not so marked in the case of HZSM5 due to the different geometry of its structure when compared with FAU structure. The analysis shows that the porosity of the structure of the zeolite is partial blocked after preparation of the catalysts by impregnation method.

3.2. X-ray diffraction (XRD)

The parent zeolites and Nb_x-ZEO catalysts were evaluated by XRD. The powder XRD diffraction patterns of the samples were recorded at 2θ values between 5 and 60 º. The XRD patterns obtained for Nb_x-Y and Nb_x-ZSM5 catalysts are in agreement with the characteristic diffraction patterns of these zeolites, in terms of peak positions and their relative intensities.

Figure 3.3 shows the diffraction patterns of HZSM5 and Nb_x-HZSM5 catalysts and Figure 3.4 illustrates the diffraction patterns of the parents NaY and HUSY, with the series of the catalysts Nb_x-NaY (Figure 3.4a) and Nb_x-HUSY (Figure 3.4b) obtained as example for FAU structure.

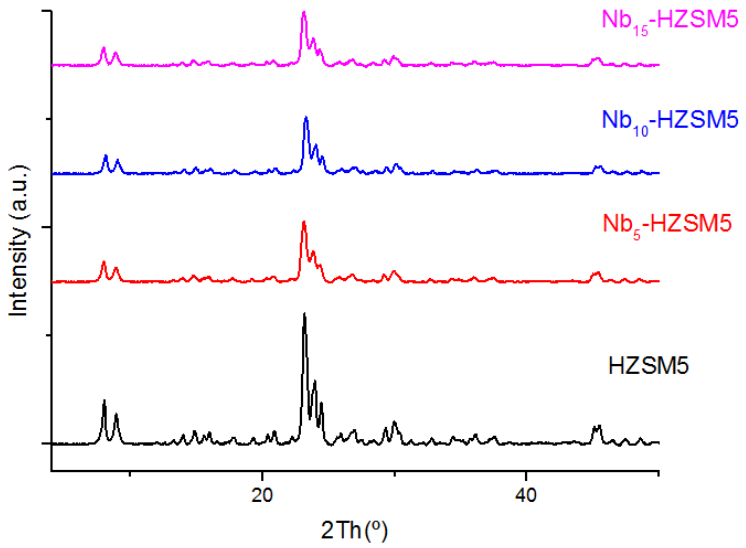

Figure 3.3: X-ray diffraction patterns of HZSM5 and Nb_x-HZSM5 catalysts.

All catalysts exhibited the typical and similar patterns of highly crystalline MFI (Figure 3.3) and FAU (Figure 3.4) zeolite structures. The XRD spectras of the parent zeolites and the catalysts showed a well crystallized framework due to the low background observed, which may be an indication of the partial absence of amorphous phase in these catalysts.

For all catalysts obtained after the impregnation method, the XRD patterns are very similar to that of the respective parent zeolite. However, after the impregnation some loss of intensity of the peaks can be observed in the XRD patterns of Nb_x-Y and Nb_x-HZSM5 catalysts. This reveals a decrease in crystallinity of the niobium-loaded zeolites in comparison with the parent zeolites.

No diffraction peaks assigned to niobium species occur either for Nb_x-Y and Nb_x-HZSM5 catalysts. The presence of niobium oxide is evident at $2\Theta = 28.5^{o}$. The crystalline phases of niobium oxide are dependent of the temperature.

(a)

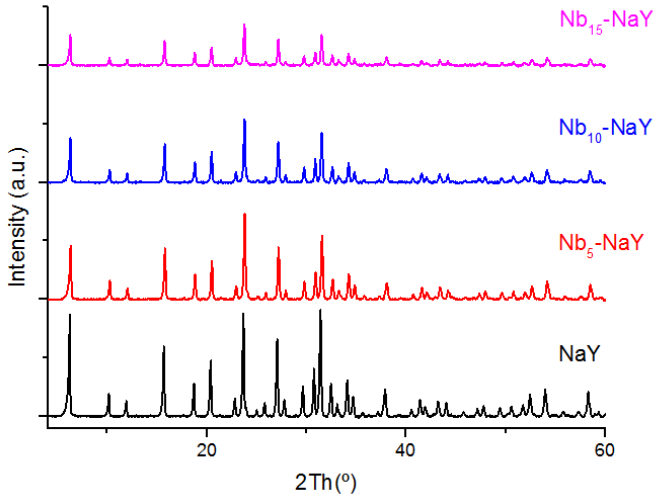

(b)

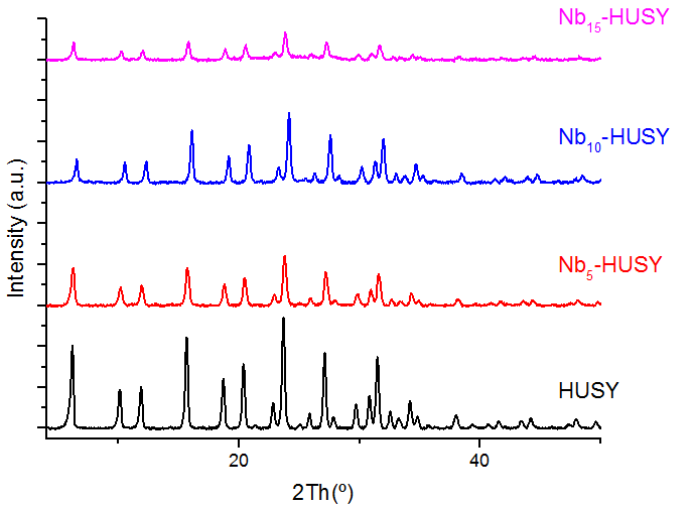

Figure 3.4: X-ray diffraction patterns of (a) NaY with Nb_x-NaY and (b) HUSY with Nb_x-HUSY.

The mixture of orthorhombic (T) and monoclinic (M and H) Nb_2O_5 phases occurs at 800 ºC while the samples treated at 500 °C showed a structure with low crystallinity and characteristic peaks with the hexagonal phase (TT phase) [139]. Barros *et al* [140] observed Nb_2O_5 crystalline T-phase in catalysts prepared with niobium supported on HZSM-5 with higher Nb content on zeolite, 19%. Our experimental conditions used in the impregnation method, 5 to 15 % of Nb and calcination temperature at 500 ºC with zeolites promote the presence niobium oxide with a crystalline phase orthorhombic (T) [139-141]. Such absence of Nb peaks even when it is present in higher amount, suggests a dispersion of Nb through the Y and ZSM5 zeolites and the niobium is present in the form of

amorphous niobium oxide hydrate. Furthermore, the presence of Nb didn't affect the integrity of the zeolite structures.

The relative crystallinity of HY and HUSY zeolites was estimated by comparing the peak intensities of the samples with NaY used as a standard sample (100 % crystalline). The total intensities of the six peaks assigned to [3 3 1], [5 1 1], [4 4 0], [5 3 3], [6 4 2] and [5 5 5] reflections were used for the comparison according to ASTM D 3906-80 method. For ZSM5, the total intensities of the five peaks assigned to [5 0 1], [0 5 1], [1 5 1], [3 0 3] and [1 3 3] reflections were used for the comparison with HZSM5 as a standard sample (100 % crystalline) according to ASTM D 5758 method. Table 3.3 summarizes the relative crystallinity of the parents and modified Y and ZSM5 zeolites.

Table 3.3: Structural properties of Y and ZSM5 samples determined from XRD.

Sample	Relative crystallinity (%)
NaY	100
Nb_5-NaY	69
Nb_{10}-NaY	69
Nb_{15}-NaY	57
HY	75
Nb_5-HY	69
Nb_{10}-HY	32
Nb_{15}-HY	35
HUSY	80
Nb_5-HUSY	42
Nb_{10}-HUSY	29
Nb_{15}-HUSY	31
HZSM5	100
Nb_5-HZSM5	47
Nb_{10}-HZSM5	53
Nb_{15}-HZSM5	44

It may be observed that the catalysts lost the crystallinity after the impregnation of Nb, as compared to the respective parent zeolites. The increase in the loss of cristallinity is obtained with higher amount of Nb supported in all zeolites. The Nb_x-NaY and Nb_x-HY series of the catalysts shows a similar tendency. However, the losses of cristallinity are more affected in the Nb_x-HUSY and Nb_x-HZSM5 series of the catalysts by the impregnation method used in this work.

3.3. Chemical analysis by inductively coupled plasma emission spectroscopy (ICP-OES)

The amount of Si, Al and Nb either from the modified samples and the parent zeolites were determined by elemental analysis. The results are present in Table 3.4.

Table 3.4: Amounts of Si, Al and Nb present in all samples.

Zeolite	Si (%)	Al (%)	Si/Al	Nb (%)[a]	Nb (%)
NaY	26.5	9.0	2.83	------	------
Nb_5-NaY	19.4	8.0	2.34	5.0	2.1
Nb_{10}-NaY	21.8	9.2	2.28	10.0	4.7
Nb_{15}-NaY	19.5	8.1	2.32	15.0	6.9
HY	34.2	11.7	2.80	------	------
Nb_5-HY	22.8	9.2	2.39	5.0	4.0
Nb_{10}-HY	21.1	8.8	2.31	10.0	7.6
Nb_{15}-HY	17.6	7.8	2.18	15.0	9.6
HUSY	34.1	10.9	3.00	------	------
Nb_5-HUSY	24.4	9.2	2.56	5.0	3.5
Nb_{10}-HUSY	22.7	8.8	2.49	10.0	6.8
Nb_{15}-HUSY	19.5	8.1	2.32	15.0	8.3
HZSM5	34.9	2.25	15.00	------	------
Nb_5-HZSM5	30.4	2.2	13.32	5.0	1.2
Nb_{10}-HZSM5	33.1	2.4	13.30	10.0	3.0
Nb_{15}-HZSM5	31.2	2.3	13.08	15.0	4.4

[a]percentage of Nb expected

Apart from the geometrical aspects related to the pore structure, the composition of zeolites confers different properties to these materials. The results of chemical analysis reveal that the total Si/Al ratio of Y zeolites is significantly lower than that of HZSM5 zeolite. This is explained by the difference of the aluminium content in the framework of the zeolites which is higher for all Y zeolites. ZSM5 zeolite is characterized by a high silica zeolite. It can also be seen that the total Si/Al ratio of the Nb_x-ZEO samples after impregnation decrease as the amount of Nb increases, which indicates that no dealumination was observed after the treatment. Therefore, it can be concluded that the structure of Y and ZSM5 zeolites remained practically unchanged after the impregnation treatment performed, which in agreement with N_2 adsorption and XRD analyses.

All Y zeolites used in this work present similar total Si/Al ratio. However, the difference between the Si/Al ratios determined by FTIR and XRD (framework) and those determined by chemical analysis (total) indicates an irregular distribution of silicon and aluminum throughout the zeolite structures.

From FTIR analysis, the Si/Al ratio of framework could be determined for the FAU structure contrasting of ZSM5 zeolite, due to the zeolite Y have a cubic symmetry [142]. The infrared region between 570 and 600 cm^{-1} shows the most sensitive band in the zeolite Y structure and can be used to calculate framework Si/Al ratios using the equation 11 [143, 144]:

$$x = 3.857 - 0.00621 w_{DR}\ (cm^{-1}) \quad (11)$$

where $x = [1+(Si/Al)]^{-1}$, with $0.1 < x < 0.3$, and w_{DR} is the zeolite specific double ring vibration mode between 570-600 cm^{-1}. Also, for the zeolites Y, the framework Si/Al ratio was obtained by XRD from the calculated unit cell parameters by using the Breck and Flanigen equation (equation 12) [143]:

$$N_{Al} = 115.2\ (a_0 - 24.191), \quad (12)$$

where N_{Al} is the framework aluminum number and a_0 is the cell parameter. The unit cell parameters were calculated from the values of the [5 3 3], [6 4 2] and [5 5 5] reflection peaks according to the ASTM D 3942-80 method.

Table 3.5 shows the Si/Al ratios determined from XRD, FTIR and chemical analysis for the parent Y zeolites.

Table 3.5: Si/Al ratios of the parent Y zeolites.

Zeolite	NaY	HY	HUSY
Si/Al[a]	2.83	2.80	3.00
Si/Al[b]	2.80	4.05	3.90
Si/Al[c]	2.82	4.10	3.96
EFAL[d]	0	17	11

[a]Total Si/Al ratio and sodium amount determined from ICP-OES.
[b]Framework Si/Al ratio determined from XRD.
[c]Framework Si/Al ratio determined from FTIR.
[d]EFAL is the number of extraframework aluminium species drawn from the framework Si/Al ratio of the zeolites [145].

In the case of NaY, the total and framework Si/Al ratios are similar, which means that both species are tetrahedrally coordinated in the framework. For HY and HUSY, the framework Si/Al ratio is higher than the total Si/Al ratio indicating the presence of extra-framework alumina species (EFAL) [146].

It is not possible to determine the Si/Al ratio of the framework from FTIR and XRD analysis for HZSM5 zeolite due to their structure which possesses an orthorhombic symmetry [147]. ZSM5 zeolite (MFI-type structure) is a high silica zeolite that is composed of several *pentasil* units linked together by oxygen bridges to form *pentasil* chains. The *pentasil* chains are interconnected by oxygen bridges to form corrugated sheets with 10-ring holes. ZSM5 is a medium pore zeolite with pore diameters of 5.4-5.6 Å that are defined by these 10 member oxygen rings [148].

It is known that the catalytic properties of zeolites are essentially related to their shape selectivity, pore structure, acidity and thermal stability. The zeolites used in this work are different in these properties. The shape selectivity for sorption and catalysis of ZSM5 is distinctly different from that of Y (FAU-type structure) zeolite, due to their pore openings are 10-rings rather than 12-rings [148]. This wide aperture of Y zeolites gives access to the microporosity and to the active sites for a wide range of organic molecules [149]. The catalytic properties can be also related to the Si/Al ratio. Lower Si/Al ratio generally implies a higher catalytic activity due to the presence of a higher number of Brønsted acid sites. The acidity of zeolites is related with Brønsted and Lewis acid sites, both contributing to the total acidity of the solid [150]. The most important sites the Brønsted sites are acidic hydroxyl groups bridging silicon to framework aluminium in the zeolite structure, while the Lewis sites are associated with extra-framework aluminium

oxide species. Also, the Lewis acidity can be achieved by loss of water of the Brønsted acid sites upon heating [150]. NaY, HY and HUSY zeolites present lower and similar total Si/Al ratio. Due to the high density of Al substitutions at nearest of neighbor positions implies highest number of acid sites.

The acidity tends to increase in strength with increasing Si/Al ratio. However, high Si/Al ratio in HZSM5 confer that the framework presents a low concentration of acid sites but with high acid strength due to their isolation of these sites [150]. The zeolitic acidic sites can be generated in several ways. In the catalysts based in (NH_4)USY and (NH_4)ZSM5 after calcination, the ammonium present by heating was decomposed into NH_3 and H^+. The NH_3 molecules desorb and the presence of the protons increases the number of acid sites [150].

In relation to the amount of niobium present in the catalysts, it was less than expected which suggest that the dispersion of Nb on the zeolites by impregnation method was not homogeneous. The impregnation method used in this work practically unchanged the zeolitic structure but the deposition of the metal was not uniform.

3.4. Fourier Transform Infrared Spectroscopy (FTIR)

From the structural point of view, FTIR analysis confirms the integrity of the parent zeolites and the catalysts. All FTIR spectra of the heterogeneous catalysts are dominated by the strong bands attributable to the zeolite structure. No shift or broadening of the zeolite vibration bands is observed upon incorporation of the niobium.

Figure 3.5 shows the infrared spectroscopy (FTIR) spectra of NaY and Nb_x-NaY catalysts. FTIR spectra of Nb_x-NaY catalysts show a very intense broad band at 3700-3200 cm^{-1}, which is attributed to Si-OH with a poorly resolved shoulder at 3600 cm^{-1} which can be attributed to the hydroxyl groups in the supercages and in the sodalite cages respectively and the characteristic bands at 1200 to 500 cm^{-1}, which are assignable to Si-O-Al, Si-O-Si, Al-O, Si-O-M and T-O species, where M is the exchangeable Na^+ ion metal species [151-153]. The presence of water in the zeolite structure also gives an absorption band in the region of 1600-1650 cm^{-1} [154].

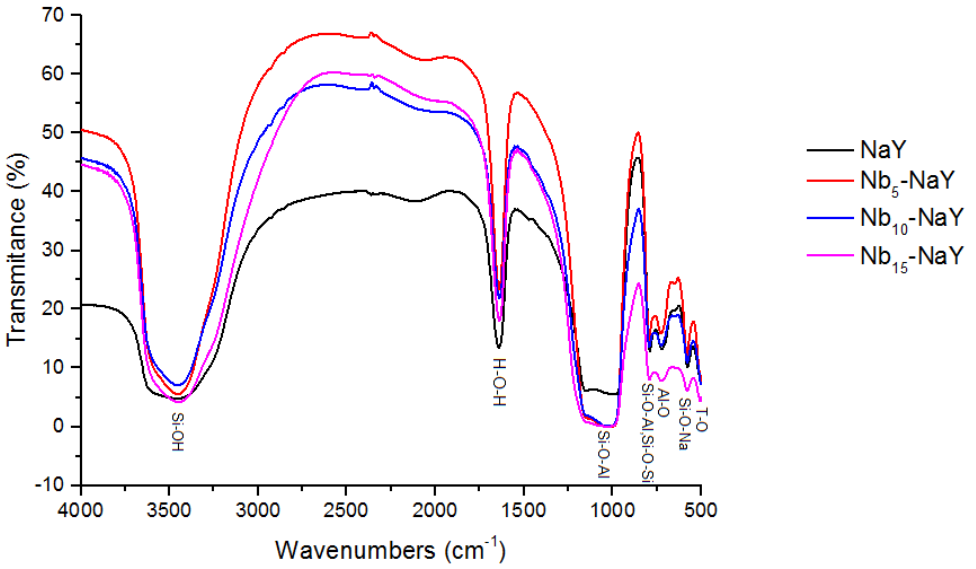

Figure 3.5: FTIR spectra of Nb_x-NaY heterogeneous catalysts and the parent zeolite.

The same conclusions were taken after analyze the spectra obtained by the others Y-zeolies, HY and HUSY, when impregnated with different amount of niobium. Figure 3.6 shows the FTIR spectra obtained by Nb_x-HY, Nb_x-HUSY and they respective parent zeolite.

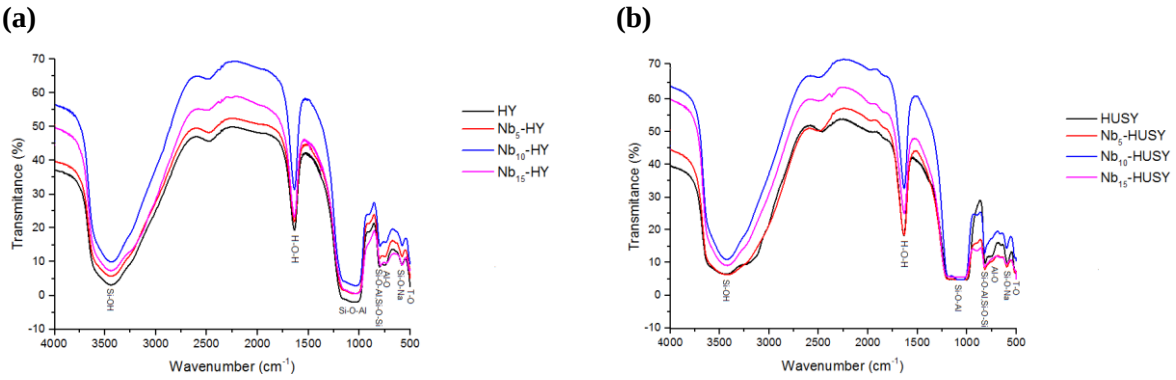

Figure 3.6: FTIR spectra of Nb_x-HY and HY (a), Nb_x-HUSY and HUSY (b) heterogeneous catalysts.

Figure 3.7 shows FTIR spectra of HZSM-5 and Nb_x-HZSM5 heterogeneous catalysts.

The findings emerge that the band at 3700 cm^{-1}, can be attributed to isolated or terminal silanol groups, and the intensive broad band at 3400 cm^{-1} is assigned to Brønsted acidic sites of Al-O(H)-Si bridges [140].

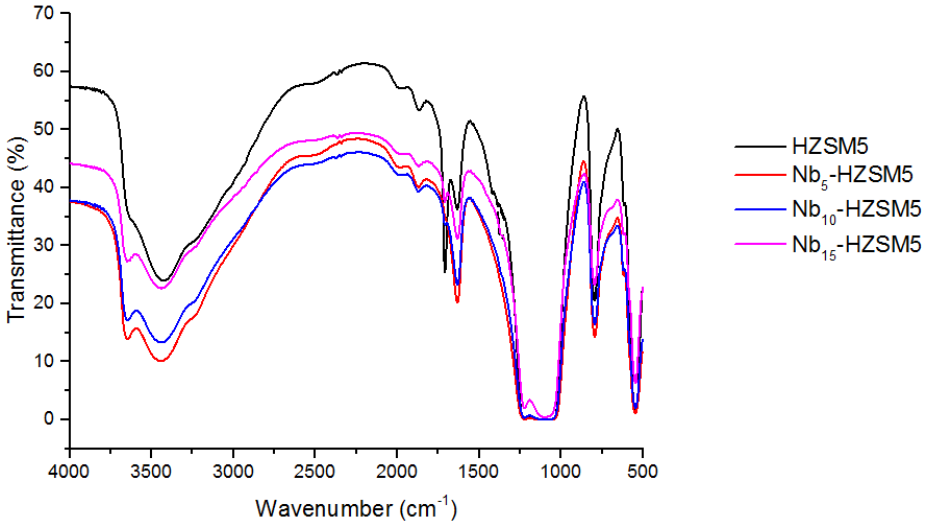

Figure 3.7: FTIR spectra of Nb_x-HZSM5 and its parent zeolite HZSM5.

The band at 1225 cm^{-1} is assigned to external asymmetric stretching vibration of the T–O bond. The band at 1100 cm^{-1} is assigned to internal asymmetric stretching of Si-O-T bonds [140, 155]. A band at about 798 cm^{-1} is related to symmetric stretching of external bonds between tetrahedral and at 550 cm^{-1} there is a vibration sensitive to the MFI zeolite topology, which is assigned to the five-membered ring of the pentasil zeolite structure [140, 155]. Vibrations related to Nb-O stretching are usually observed between 600 and 950 cm^{-1} [156-158]. However, in all FTIR spectra of the Nb_x-HZSM5 heterogeneous catalysts no new peak was observed in this region.

3.5. X-ray photoelectron spectroscopy (XPS)

XPS is a powerful technique which provides an elemental analysis of a shallow layer (approx. 20 nm depths for soft X-rays) of the zeolite grain. XPS analysis can be quantitative by integrating the area of the peak corresponding to each element and calibrating the response of each atom using standards [159]. About the information regarding the oxidation states, it must be considered with some reserve because these experiments were not carried out *in situ* and therefore, some surface oxidation may result from the contact with air during sample manipulation [159]. However, for our samples the niobium is already oxidized after the calcination treatment.

X-ray photoelectron spectroscopy experiments were carried out to detect the oxidation state of Nb species present in the zeolite structures as well as composition and related distribution of the surface elements. All samples revealed the presence of oxygen,

sodium, silicon and aluminium in their survey XPS resolution spectra. Figure 3.8 shows the XPS spectra of the parent zeolites based in FAU structure and Figure 3.9 shows the spectrum of MFI structure which display the characteristic peaks of the zeolites.

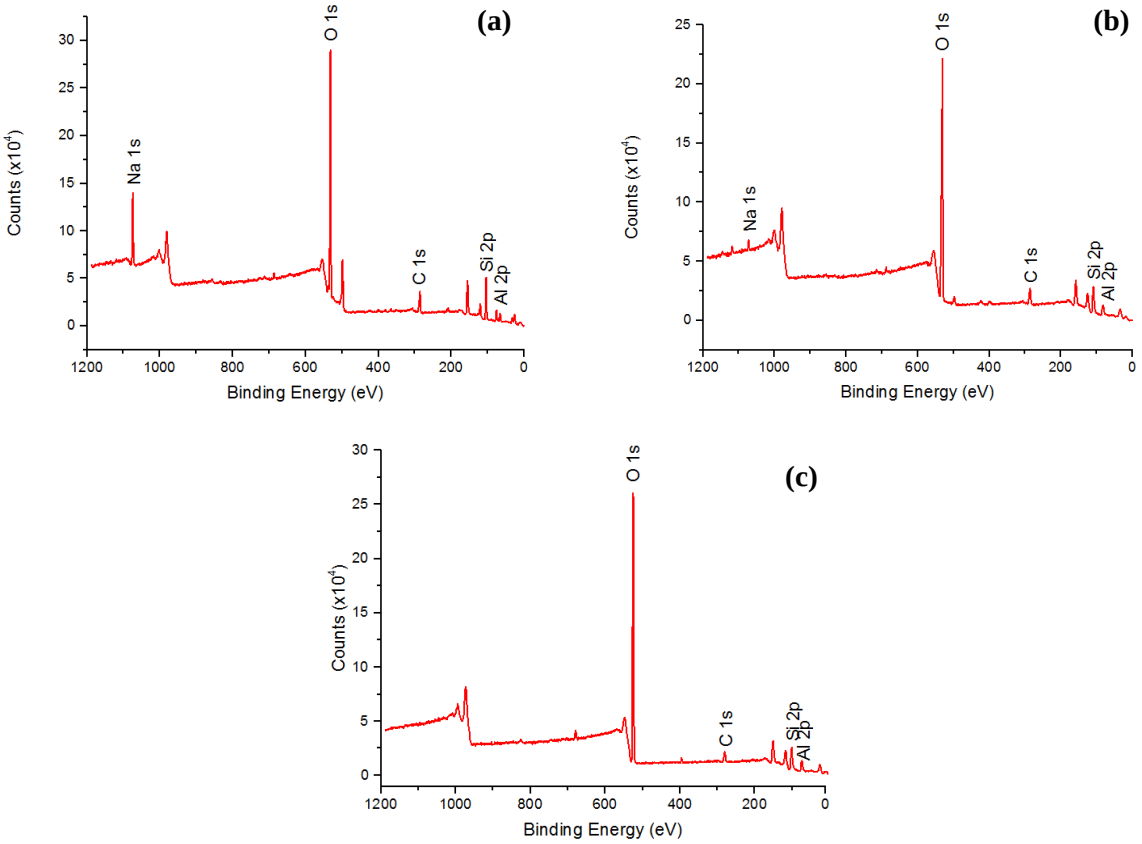

Figure 3.8: XPS spectra of (a) NaY, (b) HY and (c) HUSY.

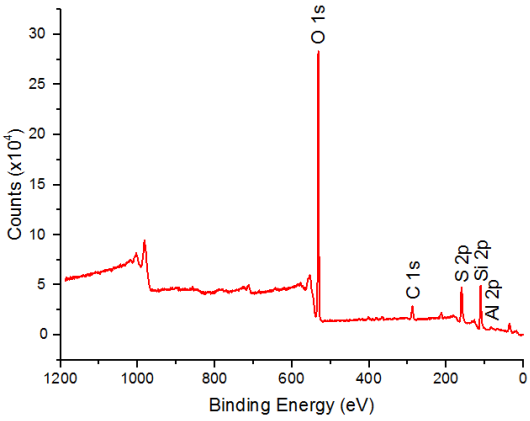

Figure 3.9: XPS spectrum of HZSM5.

The presence of niobium in the region of Nb 3p between 364.74 – 366.74 eV was detected in all catalysts. Figure 3.10 shows the presence of niobium in the catalysts

prepared with higher amount of niobium, Nb_{15}-NaY, Nb_{15}-HY, Nb_{15}-HUSY and Nb_{15}-HZSM5.

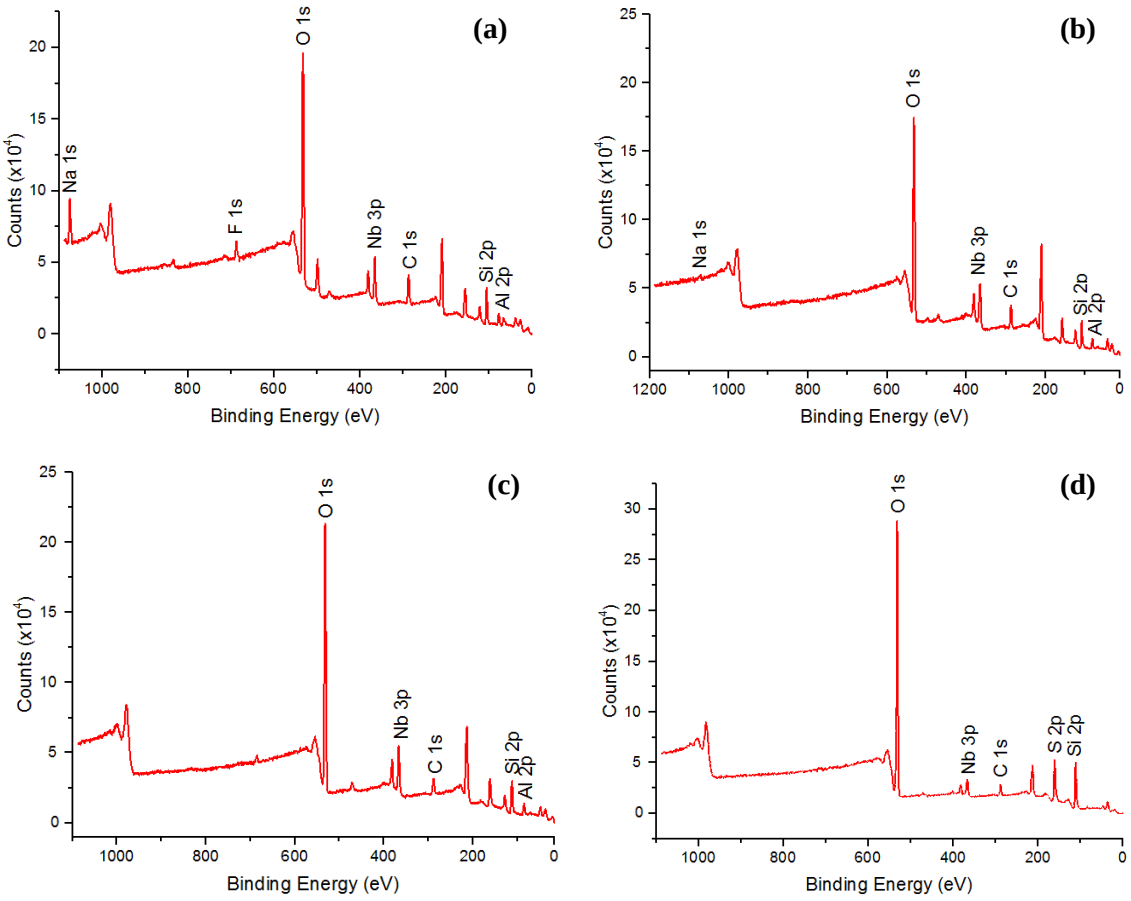

Figure 3.10: XPS spectra of (a) Nb_{15}-NaY, (b) Nb_{15}-HY, (c) Nb_{15}-HUSY and (d) Nb_{15}-HZSM5 catalysts.

The binding energies (BE) of the elements detected by XPS are summarized in Table 3.6.

All spectra show peaks in the Si 2p region between 103.74-110.74 eV due to the tetrahedral Si atoms present in the zeolite, such as SiO_4 and terminal Si-OH groups; in the Al 2p region between 75.74-82.74 eV from the tetrahedral AlO_4 groups and a wide symmetrical large peak in the O 1s region between 530.74-531.74 eV, corresponding respectively to SiO_4 tetrahedra and Si-OH groups, AlO_4 tetrahedra and oxygen atoms which are attached to the primary tetrahedrons of the structure. Finally, the peak at 1070.74-1074.74 eV corresponds to the Na 1s region located in the zeolite structure [123]. The sodium in the surface is not observed for HUSY and HZSM5 because these zeolites have small amounts of Na in the framework, 0.12 % and 0.08 %, respectively.

Table 3.6: The binding energies (BE) of the elements present in the zeolite structures.

Zeolite	Binding energy (eV)				
	Si 2p	**Al 2p**	**Nb 3p**	**Na 1s**	**O 1s**
NaY	103.74	75.74	-------	1073.74	531.74
Nb_{15}-NaY	104.74	76.74	364.74	1074.74	531.74
HY	108.74	82.74	-------	1071.74	530.74
Nb_{15}-HY	107.74	67.74	364.74	1070.74	531.74
HUSY	106.74	79.74	-------	nd	531.74
Nb_{15}-HUSY	108.74	69.74	366.74	nd	531.74
HZSM5	110.74	82.74	-------	nd	531.74
Nb_{15}-HZSM5	110.74	82.74	366.74	nd	531.74

nd – Not defined.

The peak in the Nb 3p region at binding energies close to 364.74 eV and 366.74 eV corresponds to the photoelectron peak of Nb $3d_{3/2}$. In reference compounds, the binding energy value found of Nb $3d_{3/2}$ is reported to Nb_2O_5 [160].

The atomic composition of the surface of parent zeolites NaY, HY, HUSY HZSM5 and their respective Nb_{15}-ZEO catalysts detected by XPS is summarized in Table 3.7.

The Si/Al ratio of the external surface measured by XPS shows that the surface of all samples is rich in silicon groups. The difference between Si/Al ratios determined by XPS (Table 3.7) and those determined by chemical analysis, bulk (Table 3.4) indicates an irregular distribution of silicon and aluminium throughout the zeolite structures.

Comparing the values of niobium atomic percent obtained by ICP-OES (Table 3.4) and XPS (Table 3.7), it can be seen that the amount of niobium in the surface is different from the amount of niobium within the structures, suggesting that this metal is not homogeneously distributed. Furthermore, the percentage of niobium on the surface is lower than the percentage of niobium existing within the structure for Nb_{15}-HUSY and Nb_{15}-HZSM5 due to the existence of the large porous in these zeolites.

Table 3.7: The surface atomic composition of NaY, Nb_{15}-NaY, HY, Nb_{15}-HY, HUSY, Nb_{15}-HUSY, HZSM5 and Nb_{15}-HZSM5 samples.

Zeolite	XPS (atom %)					
	Si	Al	Nb	Na	O	Si/Al
NaY	25.1	8.3	-------	5.8	45.6	2.92
Nb_{15}-NaY	17.4	8.2	2.6	3.0	47.3	2.05
HY	24.2	9.0	-------	0.8	47.1	2.59
Nb_{15}-HY	18.8	3.2	4.2	0.5	57.2	5.67
HUSY	22.5	16.2	-------	nd	51.9	1.34
Nb_{15}-HUSY	18.1	2.5	2.9	nd	46.9	7.24
HZSM5	36.7	6.4	-------	nd	50.8	5.71
Nb_{15}-HZSM5	29.7	0.8	1.2	nd	47.1	35.80

nd – Not defined.

3.6. SEM analysis

In order to obtain morphological information about the different supports before and after niobium impregnation, SEM analysis was performed with the samples. Figure 3.11 presents the SEM images of the parent zeolites.

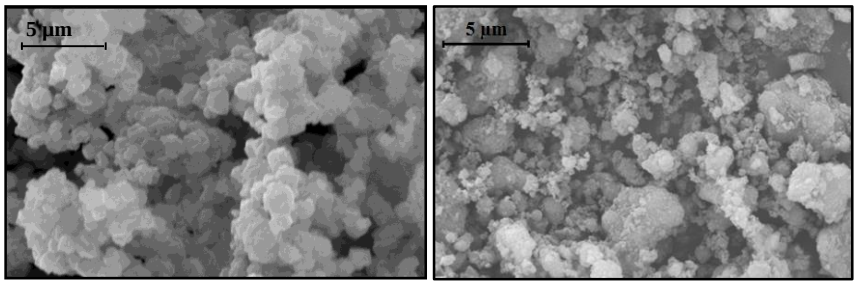

Figure 3.11: SEM photographs of the parent zeolites Y (left) and ZSM5 (right) with same resolution.

It can be observed that the parent zeolites have different morphology and particle size. The parent Y zeolite presents well-formed cubic particles with average size of about 0.7 µm. For ZSM5 zeolite, the morphology present the individual particles form larger and

irregular aggregates, being therefore difficult to determine the mean size of the primary particles from the SEM image.

Figure 3.12 presents the SEM images of the heterogeneous catalysts obtained with 15% of niobium with different resolutions.

(a)

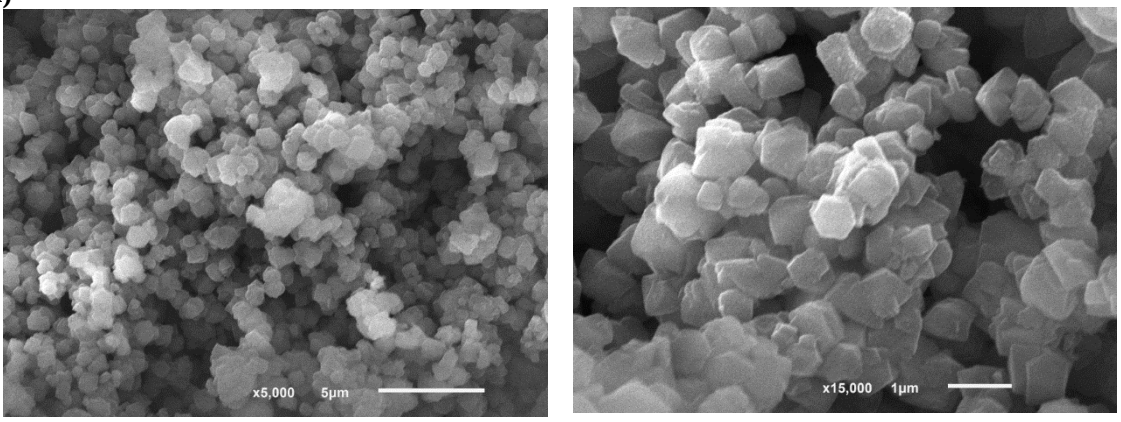

(b)

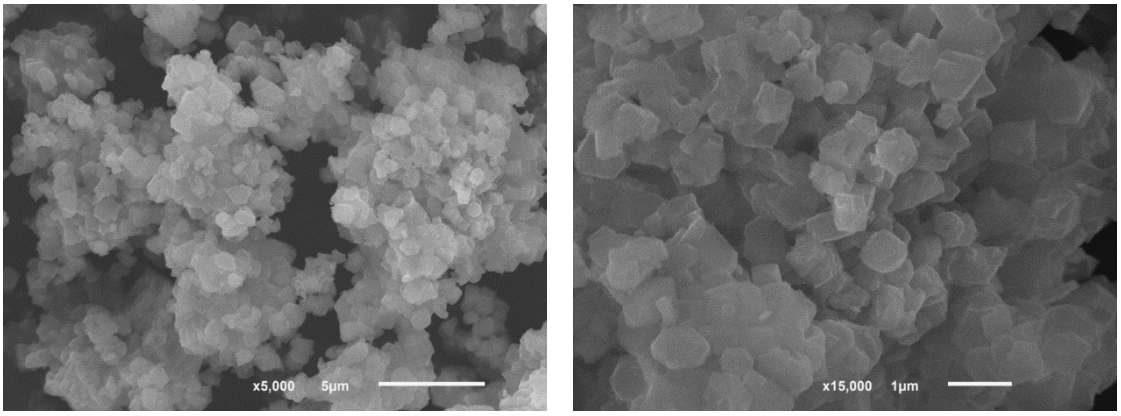

(c)

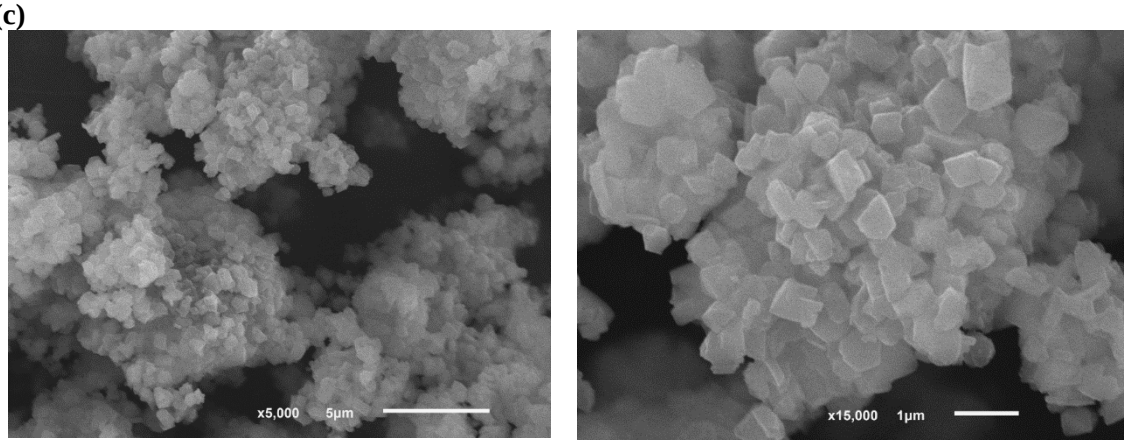

(d)

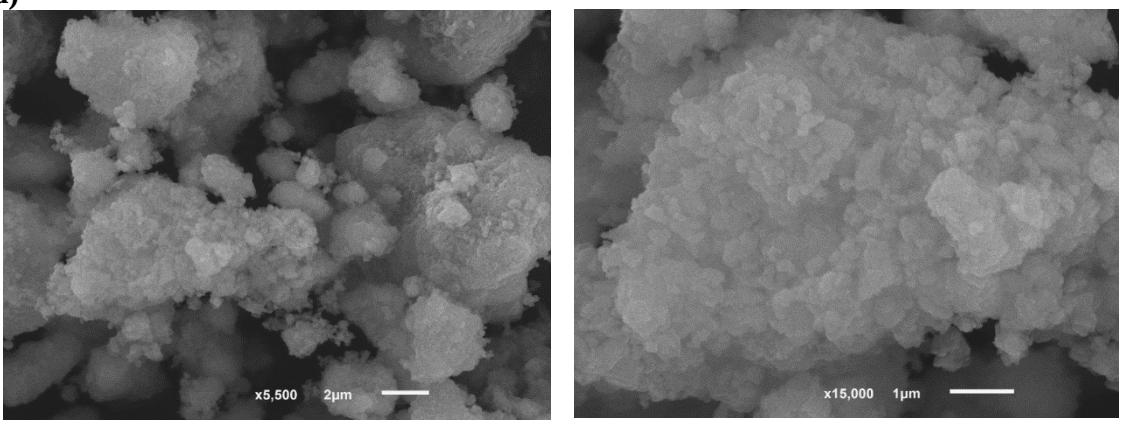

Figure 3.12: SEM images of (a) Nb_{15}-NaY, (b) Nb_{15}-HY, (c) Nb_{15}-HUSY and (d) Nb_{15}-HZSM5.

Comparing the photographs of the parent and the Nb_{15}-ZEO heterogeneous catalysts, respectively, no significant differences on morphology and particle size were found. Similar morphology and particle size were observed for Nb_{15}-ZEO, obtained after the higher concentration of Nb. Therefore, it can be concluded that the morphology of Y and ZSM5 zeolites remained practically unchanged after the impregnation treatment performed.

3.7. Thermogravimetric analysis (TGA)

The hydrophobicity of the zeolites was quantified by thermogravimetric analysis. The zeolites with low silica but higher amount of aluminium (Si/Al of 2-5) show a strongly hydrophilic surface selectivity. However, high silica zeolites with Si/Al of 10-100 are known to be hydrophobic [142].

The TGA/DTG/DSC curves of NaY and the TGA curves of the Nb_x-NaY catalysts are shown in Figures 3.13 and 3.14, respectively. The hydrated NaY lost ≈25 wt% of the initial mass of the zeolite sample upon heating from 25 to 800 ºC. This loss is mainly attributed to desorption of the adsorbed water on the zeolite. Most of mass loss occurs in temperatures up to 25 ºC to 200 ºC reaching a maximum around 130 ºC as showed by the peak obtained from the derivative weight while the rest mass loss takes place at higher temperatures. This behavior agrees with that expected: a single-stage weight loss due to the loss of water from the NaY structure. At same time is developed an exothermic process because heat flows out of the sample as a result of the sample heat capacity.

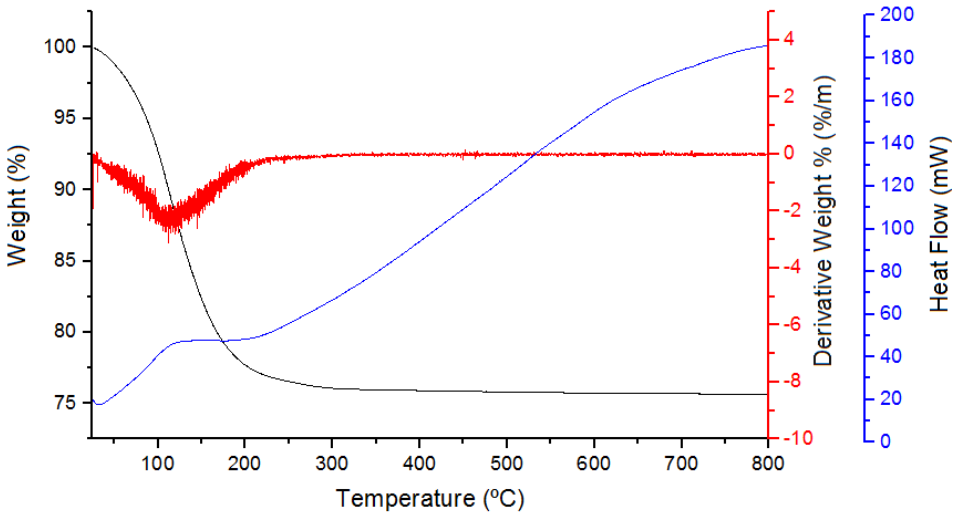

Figure 3.13: TGA/DTG/DSC curves of NaY.

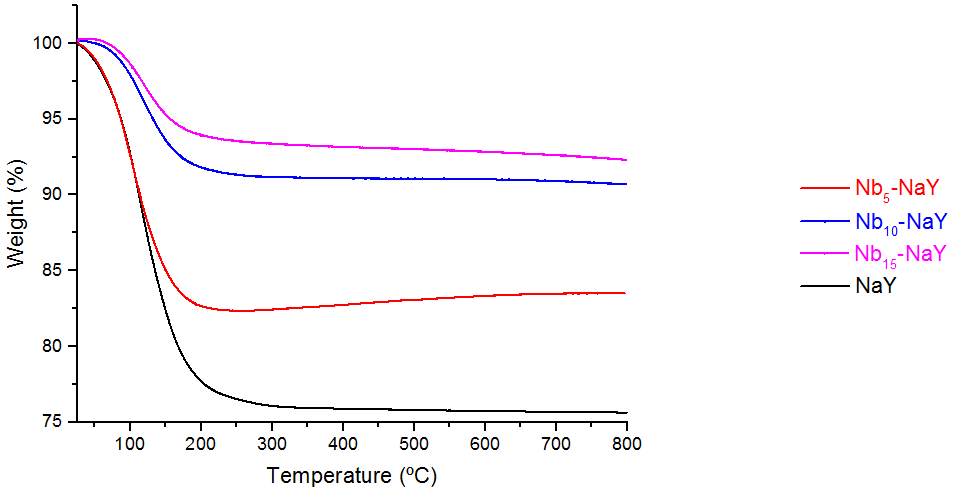

Figure 3.14: TGA curves of Nb_x-NaY.

NaY samples impregnated with different amounts of Nb_2O_5 revealed the same behavior as the parent zeolite. The weight loss observed is lower than NaY (7.5 to 10%). The presence of Nb_2O_5 not affects the thermal stabilization of the catalyst.

A different TGA heating profile was observed for HY zeolite which showed three main steps of weight loss (Figure 3.15). The first step (25-200 °C) and the second step (200-300 °C) are attributed to the water desorption from the zeolite while the third step (650-700 ºC) probably is due to the contaminants from the synthesis of the zeolite. The total mass lost is around 24%. Through DSC analysis is possible to conclude that is an exothermic process as well as observed for NaY zeolite.

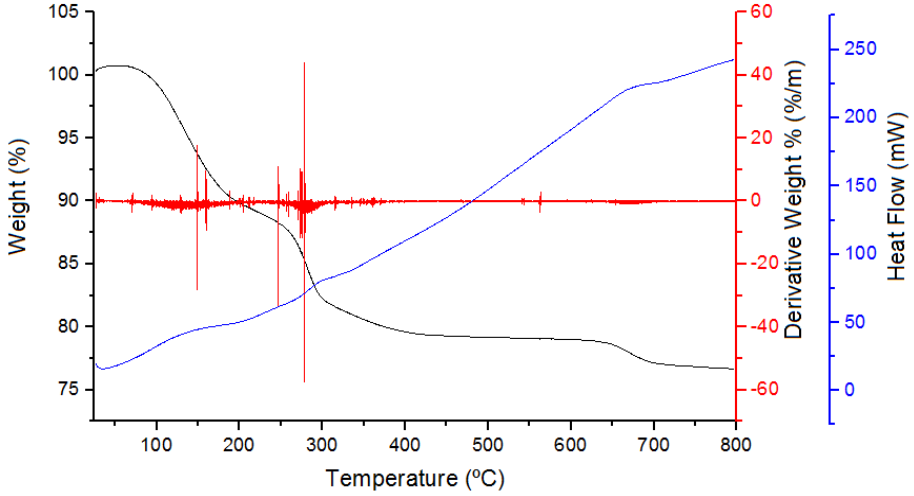

Figure 3.15: TGA/DTG/DSC curves of HY.

In Figure 3.16 the TGA curves of Nb_x-HY show the same behavior as the parent zeolite despite the shoulders are less pronounced. The total weight loss observed is around 4%. The presence of Nb_2O_5 not affects the thermal stabilization of the catalyst.

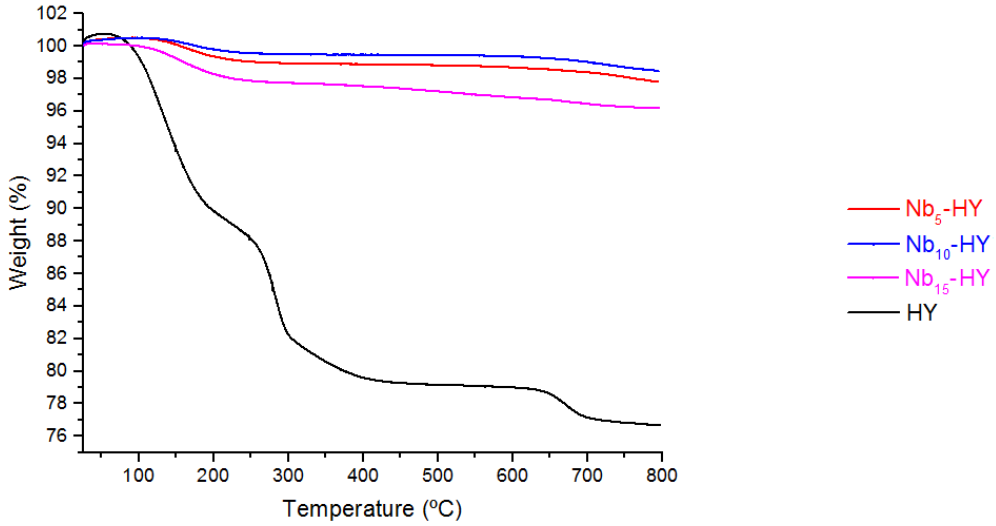

Figure 3.16: TGA curves of Nb_x-HY.

The parent HUSY has a similar thermal behavior as NaY, with high loss of mass between 25-200ºC due to the water desorption (Figure 3.17). The total mass loss was around 13%.

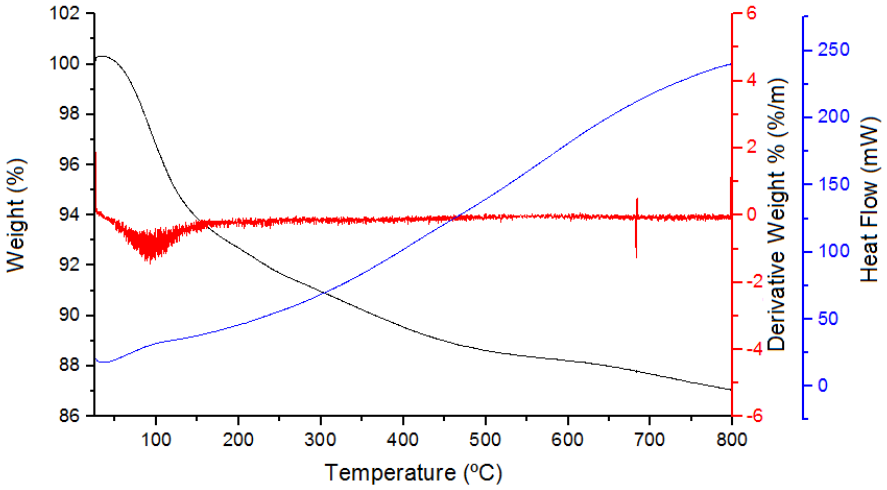

Figure 3.17: TGA/DTG/DSC curves of HUSY.

The impregnated samples (Nb_x-HUSY) showed also a loss mass between 25-200ºC of 7% (Figure 3.18).

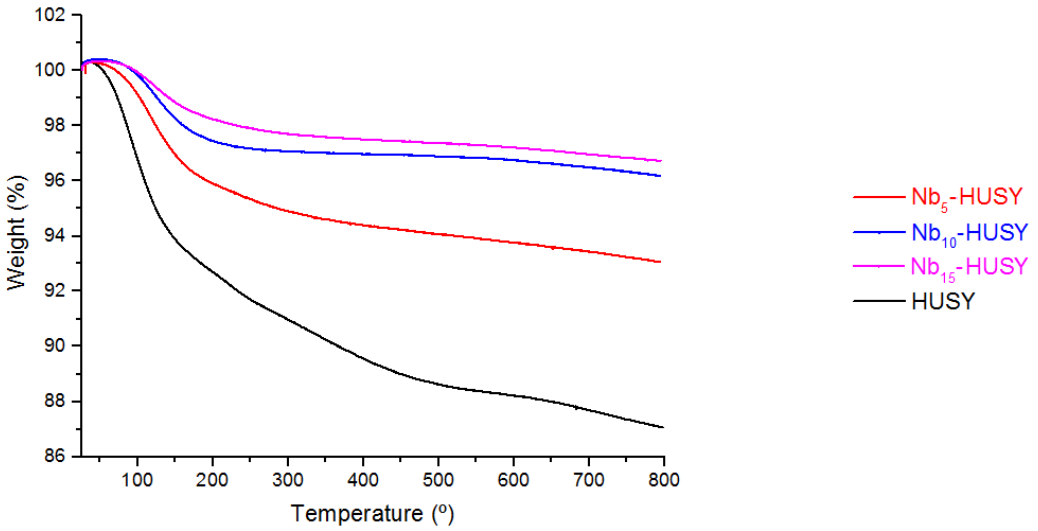

Figure 3.18: TGA curves of Nb_x-HUSY.

Figures 3.19 and 3.20 show the TGA curves of HZSM5 and modified Nb_x-HZSM5 catalysts. HZSM5 shows a total weight loss of ≈5% which occurs between 25-200 ºC, attributed to water molecules physically adsorbed. The same behavior was observed for Nb_x-HZSM5 catalysts.

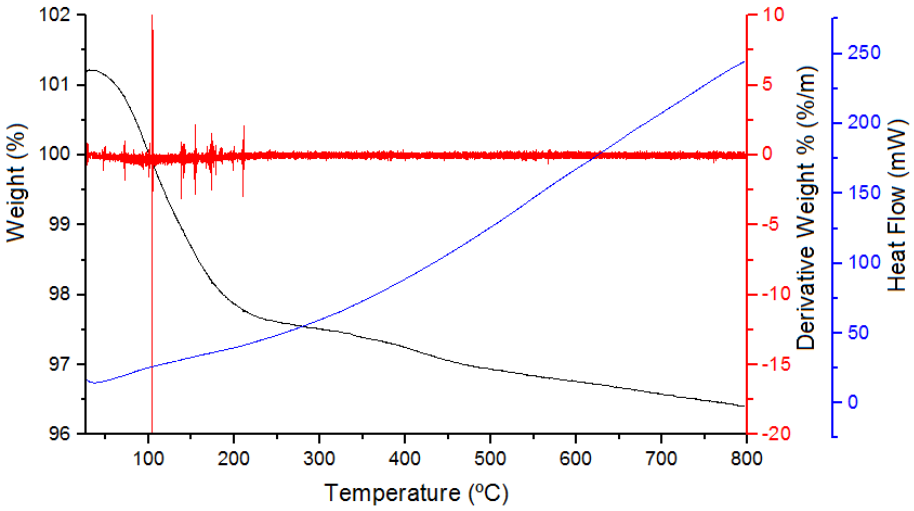

Figure 3.19: TGA/DTG/DSC curves of HZSM5.

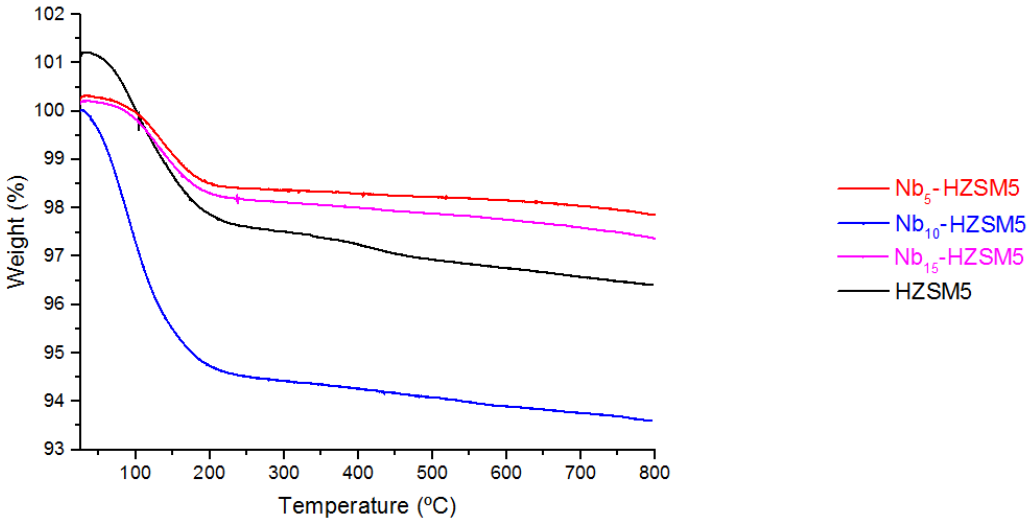

Figure 3.20: TGA curves of Nb_x-HZSM5.

The total weight loss of each sample during the analysis is summarized in table 3.8.

Table 3.8: Percentage of the weight loss in each sample during TGA analysis.

Sample	Weight loss (%)
NaY	25
Nb_5-NaY	18
Nb_{10}-NaY	10
Nb_{15}-NaY	8
HY	24
Nb_5-HY	3
Nb_{10}-HY	2
Nb_{15}-HY	4
HUSY	13
Nb_5-HUSY	7
Nb_{10}-HUSY	4
Nb_{15}-HUSY	3
HZSM5	5
Nb_5-HZSM5	7
Nb_{10}-HZSM5	2
Nb_{15}-HZSM5	3

In conclusion, the zeolites used in this work present the follow hydrophilic behavior: NaY > HY > HUSY > HZSM5. In consequence of these, the catalysts show different catalytic behavior due to the presence of the water produce in the reaction.

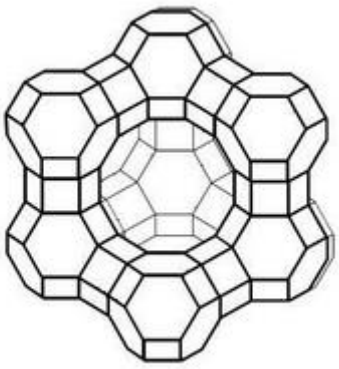

CHAPTER IV– CATALYSIS

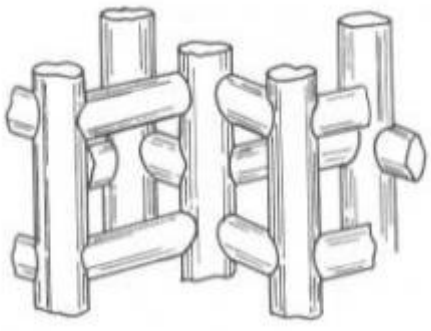

CHAPTER IV – CATALYSIS

This chapter presents the experimental results obtained from the catalytic acetalization of glycerol conducted with the heterogeneous catalysts NaY, Nb_x-NaY, HY, Nb_x-HY, HUSY, Nb_x-HUSY, HZSM5 and Nb_x-HZSM5, previously described in Chapter III.

4.1. Catalytic acetalization of glycerol with acetone

The glycerol acetalization reaction mainly yields a five-membered ring ketal (*solketal*), but gives rise a six-membered ring ketal, whose relative formation depends on the acetalization position within the glycerol molecule [161]. However, glycerol acetalization with acetone favors the formation of the five-membered ring transition state, giving rise to *solketal* formation [3]. In the present study, the active catalysts studied in the glycerol acetalization reaction showed a maximum selectivity of 98% towards *solketal*, in line with data reported before for the same reaction over heterogeneous Brønsted acid catalysts [3]. All parent zeolites choose in this work are Brønsted and Lewis acid sites with the former being in larger amount.

The niobium supported catalysts based in zeolites were carried out under semi-batch conditions for the reaction of glycerol with acetone. The parent zeolites used in this work present the follow hydrophilic behavior: NaY > HY > HUSY > HZSM5 (Table 3.8). The formation of water in this reaction is a problem due to the decrease of the acid strength of the catalyst and favors the reversibility of the reaction [3]. In order to enhance the catalytic properties of the parent zeolites, they were modified by impregnation with niobium. Before the reaction all heterogeneous catalysts were submitted to the same pre-treatment temperature in order to activate the acid sites and remove the water from the pores. The temperature used was 220 ºC. The effect of the reaction temperature and the amount of catalyst used were studied for the modified catalysts. The progress of each acetalization reaction was monitored following the variation in intensity of characteristic Raman bands. Thus, a real-time control of the reaction could be done by Raman spectroscopy. Gas chromatography analysis was also performed in order to quantify the conversion of glycerol.

To better understand the glycerol acetylation, Raman spectra of neat glycerol and acetone were first examined at room temperature in a spectral range of 3400-200 cm^{-1} (Figures 4.1 and 4.2).

Figure 4.1 shows the Raman bands characteristic of glycerol. The region of the Raman spectra between 3050 and 3400 cm^{-1} contains glycerol ν(CO–H) vibrations. According to the literature [162, 163], this region can be decomposed into two broad peaks, 3240 and 3340 cm^{-1}, that are assigned to the symmetric OH stretch, ν_s(CO–H) vibrations, of oligomers with an aggregation number greater than two. Another sub-band related to the antisymmetric OH stretch, ν_a(CO–H) vibration, of glycerol dimers is achieved at 3440 cm^{-1}, when the spectra is acquired until 3700 cm^{-1}. The spectral region between 2600-3040 cm^{-1} is decomposed into three visible peaks at 2940, 2890 and 2756 cm^{-1} assigned to the antisymmetric CH stretch from CH_2 ($\nu_a(CH_2)$), the symmetric CH stretch from CH_2 $\nu_s(CH_2)$, and the (CH) stretch mode from C-2 in the glycerol molecule, respectively [163, 164]. Both the 2940 and 2890 cm^{-1} peaks are arising from C-1, which is equivalent to C-3.

In the 900–1500 cm^{-1} spectral region are found the vibrational modes due to CCO, CH_2 and COH deformations of primary alcohols (-OH groups). The band at 1468 cm^{-1} is assigned to CH_2 deformation ($\sigma(CH_2)$) in glycerol, and the others bands at 1316 and 1258 cm^{-1} are related to the CH_2 twist ($\tau(CH_2)$) vibrations [164]. The band at 1362 cm^{-1} is due to COH deformation (σ(COH)) and it is very broad due to the extensive hydrogen-bonding within glycerol from both C1–OH and C2–OH environments [163]. The bands at 1114 and 1056 cm^{-1} are assigned to the C–OH stretch of C-2 (ν_s(C-OH)), and ν_s(C–OH) vibrations of C-1 and C-3 atoms, respectively. Two non-polarized Raman bands are also seen at 978 and 926 cm^{-1}, suggesting the rocking CH_2 vibration in glycerol.

At 852 cm^{-1} is shown a strongly polarized peak assigned to a C-C stretching vibration in glycerol and next to it, another peak at 822 cm^{-1} with similar characteristics and behavior. However, the significant decrease in the intensity of the peak could suggest that the 852 and 822 cm^{-1} vibrations in glycerol are related to C-C symmetric stretches arising from C-1 and C-2, respectively. The peak at 676 cm^{-1}, is only slightly polarized and its assignment remains controversial due to the different meaning in different works [165-167].

The Raman peak listed at 550 cm^{-1} is not polarized and is assigned to a CCC bending vibration in glycerol, as it is located in the spectral range where CCC and CCO

deformation modes are found [164]. Finally, the bands showed at 486 and 418 cm^{-1} are attributed to CCO rock vibrations [164, 166].

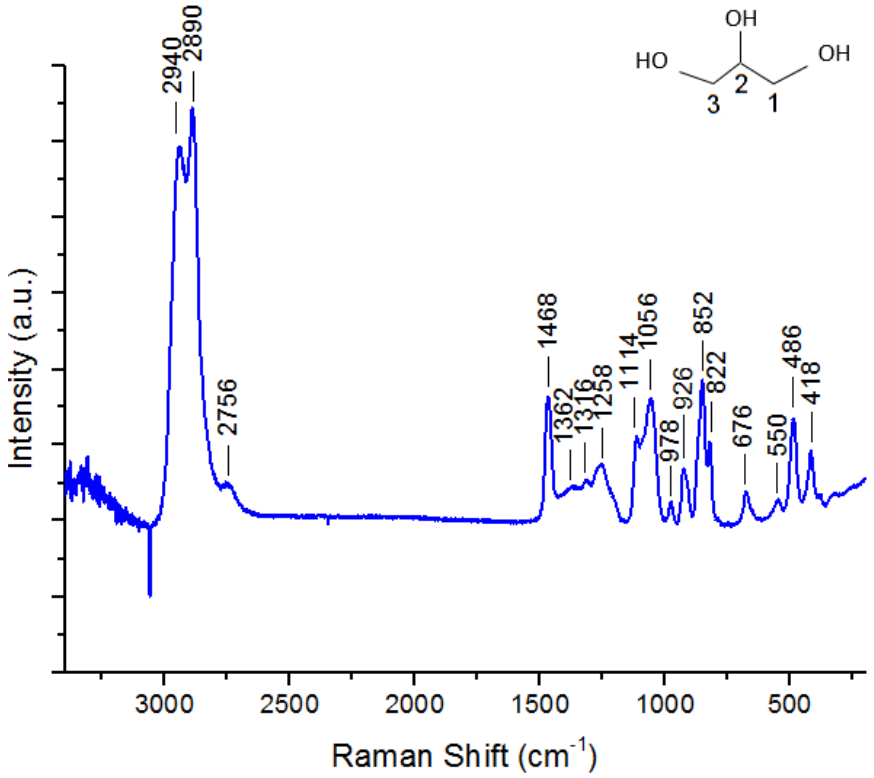

Figure 4.1: Raman spectra between 3400 and 200 cm^{-1} of glycerol molecule.

The Raman spectrum of acetone (Figure 4.2) shows a high-intensity polarized peak at 2924 cm^{-1} assigned to a CH_3 symmetric stretch and two peaks, at 3008 and 2066 cm^{-1}, assigned to d-stretching modes of CH_3 [168, 169]. AT 1710 cm^{-1}, it is found other polarized peak that represents C=O stretch [169]. The peaks at 1432 and 1358 cm^{-1} represent the CH_3 d-deformation and CH_3 s-deformation, respectively [168]. The designation "d-stretching", "d-deformation", and "d-derformation" is because none of the normal vibrations are genuinely "symmetrical" or "degenerate" in respect to the three-fold symmetric axis of CH_3 group. At 1222 cm^{-1} (depolarized peak) is assigned to C–C asymmetric stretch and at 1068 (polarized) and 904 cm^{-1} (depolarized) is suggested to be the rocking CH_3 vibration in acetone [168, 169]. A very strong polarized peak is achieved at 788 cm^{-1}, which represents a C–C symmetric stretch [169]. The subsequent Raman peaks listed at 532, 492 and 394 cm^{-1} are all not polarized and are assigned to C=O in-plane bend, C=O out-of-plan bend and C-C-C deformation, respectively [168].

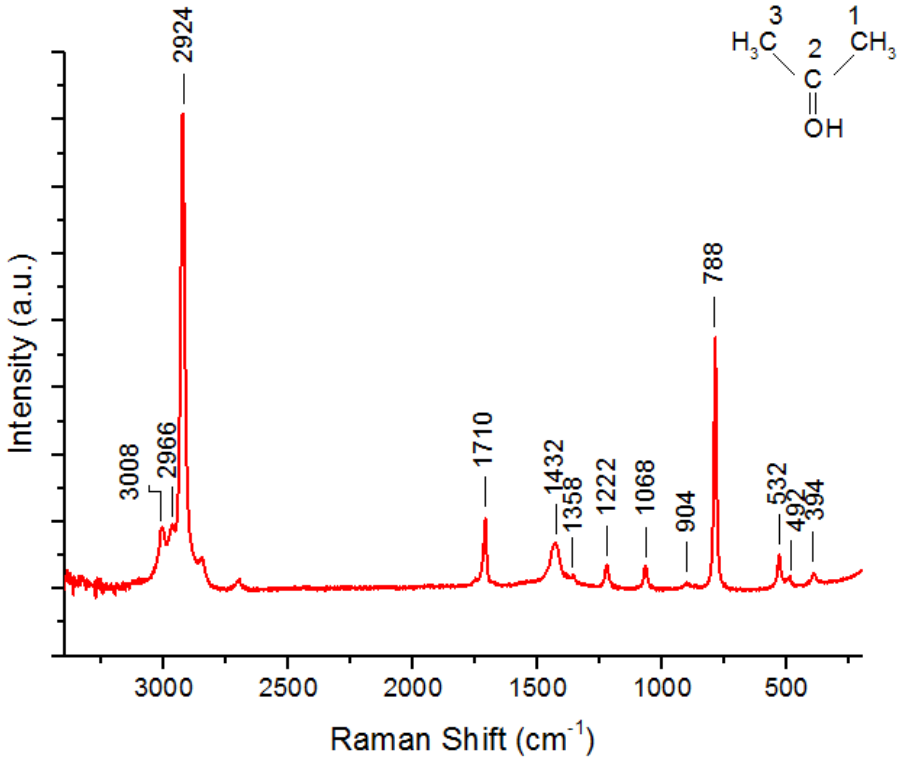

Figure 4.2: Raman spectra between 3400 and 200 cm^{-1} of acetone molecule.

The reaction between these two compounds was previous study by Calvino-Garcia et al. at 80 ºC [46], in the absence of catalyst using an excess of acetone, since this reaction temperature cause acetone evaporation, reversing the *solketal* formation (Figure 4.3). In addition the Raman bands characteristic of each reactant, the authors found a new Raman band at 732 cm^{-1} after 30 min reaction time, which was associated to strong interactions between glycerol and acetone molecules (G-A). This new band is assigned to O···C=O vibrations due to the interaction between the primary hydroxyl group of the glycerol molecule and the carbonyl group of the acetone molecule. However, this initial interaction between reactants hardly delivered any reaction, only affording 13 % conversion and 96 % selectivity of *solketal* after 30 min of reaction. The *solketal* bands became apparent at 650, 638 and 604 cm^{-1}.

During the blank reaction, Raman spectra also showed strong interactions between glycerol molecules (G-G) at 3324 cm^{-1}, revealing the self-association of glycerol molecules through intermolecular hydrogen bonds to form dimeric, trimeric and oligomeric structures. These O-H interactions in the G-G interactions are temperature dependent and because of that, may be not enough to produce *solketal* depending on the temperature studied [46, 162].

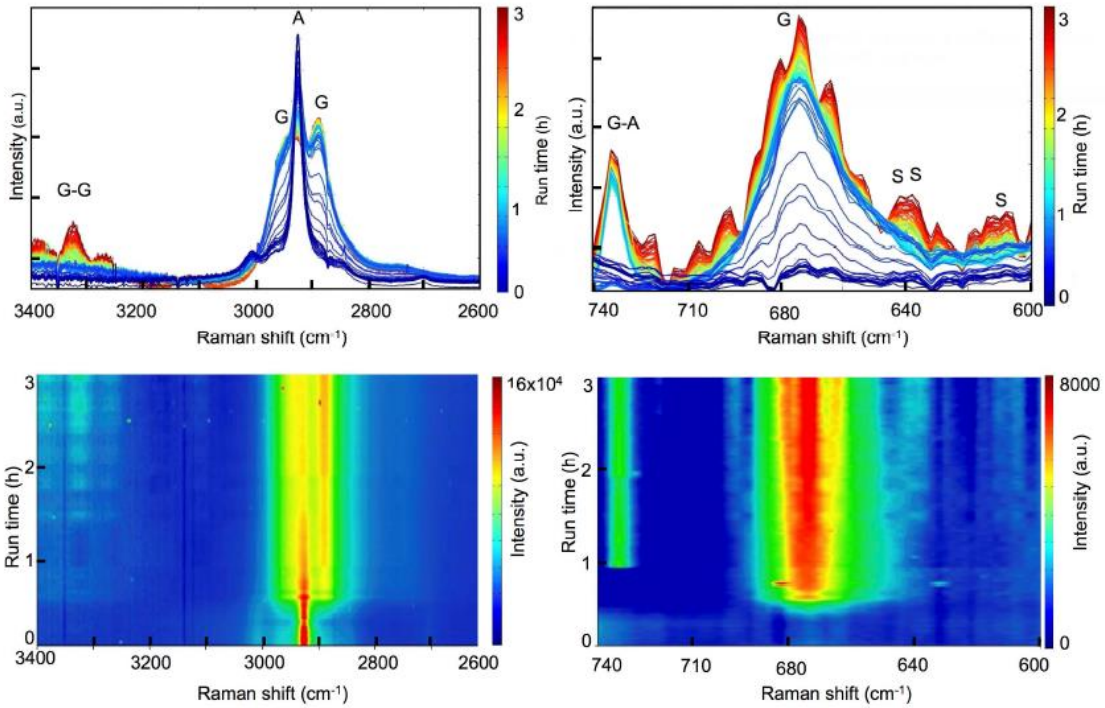

Figure 4.3: Raman monitoring of the reaction between glycerol and acetone under continuous stirring at 80 ºC for 3 hours without catalyst (40 mmol of glycerol, 80 mmol of acetone). G- glycerol, A- acetone, G-A- glycerol-acetone interaction, G-G- glycerol-glycerol interaction, S- *solketal*. (3400 cm^{-1} G-G / 2946 and 2886 cm^{-1} G / 788 cm^{-1} A / 732 cm^{-1} G-A / 676 cm^{-1} G / 650, 638, 604 cm^{-1} S) [46].

High temperatures would be favorable to increase glycerol conversion and *solketal* production, but the reaction only will progress normally until the presence of acetone remains enough. In another way, acetone evaporation will create a reactant deficit and the reaction will not progress any longer. As Calvino-Garcia et al. [46] had problems with acetone evaporation when tested the reaction in the presence of MP-NbMCF catalysts at 80 ºC, causing reaction reversion after few time of start the reaction, we choose decrease the reaction temperature to 70 ºC with our catalysts.

4.1.1. Influence of the temperature in the acetalization of glycerol with acetone

Effects of temperature on acetalization of glycerol were studied under continuous stirring at 70 ºC, 40 ºC and room temperature with acetone/glycerol = 2:1 and the weight of the catalyst was 2 wt.%, based on the amount of glycerol used in this reaction. All parent zeolites and the catalysts prepared with Nb were continuously monitored by Raman

spectroscopy. In consequence of this study, the heterogeneous catalysts which have presented the best catalytic results were analyzed by GC analysis.

4.1.1.1. Acetalization of glycerol with acetone at 70 ºC

The parent zeolite and the modified Nb_x-NaY catalysts do not show any activity for the reaction at long time. Figure 4.4 illustrates the representative Raman spectra acquired every 30 min at 70 ºC for Nb_{15}-NaY, as an example, and the relationships between the intensity of the *solketal* signal, conversion of glycerol and time of the reaction is shown, respectively.

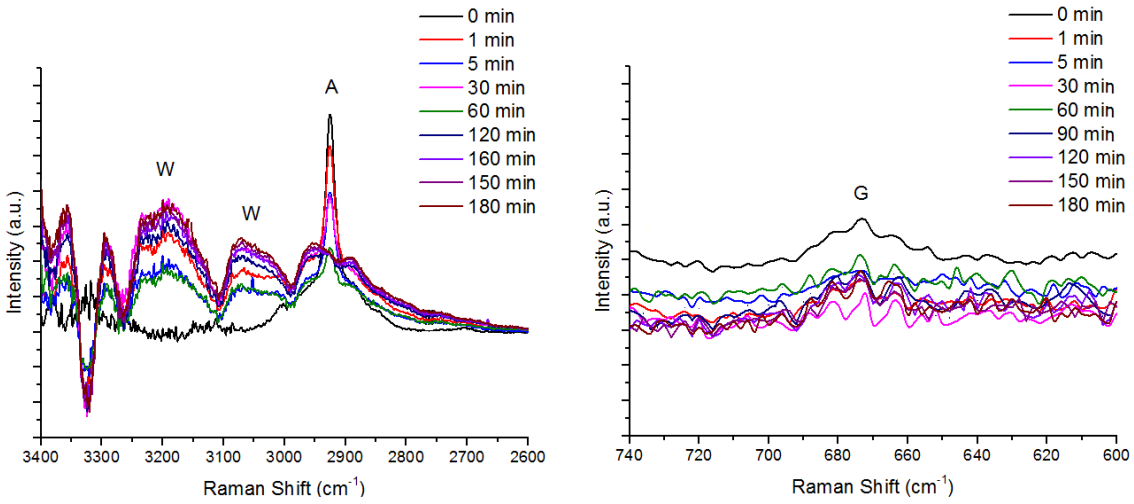

Figure 4.4: Raman monitoring of the reaction between glycerol and acetone under continuous stirring at 70 ºC for 180 min (3 h) with catalyst Nb_{15}-NaY.

The background Raman spectra of the reaction show the characteristic Raman bands of the two reactants used, acetone and glycerol. After addition of Nb_{15}-NaY catalyst, the reaction between glycerol and acetone didn't occur. No characteristic bands of G-G and G-A interactions become apparent at 3325 cm^{-1} or 732 cm^{-1}, respectively. In addition, the intensity of the characteristic Raman bands of glycerol and acetone decreased at long time. Nb_{15}-NaY catalyst is not active for this reaction. Similar behavior was observed for the parent zeolite. The presence of high amount of water in the reaction medium provokes the deactivation of the acid sites of the zeolite NaY due to their hydrophilic character [3]. Even with the presence of niobium which decreases the microporosity of NaY (Table 3.1), the modified heterogeneous catalysts do not present catalytic activity for this reaction. The

Raman bands of *solketal* at 638 and 648 cm^{-1} also do not appears for the others Nb_x-NaY catalysts.

Similar behaviour was observed for HY and the modified Nb_x-HY catalysts. Figure 4.5 shows the Raman spectrum of Nb_{15}-HY obtained at 70 ºC during 180 min, as an example.

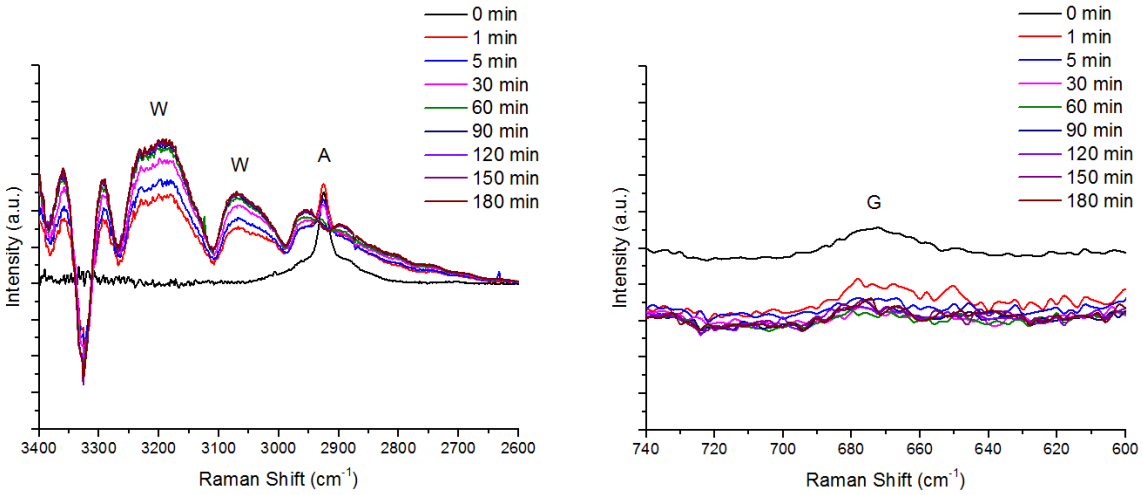

Figure 4.5: Raman monitoring of the reaction between glycerol and acetone under continuous stirring at 70 ºC for 3 h with catalyst Nb_{15}-HY.

From these results, the parent HY zeolite and the Nb_x-HY catalysts were not active in this reaction. In all Raman spectrum from NaY and HY the water is observed in the region of 3300-3000 cm^{-1}.

As water is the side-product of this reaction, the hydrophilicity of the catalysts should be taken into account. NaY, HY has high affinity with water (Table 3.8). The effect of the water was studied by Pescarmona [37] with modified TUD-1 and MCM-41 materials. These authors suggested that the deactivation of the catalysts during the acetalization of glycerol with acetone is provoked by reaction residues deposited on the active sites rather than by the water absorbed on the porous structure of the catalysts. However, they observed that the catalysts which present aluminium (Al-TUD-1 and USY), the water formed during the reaction favored the hydrolysis of *solketal*, i.e. the reverse reaction [12]. In the case of zeolites as NaY and HY with higher amount of aluminium the water affect the activity in this reaction [3]. Additional, the smaller size of the micropores of zeolite NaY and HY and subsequent impregnation by niobium (Table 3.1) limit the diffusion of reagents and products and, thus, negatively affect its catalytic activity.

Conversely, the modified catalysts based on HUSY and HZSM5 are active in the reaction. Both parent zeolites are active and the impregnation of niobium in these zeolites enhances their catalytic properties for the glycerol acetalization. Figure 4.6 shows the Raman monitoring of the HUSY (A) and Nb_{15}-HUSY (B) catalysts. Raman spectra show that these catalysts promote the reaction between glycerol and acetone.

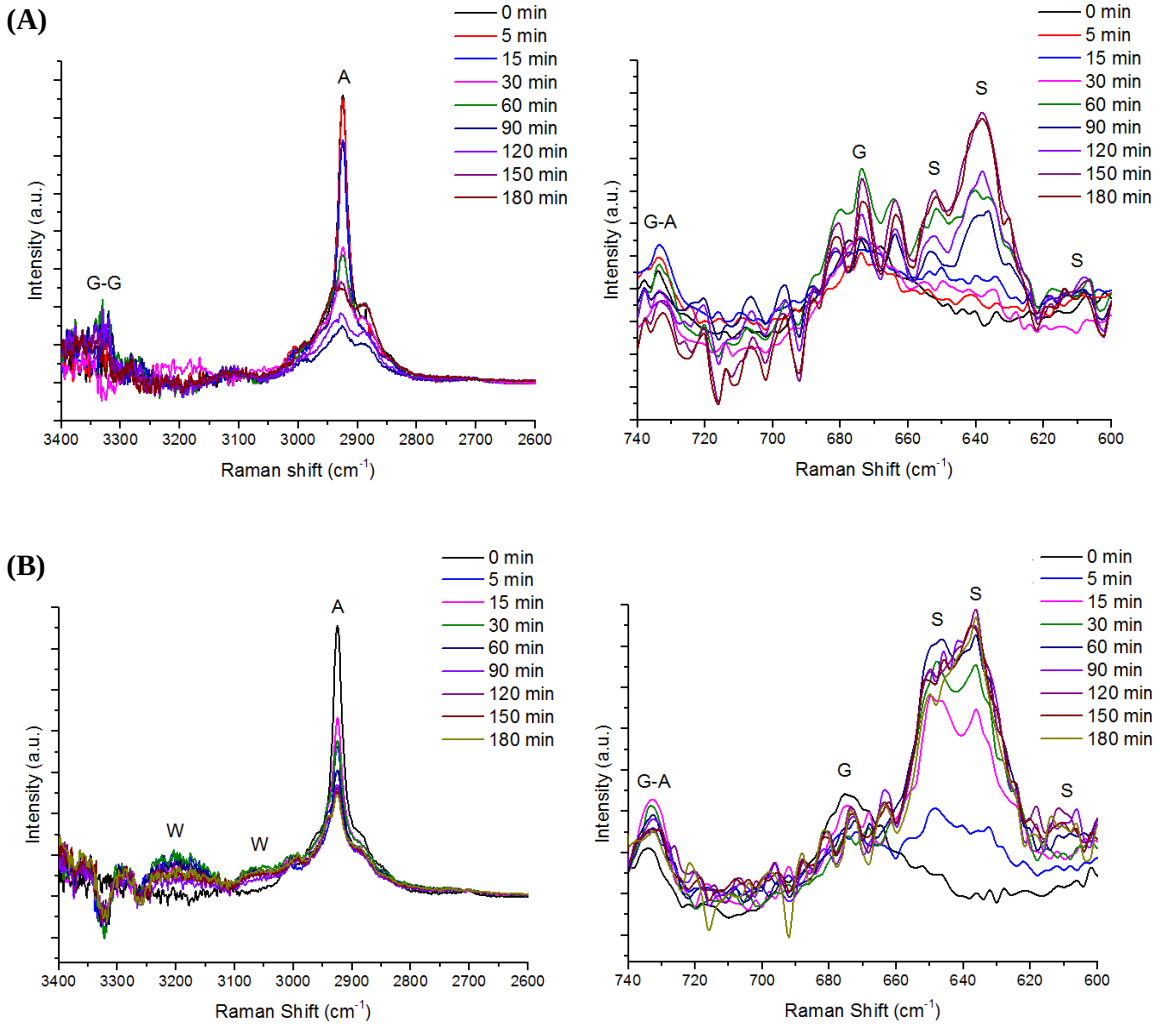

Figure 4.6: Raman monitoring of the reaction between glycerol and acetone under continuous stirring at 70 ºC for 180 min (3 h) with HUSY (A) and Nb_{15}-HUSY (B) catalysts. G- glycerol, G-A- glycerol-acetone interaction, G-G- glycerol-glycerol interaction, S- *solketal.*

In addition to the characteristic Raman bands of reactants, new bands are apparent at 2992, 1462, 1440, 1120, 1070, 1056, 970, 920, 850, 792, 648, 638, 482, 418, 348 and 316 cm^{-1}, which corresponds to the reaction product *solketal* [46]. However, the Raman band at 3324 cm^{-1}, characteristic of G-G interaction, appeared in both reactions, but for Nb_{15}-HUSY the negative intensity was indicating the inexistence of G-G interaction during

the reaction, although the formation of *solketal* becomes apparent from the first few minutes of reaction. So, we conclude that glycerol-glycerol interaction was not critical for the *solketal* production.

The Raman band related to G-A interaction appears at 732 cm^{-1} as soon as the catalyst is added and are related to the *solketal* formation, showing a similar trend for both catalysts. The *solketal* Raman bands at 638 and 648 cm^{-1} form readily due to significant amount of mesoporous with a radius larger than 50 Å in HUSY which permit the access of acid sites of the catalyst. The formation of *solketal* was improved in the presence of Nb_{15}-HUSY. Figure 4.7 shows the concentration profile of Raman bands characteristics of the reactants acetone, glycerol and the *solketal* product for both catalysts.

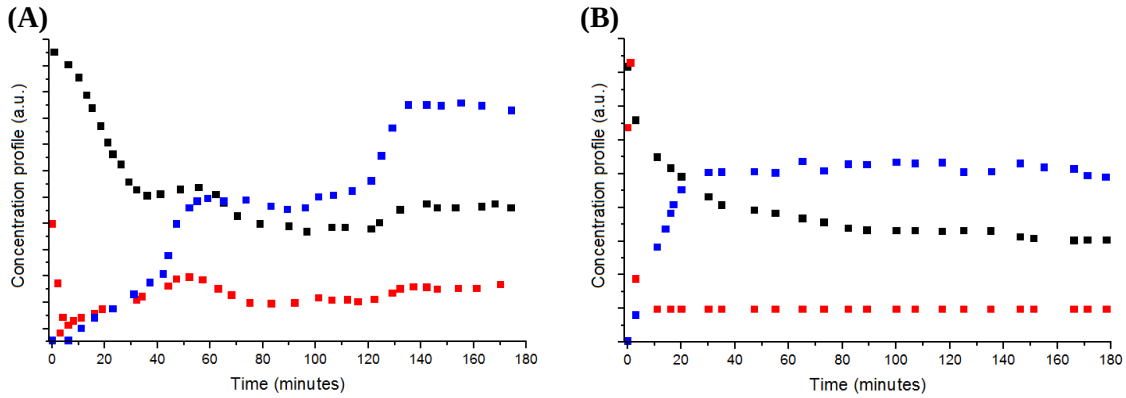

Figure 4.7: Concentration profile of reactant acetone and the product *solketal* versus time for the acetalization of glycerol at 70ºC for 180 min over HUSY (A) and Nb_{15}-HUSY (B) catalysts. ■Acetone, ■Glycerol and ■*Solketal*.

Figure 4.7 shows that the glycerol concentration decreases noticeably in the first minutes of the reaction followed by the decrease of the acetone due to the G-A interactions. The *solketal* Raman bands reach a maximum at 140 min for the parent zeolite and 30 min for the Nb_{15}-HUSY of reaction and keep constant during the reaction. Similar behavior was observed for the reactants.

Figure 4.8 shows the Raman monitoring of the HZSM5 (A) and Nb_{15}-HZSM5 (B) catalysts.

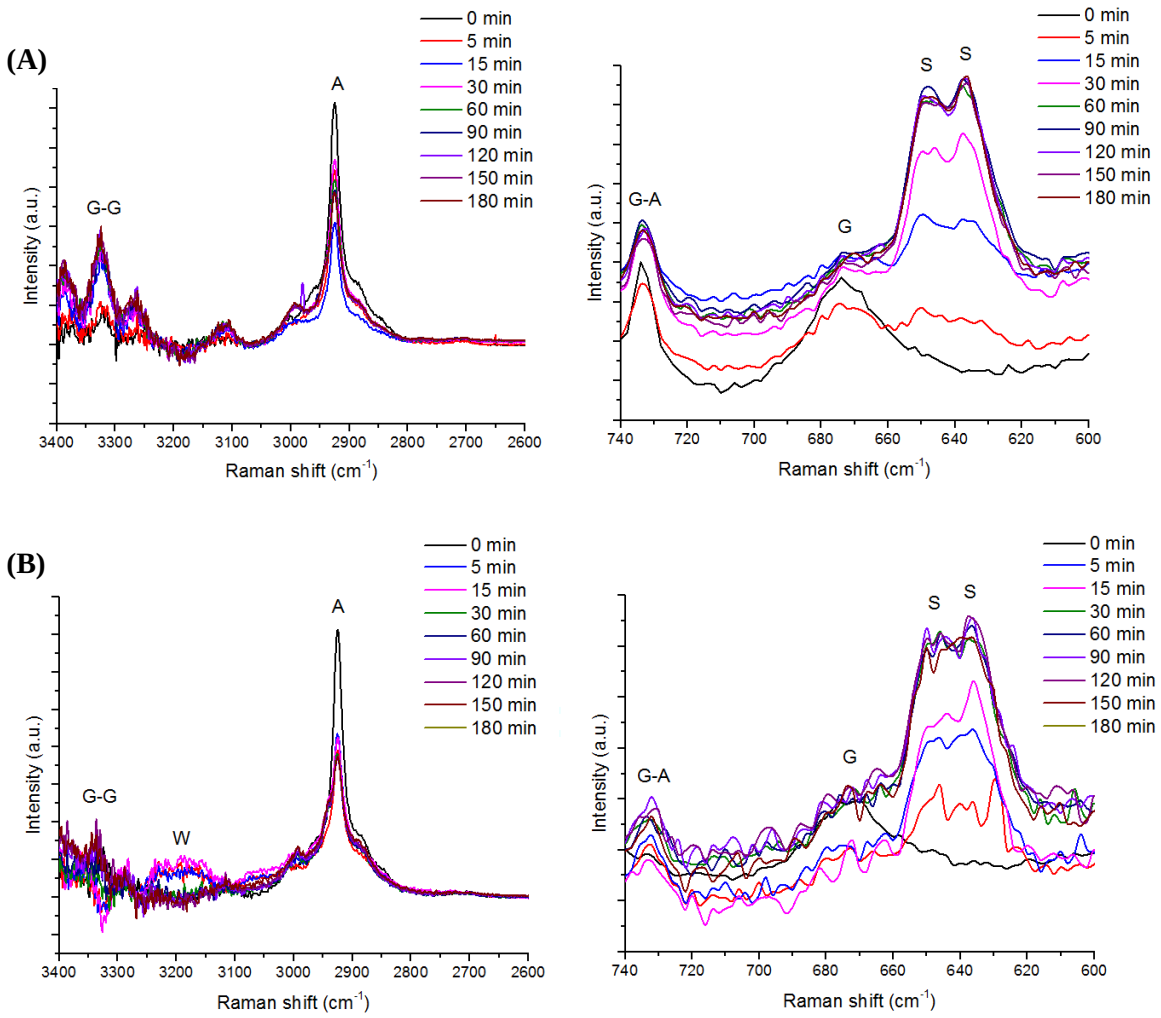

Figure 4.8: Raman monitoring of the reaction between glycerol and acetone under continuous stirring at 70 ºC for 180 min (3 h) with HZSM5 (A) and Nb_{15}-HZSM5 (B) catalysts. G-glycerol, G-A- glycerol-acetone interaction, G-G- glycerol-glycerol interaction, S- *solketal.*

Similar Raman spectrum was observed for HZSM5 and Nb_{15}-HZSM5 with the intensity bands more pronounced. Figure 4.9 displays the concentration profile of Raman bands characteristics of the reactants acetone, glycerol and the *solketal* product obtained for HZSM5 (A) and Nb_{15}-HZSM5 (B) catalysts.

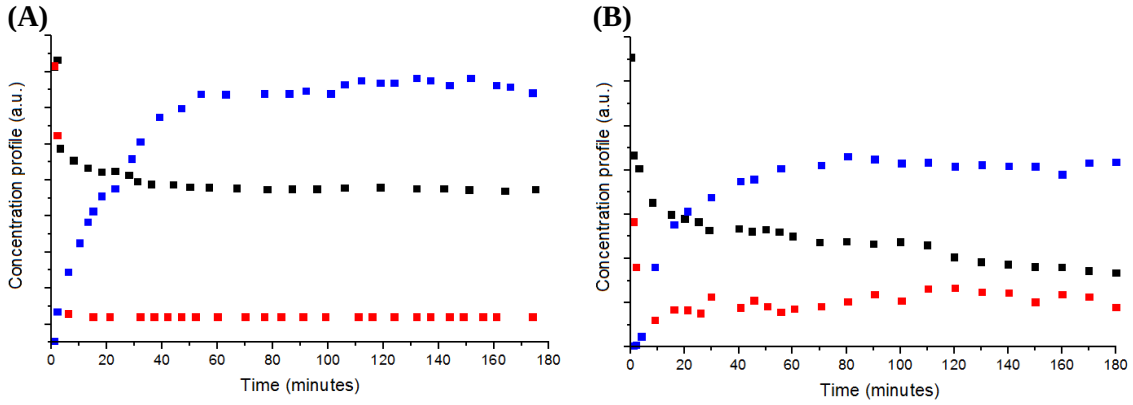

Figure 4.9: Concentration profile of reactant acetone, glycerol and the product *solketal* versus time for the acetalization of glycerol at 70ºC for 180 min over HZSM5 (A) and Nb_{15}-HZSM5 (B) catalysts. ■ Acetone, ■ Glycerol and ■ *Solketal*.

HZSM5 and Nb_{15}-HZSM5 catalysts presents similar plots as HUSY and Nb_{15}-HUSY. Both reactants decrease in the first minutes of the reaction due to the G-A interactions. However, the stabilization of the *solketal* Raman bands was achieved around 40 min of reaction and keep constant during the reaction. The plots of the reactants show that the amount of G and A stabilize after c.a. 40 min.

The behavior observed to the concentration profile of Raman bands characteristics of the reactants acetone, glycerol and the *solketal* product for the parent zeolites, Nb_{15}-HUSY and Nb_{15}-HZSM5, indicating that the reaction is approaching equilibrium conditions. These results showed good reaction efficiency for selectivity *solketal* formation and the reverse reaction is minimized.

Gas chromatography analysis confirms that the conversion of glycerol and the *solketal* formation were achieved only in the presence of HUSY and HZSM5 and the modified Nb_x-HUSY/HZSM5 catalysts. Table 4.1 summarizes the GC results obtained for the parent zeolites and the modified heterogeneous catalysts at 70 ºC for 30 min and 180 min of reaction.

Notably, all modified catalysts give higher conversion of glycerol to *solketal* than the parent zeolites. The presence of niobium on HUSY and HZSM5 played an important role for being responsible of the significant increase in the glycerol conversion.

All Nb_x-HUSY catalysts showed a similar behavior for the glycerol conversion with ~ 60 % and 98 % of selectivity. In the case of HZSM5, the maximum of the conversion at different reaction time was obtained for the catalyst with higher amount of niobium. For Nb_{15}-HZSM5, the conversion of the reaction reaches a maximum of 65 % (98

% selectivity) at 30 min and increase for 74 % (98 % selectivity) at 180 min, suggesting that HZSM5 are dependent of the concentration of Nb used for the impregnation. The hydrophobic character of this zeolite favors the higher conversion of glycerol to *solketal.*

Table 4.1: GC results obtained for the parent HUSY and HZSM5 and all modified Nb_x-HUSY/HSZM5 catalysts at 70 ºC for 30 and 180 min.

Catalyst	Conversion (%)		Selectivity (%)		Yield (%)	
Time (min)	**30**	**180**	**30**	**180**	**30**	**180**
HUSY	-	29	-	97	-	28
Nb_5-HUSY	64	60	98	98	63	59
Nb_{10}-HUSY	60	65	98	98	59	64
Nb_{15}-HUSY	60	58	98	98	59	57
HZSM5	-	25[a]	-	97	-	24
Nb_5-HZSM5	44	55	95	98	42	54
Nb_{10}-HZSM5	55	59	98	98	54	58
Nb_{15}-HZSM5	65	74	98	98	64	73

[a]Conversion of glycerol obtained from reference [3].

The same behavior observed for glycerol conversion for all modified catalysts suggest that the reaction achieve the thermodynamic equilibrium in agreement of Raman analysis.

4.1.1.2. Acetalization of glycerol with acetone at 40 ºC

On behalf of this temperature both parent zeolites, HUSY and HZSM5 do not show any conversion of glycerol. Remarkably, the modified heterogeneous catalysts are active and selective for the reaction. Figure 4.10 shows the Raman spectra of the reaction between glycerol and acetone at 40 ºC for 240 min (4 h) with the selected modified heterogeneous catalysts. In this case, the reaction was followed during 240 min (4 h) due to the acetone. Calvino-Garcia et al. [46] observed that the intensity of acetone Raman band only decrease at 40 ºC after long reaction time.

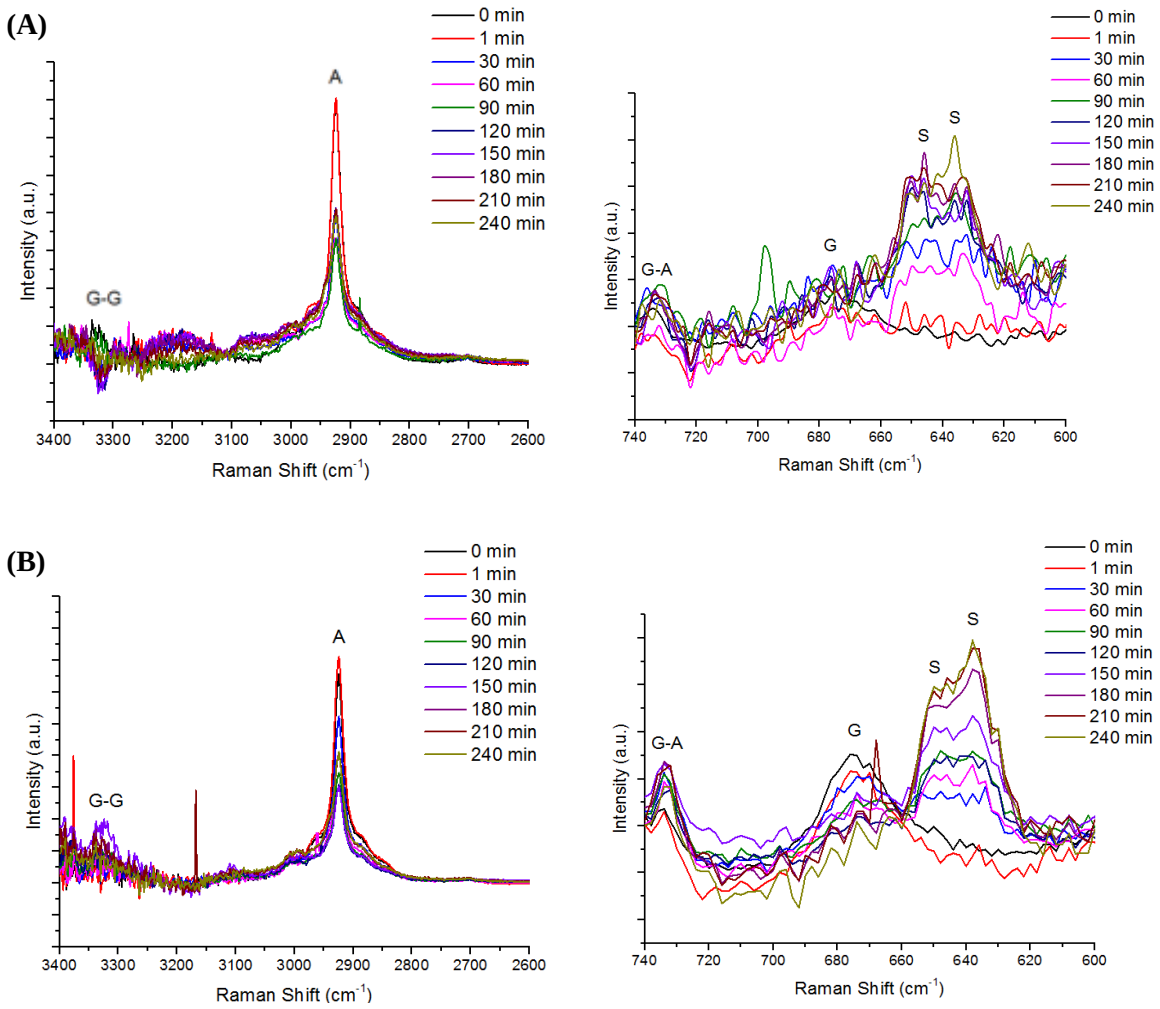

Figure 4.10: Raman monitoring of the reaction between glycerol and acetone under continuous stirring at 40 ºC for 240 min (4 h) with Nb_{15}-HUSY (A) and Nb_{15}-HZSM5 (B) catalysts. G- glycerol, G-A- glycerol-acetone interaction, G-G- glycerol-glycerol interaction, S- *solketal*.

In both modified heterogeneous catalysts with 15 % of niobium, the Raman bands of reactants, acetone and glycerol, and the *solketal* product are apparent. The intensity of the *solketal* Raman bands are more pronounced for Nb_{15}-HZSM5, suggesting this catalyst beneficiate the production of the five-membered-ring product. A decrease on temperature reaction led to some G-G interaction. As expected, the intensity Raman bands of acetone decrease after long reaction time, which confirms a minimized volatilization of acetone. Glycerol-acetone interaction showed, once more, a similar behavior to *solketal* formation, growing fast at first minutes of reaction and then at a slower rate. Figure 4.11 shows the concentration profile of Raman bands characteristic of the reactants acetone, glycerol and the *solketal* product for both catalysts with 15 % of niobium at 40 ºC.

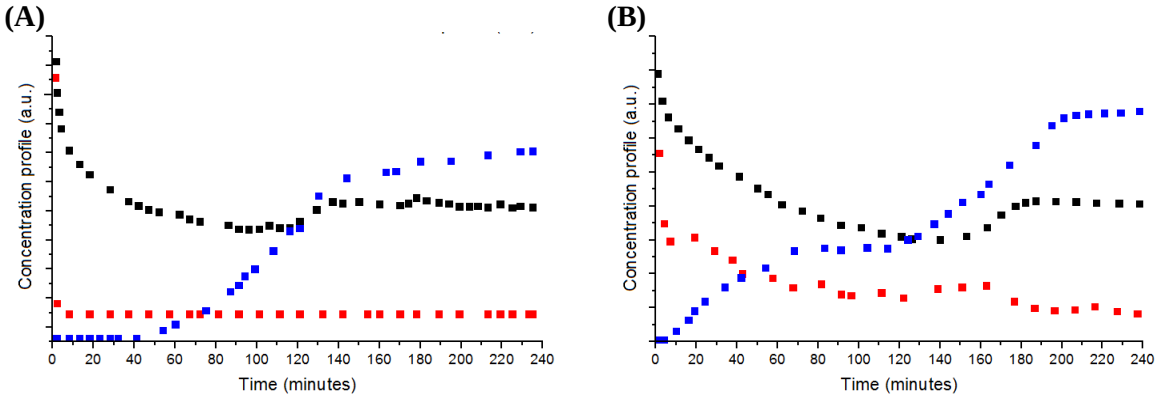

Figure 4.11: Concentration profile of reactant acetone, glycerol and the product *solketal* versus time for the acetalization of glycerol at 40 ºC for 240 min over Nb_{15}-HUSY (A) and Nb_{15}-HZSM5 (B) catalysts. ■ Acetone, ■ Glycerol and ■ *Solketal*.

The concentration profile of reactants and the product are similar to those observed for the modified catalysts at 70 ºC (Figure 4.9). Both reactants decrease in the first minutes of the reaction due to the G-A interactions and their plots stabilize after c.a. 20 min. However, the *solketal* product increase with the time and their stabilization was achieved later after 100 min of reaction. Gas chromatography analysis confirms that the conversion of glycerol and the *solketal* formation were achieved only in the presence of the modified Nb_x-HUSY/HZSM5 catalysts. Table 4.2 summarizes the GC results obtained for the modified heterogeneous catalysts at 40 ºC for 240 min of reaction.

Table 4.2: GC results obtained for the parent HUSY and HZSM5 and all modified Nb_x-HUSY/HSZM5 catalysts at 40 ºC for 240 min (4 h).

Catalyst	X (%)	S (%)	Y (%)
HUSY	< 5	97	5
Nb_5-HUSY	66	98	65
Nb_{10}-HUSY	65	98	64
Nb_{15}-HUSY	61	98	60
HZSM5	< 5	97	5
Nb_5-HZSM5	51	97	50
Nb_{10}-HZSM5	62	98	61
Nb_{15}-HZSM5	63	98	62

X (%) = conversion of glycerol; S (%) = *solketal* selectivity; Y (%) = *solketal* yield

Once again, the modified catalysts give higher conversion of glycerol to *solketal* than the parent zeolites. The modified Nb_x-HZSM5 shows the same trend as observed at 70 ºC, with the best results with higher amount of Nb (15 %). The conversion of glycerol was improved with the increase of niobium. For HUSY, the conversion of glycerol was slight decrease by the increase of Nb. Also, for lower temperature the conversion of glycerol reach the thermodynamic equilibrium, as we can see in Figure 4.11. Figure 4.12 compares the conversion of glycerol obtained at 70 ºC and 40 ºC in the presence of the modified catalysts, at the end of each reaction.

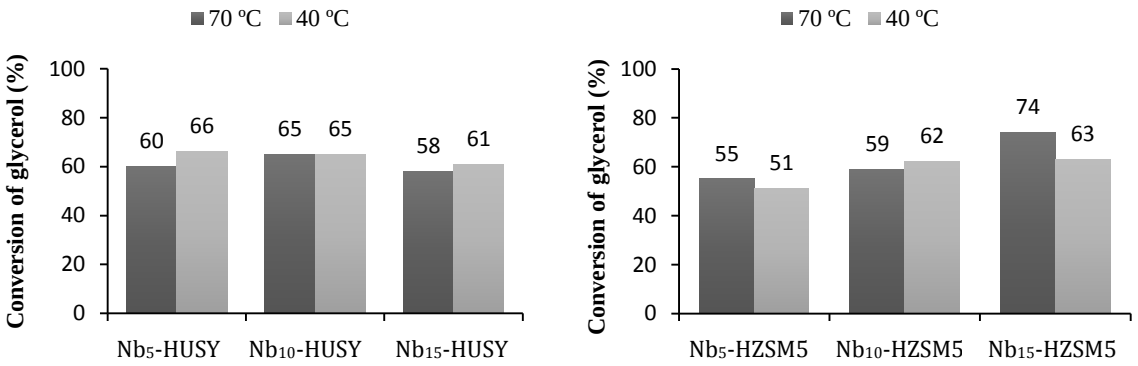

Figure 4.12: Catalytic conversion of glycerol with acetone with different modified catalysts at 70 and 40 ºC, at the end of each reaction.

In the case of Nb_x-HUSY, different amounts of Nb impregnated enhance the same conversion of glycerol to *solketal* in both temperatures studied. Again, for these conditions the modified catalyst with 10 % of Nb achieved the best results. For Nb_x-HZSM5 the increase of Nb improve higher conversion of glycerol with a maximum obtained 74 % at 70 ºC. From these results, even in moderate temperature, the reaction achieved the thermodynamic equilibrium in terms of *solketal* yield (60-65 %), in agreement of Raman analysis [2]. In summary, highly efficient conversion of glycerol to *solketal* over the Nb_x-HUSY/HZSM5 catalysts could be achieved with 10 % of Nb and 40 ºC, showing that our catalysts can be used in moderate temperatures.

4.1.1.3. Acetalization of Glycerol with Acetone at room temperature

During the reaction between glycerol and acetone at room temperature for 6 h, only the Raman bands of reactants, acetone and glycerol are clearly detectable. Both, Raman

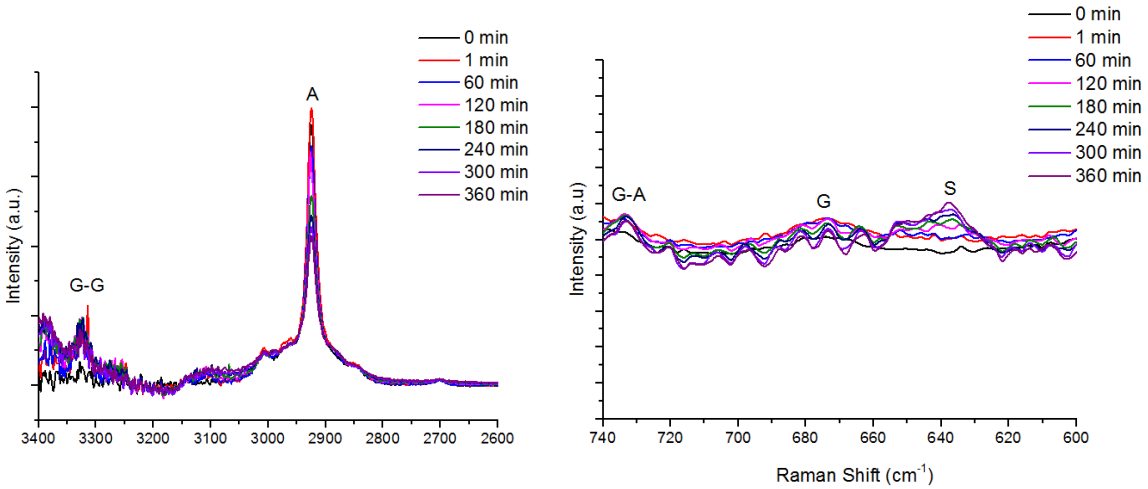

Figure 4.13: Raman monitoring of the reaction between glycerol and acetone under continuous stirring at room temperature for 360 min (6 h) with Nb_{15}-HZSM5 as catalyst. G- glycerol, G-A- glycerol-acetone interaction, G-G- glycerol-glycerol interaction, S- *solketal*.

spectroscopy and gas chromatography show that the parent zeolites and the modified Nb_x-HUSY and Nb_x-HZSM5 catalysts are not active at these conditions. Figure 4.13 shows the Raman spectra obtained for Nb_{15}-HZSM5 catalyst, which showed only 2 % of conversion at the end of 6 h of reaction with 97 % of selectivity. The interactions between glycerol-glycerol and glycerol-acetone created are not sufficient to trigger the reaction.

4.1.2. Effect of the amount of the catalyst

The effects of catalyst addition amount on glycerol conversion were studied by varying the amount of catalyst from 1 to 5 % in relation to glycerol at 70 ºC and acetone/glycerol = 2:1 over the parent HUSY and HZSM5 zeolites and the modified Nb_x-HUSY and Nb_x-HZSM5 catalysts. Table 4.3 summarizes the GC results obtained for all catalysts.

Table 4.3: GC results obtained for the parent HUSY and HZSM5 and all modified Nb_x-HUSY/HSZM5 catalysts at 70 ºC for 180 min.

Amount of catalyst (wt %)	**1**			**2**			**5**		
Catalyst	**X (%)**	**S (%)**	**Y (%)**	**X (%)**	**S (%)**	**Y (%)**	**X (%)**	**S (%)**	**Y(%)**
HUSY	-	-	-	29	98	28	-	-	-
Nb_5-HUSY	57	98	56	60	98	59	62	98	61
Nb_{10}-HUSY	58	98	57	65	98	64	57	98	56
Nb_{15}-HUSY	51	98	50	58	98	57	55	98	54
HZSM5	-	-	-	25[a]	97	24	-	-	-
Nb_5-HZSM5	63	98	62	55	98	54	56	98	55
Nb_{10}-HZSM5	64	98	63	59	98	58	55	98	54
Nb_{15}-HZSM5	67	98	66	74	98	73	50	98	49

X (%) = conversion of glycerol; S (%) = *solketal* selectivity; Y (%) = *solketal* yield
[a]from the reference [3]

Figure 4.14 compares the effect of the amount of catalyst in the conversion of glycerol obtained at 70 ºC at the end of 3 h.

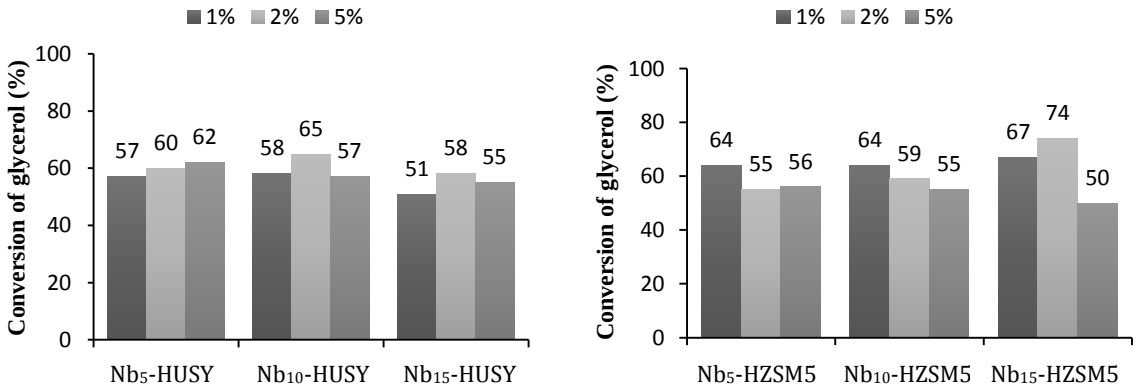

Figure 4.14: Catalytic conversion of glycerol with acetone with different amount of modified catalysts at 70 ºC at the end of 3 h.

The results present in Table 4.3 and Figure 4.14 show that the best results in glycerol conversion to *solketal* was achieved with 2 % of catalyst. Once again, these results indicate that the addition amount of catalyst from 1 % to 5 % does not change the thermodynamic equilibrium in terms of *solketal* yield (60-65 %) [2].

In summary, on the basis of the characterization of our catalysts we can conclude that the acetalization of acetone with glycerol to yield *solketal* can be efficiently catalyzed even with moderate temperature (40 ºC) by the Nb_x-HUSY/HZSM5. The final catalytic activity does not depend only on the amount of acid sites: wide pores and high surface area help optimizing the diffusion of reagents and products and the contact with the active sites, while a relatively hydrophobic surface in the case of HZSM5 favors removal of water, minimizing the hydrolysis of the formed *solketal*. The modified Nb_x-HUSY/HZSM5 catalysts present the most suitable balance of all these parameters, leading to the best catalytic performance in the conversion of glycerol to *solketal*.

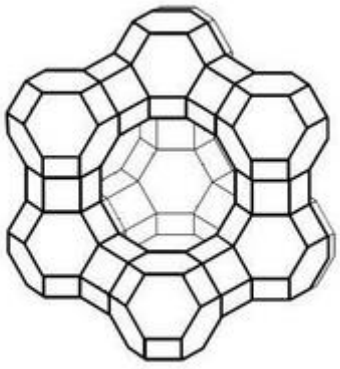

CHAPTER V– CONCLUSIONS

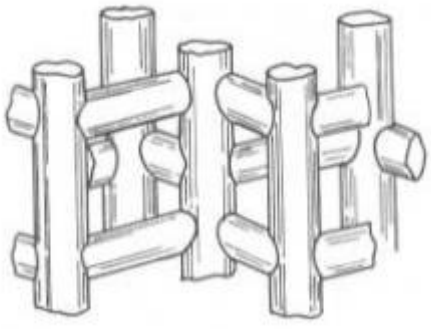

CHAPTER V – CONCLUSION

A series of niobium-containing zeolites were prepared by impregnation method and evaluated in the acetalization of glycerol with acetone to produce five-membered ring ketal (2,2-dimethyl-1,3-dioxolane-4-methanol, *solketal*). The experimental parameters, type of catalyst, effect of the temperature and amount of catalyst used, were tested during the catalytic experiments. A real-time control of the reaction was made by Raman spectroscopy and the conversion results confirmed by Gas chromatography analysis.

The characterization results show that the impregnation method used to prepare the heterogeneous catalysts (Nb_x-NaY, Nb_x-HY, Nb_x-HUSY and Nb_x-HZSM5, where x represents 5, 10 or 15 wt% of Nb_2O_5) practically didn't affect the structure of the respective parent zeolites. However, as expected, a significant decrease of specific surface area was observed while the external surface increases after the impregnation of niobium on zeolites.

The heterogeneous Nb_x-NaY and Nb_x-HY catalysts and the parent zeolites, NaY and HY, do not show any activity for the reaction at long time at 70 ºC. No characteristic bands of G-G and G-A interactions or *solketal* become apparent. In addition, the intensity of the characteristic Raman bands of glycerol and acetone decreased at long time, showing that the reagents are being consumed. However, as water is the side-product of this reaction, its high amount in the reaction medium provoked the deactivation of the acid sites of the zeolites NaY and HY due to their hydrophilic character.

At 70 ºC, the modified catalysts based on HUSY and HZSM5 demonstrated excellent catalytic activity with a maximum selectivity of 98 % towards *solketal.* Glycerol concentration decreases noticeably in the first minutes of the reaction followed by the decrease of the acetone due to the G-A interactions. The achieved conversion of the modified catalysts was superior to those obtained with the parent zeolites. The presence of niobium on HUSY and HZSM5 played an important role for being responsible of the significant increase in the glycerol conversion. All Nb_x-HUSY catalysts showed a similar behavior for the glycerol conversion with ~ 60 % and 98 % of selectivity. In the case of HZSM5, the maximum of the conversion at different reaction time was obtained for the catalyst with higher amount of niobium. For Nb_{15}-HZSM5, the conversion of the reaction reaches a maximum of 65 % (98 % selectivity) at 30 min and increase for 74 % (98 % selectivity) at 180 min, suggesting that HZSM5 are dependent of the concentration of Nb

used. The acidity, wide porous and a relatively hydrophobic character of these zeolites favor the higher conversion of glycerol to *solketal*.

At 40 ºC, the modified Nb_x-HZSM5 show the same trend as observed at 70 ºC, obtaining the best results with higher amount of Nb (15 %). The conversion of glycerol was improved with the increase of niobium. For HUSY, the conversion of glycerol was slight decrease by the increase of niobium. A highly efficient conversion of glycerol to *solketal* over the Nb_x-HUSY/HZSM5 catalysts could be achieved with 10 % of Nb at 40 ºC with 2 % of catalyst, showing that our catalysts can be used in moderate temperatures. The addition of 1 and 5 wt% of catalyst didn't change the thermodynamic equilibrium in terms of *solketal* yield (60-65 %).

When the reaction was carried out at room temperature, the interactions between glycerol-glycerol and glycerol-acetone created are not sufficient to trigger the reaction.

The results of this study show that the selected heterogeneous catalysts based in Nb_x-HUSY/HZSM5 can be used with highly efficient for the synthesis of valuable *solketal* from a renewable feedstock such as glycerol, thus opening new perspectives for sustainable utilization of this side-product of biodiesel production.

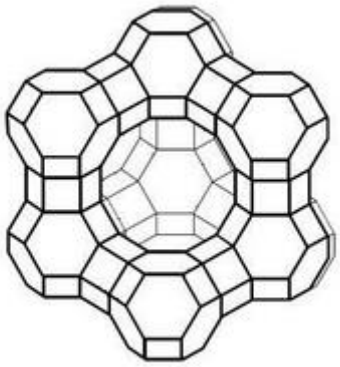

BIBLIOGRAPHY

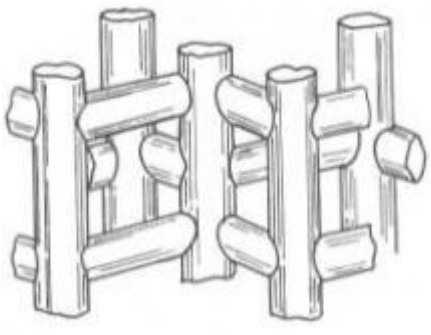

BIBLIOGRAPHY

1. Khan, M.M., et al., *Impacts of Biodiesel on the Environment.* International Journal of Environmental Engineering and Management 2013. 4(4):345-350.
2. Nanda, M.R., et al., *Thermodynamic and kinetic studies of a catalytic process to convert glycerol into solketal as an oxygenated fuel additive.* Fuel, 2014. 117, Part A(0):470-477.
3. da Silva, C.X.A., V.L.C. Goncalves, and C.J.A. Mota, *Water-tolerant zeolite catalyst for the acetalisation of glycerol.* Green Chemistry, 2009. 11(1):38-41.
4. Roldán, L., et al., *Glycerol upgrading by ketalization in a zeolite membrane reactor.* Asia-Pacific Journal of Chemical Engineering, 2009. 4(3):279-284.
5. Maksimov, A.L., et al., *Preparation of high-octane oxygenate fuel components from plant-derived polyols.* Petroleum Chemistry, 2011. 51(1):61-69.
6. Ferreira, P., et al., *Valorisation of glycerol by condensation with acetone over silica-included heteropolyacids.* Applied Catalysis B: Environmental, 2010. 98(1-2):94-99.
7. Vicente, G., et al., *Acetalization of bio-glycerol with acetone to produce solketal over sulfonic mesostructured silicas.* Green Chemistry, 2010. 12:899–907.
8. Deutsch, J., A. Martin, and H. Lieske, *Investigations on heterogeneously catalysed condensations of glycerol to cyclic acetals.* Journal of Catalysis, 2007. 245(2):428-435.
9. Royon, D., S. Locatelli, and E.E. Gonzo, *Ketalization of glycerol to solketal in supercritical acetone.* The Journal of Supercritical Fluids, 2011. 58(1):88-92.
10. Huynh, L.H., N.S. Kasim, and Y.H. Ju, *Biodiesel production from waste oils*. 2011. 375-396.
11. Knothe, G., *Dependence of biodiesel fuel properties on the structure of fatty acid alkyl esters.* Fuel Processing Technology, 2005. 86(10):1059-1070.
12. Demirbaş, A., *Biodegradability of Biodiesel and Petrodiesel Fuels.* Energy Sources, Part A: Recovery, Utilization, and Environmental Effects, 2008. 31(2):169-174.
13. Murillo, S., et al., *Performance and exhaust emissions in the use of biodiesel in outboard diesel engines.* Fuel, 2007. 86(12–13):1765-1771.

14. Balat, M., *Biodiesel fuel production from vegetable oils via supercritical ethanol transesterification.* Energy Sources, Part A: Recovery, Utilization and Environmental Effects, 2008. 30(5):429-440.
15. He, C., et al., *Comparison of carbonyl compounds emissions from diesel engine fueled with biodiesel and diesel.* Atmospheric Environment, 2009. 43(24):3657-3661.
16. Sigar, C.P., et al., *Performance and emission characteristics of vegetable oil as diesel fuel extender.* Energy Sources, Part A: Recovery, Utilization and Environmental Effects, 2009. 31(2):139-148.
17. Demirbas, A., *Biodiesel production from vegetable oils via catalytic and non-catalytic supercritical methanol transesterification methods.* Progress in Energy and Combustion Science, 2005. 31(5–6):466-487.
18. Abbaszaadeh, A., et al., *Current biodiesel production technologies: A comparative review.* Energy Conversion and Management, 2012. 63:138-148.
19. Kansedo, J., K.T. Lee, and S. Bhatia, *Cerbera odollam (sea mango) oil as a promising non-edible feedstock for biodiesel production.* Fuel, 2009. 88(6):1148-1150.
20. Ma, F. and M.A. Hanna, *Biodiesel production: a review.* Bioresource Technology, 1999. 70(1):1-15.
21. Tran, H.-L., et al., *An effective acid catalyst for biodiesel production from impure raw feedstocks.* Biotechnology and Bioprocess Engineering, 2013. 18(2):242-247.
22. Fadhil, A.B. and L.H. Ali, *Alkaline-catalyzed transesterification of Silurus triostegus Heckel fish oil: Optimization of transesterification parameters.* Renewable Energy, 2013. 60(0):481-488.
23. Nelson, L., T. Foglia, and W. Marmer, *Lipase-catalyzed production of biodiesel.* Journal of the American Oil Chemists' Society, 1996. 73(9):1191-1195.
24. Roseli Ap. Ferrari, A.L.M.T. Pighinelli, and K.J. Park, *Biodiesel Production and Quality*, in *Biofuel's Engineering Process Technology*, D.M.A.D.S. Bernardes, Editor. 2011, InTech.
25. Freedman, B., R. Butterfield, and E. Pryde, *Transesterification kinetics of soybean oil 1.* Journal of the American Oil Chemists' Society, 1986. 63(10):1375-1380.
26. Leung, D.Y.C., X. Wu, and M.K.H. Leung, *A review on biodiesel production using catalyzed transesterification.* Applied Energy, 2010. 87(4):1083-1095.
27. Demirbas, A., *Political, economic and environmental impacts of biofuels: A review.* Applied Energy, 2009. 86, Supplement 1(0):S108-S117.

28. Sonnati, M.O., et al., *Glycerol carbonate as a versatile building block for tomorrow: synthesis, reactivity, properties and applications.* Green Chemistry, 2013. 15(2):283-306.
29. Pagliaro, M. and M. Rossi, *Chapter 1 Glycerol: Properties and Production*, in *The Future of Glycerol (2)*. 2010, The Royal Society of Chemistry. 1-28.
30. Prati, L., P. Spontoni, and A. Gaiassi, *From renewable to fine chemicals through selective oxidation: The case of glycerol.* Topics in Catalysis, 2009. 52(3):288-296.
31. Ruppert, A.M., et al., *Glycerol etherification over highly active CaO-based materials: New mechanistic aspects and related colloidal particle formation.* Chemistry - A European Journal, 2008. 14(7):2016-2024.
32. Li, J. and T. Wang, *Coupling reaction and azeotropic distillation for the synthesis of glycerol carbonate from glycerol and dimethyl carbonate.* Chemical Engineering and Processing: Process Intensification, 2010. 49(5): 530-535.
33. Khayoon, M.S. and B.H. Hameed, *Synthesis of hybrid SBA-15 functionalized with molybdophosphoric acid as efficient catalyst for glycerol esterification to fuel additives.* Applied Catalysis A: General, 2012. 433–434(0):152-161.
34. Medeiros, M.A., C.M.M. Leite, and R.M. Lago, *Use of glycerol by-product of biodiesel to produce an efficient dust suppressant.* Chemical Engineering Journal, 2012. 180(0):364-369.
35. Corma, A., et al., *Lewis and Brönsted basic active sites on solid catalysts and their role in the synthesis of monoglycerides.* Journal of Catalysis, 2005. 234(2):340-347.
36. Menezes, F.D.L., M.D.O. Guimaraes, and M.J. da Silva, *Highly Selective SnCl2-Catalyzed Solketal Synthesis at Room Temperature.* Industrial & Engineering Chemistry Research, 2013. 52(47):16709-16713.
37. Li, L., et al., *Highly-efficient conversion of glycerol to solketal over heterogeneous Lewis acid catalysts.* Green Chemistry, 2012. 14(6):1611-1619.
38. Mota, C.J.A., et al., *Glycerin Derivatives as Fuel Additives: The Addition of Glycerol/Acetone Ketal (Solketal) in Gasolines.* Energy & Fuels, 2010. 24(4):2733-2736.
39. Piasecki, A., et al., *Synthesis and surface properties of chemodegradable anionic surfactants: Sodium (2-n-alkyl-1,3-dioxan-5-yl)sulfates.* Journal of the American Oil Chemists' Society, 1997. 74(1):33-37.
40. Climent, M.J., A. Velty, and A. Corma, *Design of a solid catalyst for the synthesis of a molecule with blossom orange scent.* Green Chemistry, 2002. 4(6):565-569.

41. Climent, M.J., A. Corma, and A. Velty, *Synthesis of hyacinth, vanilla, and blossom orange fragrances: the benefit of using zeolites and delaminated zeolites as catalysts.* Applied Catalysis A: General, 2004. 263(2):155-161.
42. Geerlof, A., et al., *Studies on the production of (S)-(+)-solketal (2,2-dimethyl-1,3-dioxolane-4-methanol) by enantioselective oxidation of racemic solketal with Comamonas testosteroni.* Applied Microbiology and Biotechnology, 1994. 42(1):8-15.
43. Ozorio, L.P., et al., *Reactivity of glycerol/acetone ketal (solketal) and glycerol/formaldehyde acetals toward acid-catalyzed hydrolysis.* Journal of the Brazilian Chemical Society, 2012. 23:931-937.
44. Chandrasekhar, S., *Product Stability in Kinetically-Controlled Organic Reactions.* Chem. Soc. Rev., 1987. 16:313-338.
45. Clarkson, J.S., A.J. Walker, and M.A. Wood, *Continuous Reactor Technology for Ketal Formation: An Improved Synthesis of Solketal.* Organic Process Research & Development, 2001. 5(6):630-635.
46. Calvino-Casilda, V., et al., *Real-Time Raman Monitoring and Control of the Catalytic Acetalization of Glycerol with Acetone over Modified Mesoporous Cellular Foams.* The Journal of Physical Chemistry C, 2014.
47. Nandan, D., et al., *Acid functionalized carbon–silica composite and its application for solketal production.* Microporous and Mesoporous Materials, 2013. 179(0):182-190.
48. Cablewski, T., A.F. Faux, and C.R. Strauss, *Development and Application of a Continuous Microwave Reactor for Organic Synthesis.* The Journal of Organic Chemistry, 1994. 59(12):3408-3412.
49. Krief, A., L. Provins, and A. Froidbise, *Diastereoselective synthesis of dimethyl cyclopropane-1,1-dicarboxylates from a γ-alkoxy-alkylidene malonate and sulfur and phosphorus ylides.* Tetrahedron Letters, 1998. 39(11):1437-1440.
50. Bruchmann, B., et al., *Preparation of cyclic acetals or ketals*. 1999, Google Patents.
51. Jermy, B.R. and A. Pandurangan, *Catalytic application of Al-MCM-41 in the esterification of acetic acid with various alcohols.* Applied Catalysis A: General, 2005. 288(1-2):25-33.
52. Mallick, S. and K.M. Parida, *Selective nitration of phenol over silicotungstic acid supported zirconia.* Catalysis Communications, 2007. 8(10):1487-1492.
53. Reddy, B.M., M.K. Patil, and B.T. Reddy, *An efficient protocol for Aza-michael addition reactions under solvent-free condition employing sulfated zirconia catalyst.* Catalysis Letters, 2008. 126(3-4):413-418.

54. Reddy, P.S., et al., *Synthesis of bio-additives: Acetylation of glycerol over zirconia-based solid acid catalysts.* Catalysis Communications, 2010. 11(15):1224-1228.
55. Hagen, J., *Industrial Catalysis: A Practical Approach*. 2 ed. 2006, Weinheim: Wiley-VCH Verlag GmbH&Co.KGaA.
56. Clark, J.H. and C.N. Rhodes, *Clean Synthesis Using Porous Inorganic Solid Catalysts and Supported Reagents*. 2000, Cambridge RSC Clean Technology Monographs.
57. Figueiredo, H., *Preparation of catalysts from biosorbents supported on zeolites*. 2011, Universidade do Minho: Braga.
58. Fadhel, A.Z., et al., *Combining the benefits of homogeneous and heterogeneous catalysis with tunable solvents and nearcritical water.* Molecules, 2010. 15(11):8400-24.
59. Figueiredo, J.L. and F.R. Ribeiro, *Catálise Heterogénea*. 2ª ed. 2007: Fundação Caloustre Gulbenkian.
60. Colella, C. and A.F. Gualtieri, *Cronstedt's zeolite.* Microporous and Mesoporous Materials, 2007. 105(3):213-221.
61. Guisnet, M. and F.M. Ribeiro, *Zeólitos: Um nanomundo ao serviço da catálise*, ed. F.C. Gulbenkian. 2004, Lisboa.
62. *Zeolite Characterization and Catalysis*, ed. E.G.D. Arthur W. Chester. 2010: Springer.
63. Weitkamp, J., *Zeolites and catalysis.* Solid State Ionics, 2000. 131(1–2):175-188.
64. Martins, L. and D. Cardoso, *Aplicação catalítica de peneiras moleculares básicas micro e mesoporosas*. Química Nova. Vol. 29 2006. 358-364.
65. Löwenstein, W., *The distribution of aluminium in the tetrahedra of silicates and aluminates.* American Mineralogist, 1954. 39:92.
66. Garcia-Martinez, J., et al., *Mesostructured zeolite Y-high hydrothermal stability and superior FCC catalytic performance.* Catalysis Science & Technology, 2012. 2(5):987-994.
67. Montalvo, S., et al., *Application of natural zeolites in anaerobic digestion processes: A review.* Applied Clay Science, 2012. 58:125-133.
68. McCusker, L.B. and C. Baerlocher, *Zeolite structures*, in *Studies in Surface Science and Catalysis*, J. Čejka and H.v. Bekkum, Editors. 2005, Elsevier. 41-64.
69. Kesraoui-Ouki, S., C.R. Cheeseman, and R. Perry, *Natural zeolite utilisation in pollution control: A review of applications to metals' effluents.* Journal of Chemical Technology & Biotechnology, 1994. 59(2):121-126.
70. Lowenstein, W.A., Miner, 1954. 39:92.

71. Pina, M.P., et al., *Zeolite films and membranes. Emerging applications.* Microporous and Mesoporous Materials, 2011. 144(1-3):19-27.
72. Corma, A., *State of the art and future challenges of zeolites as catalysts.* Journal of Catalysis, 2003. 216(1–2):298-312.
73. Braga; A. C. A. and N.H. Morgon, *Descrições estruturais cristalinas de zeólitos*. Vol. 30. 2007: Quimíca Nova. 178-188.
74. Lago, R.M., et al., *The Nature of the Catalytic Sites in HZSM-5- Activity Enhancement*, in *Studies in Surface Science and Catalysis*, A.I. Y. Murakami and J.W. Ward, Editors. 1986, Elsevier. 677-684.
75. Uppili, S., et al., *Probing Zeolites with Organic Molecules: Supercages of X and Y Zeolites Are Superpolar†.* Langmuir, 1999. 16(1):265-274.
76. Hensen, E.J.M. and J.A.R. van Veen, *Encapsulation of transition metal sulfides in faujasite zeolite for hydroprocessing applications.* Catalysis Today, 2003. 86(1–4):87-109.
77. Shailaja, J., et al., *Alkali Ion-Controlled Excited-State Ordering of Acetophenones Included in Zeolites: Emission, Solid-State NMR, and Computational Studies†.* The Journal of Physical Chemistry A, 2002. 107(18):3187-3198.
78. Scherzer, J., *The Preparation and Characterization of Aluminum-Deficient Zeolites*, in *Catalytic Materials: Relationship Between Structure and Reactivity*. 1984, American Chemical Society. 157-200.
79. Sohn, J.R., et al., *Acid catalysis by dealuminated zeolite Y. 2. The roles of aluminum.* Journal of Physical Chemistry, 1986. 90(20):4847-4851.
80. Almutairi, S.M.T., *The role of Lewis and Brønsted acidity for alkane activation over zeolites.* 2013, Technische Universiteit Eindhoven: Eindhoven. 153.
81. Kaduk, J.A. and J. Faber, *Crystal structure of zeolite y as a function of ion* The Rigaku Journal, 1995. 12(2):14-34.
82. Kanthasamy, R. and T.U.o. Iowa, *Characterization and Applications of Mesoporous Silica and Hollow Zeolite Structures*. 2008: The University of Iowa.
83. Dunne, L.J. and G. Manos, *Adsorption and Phase Behaviour in Nanochannels and Nanotubes*. 2009: Springer.
84. *Zeolites and Ordered Porous Solids: Fundamentals and Applications*. 2011: Universitat Politècnica de València.

85. Geus, J.W., *Preparation of Catalysts III Scientific Bases for the Preparation of Heterogeneous Catalysts*, ed. P.G.a.P.A.J. G. Poncelet. Vol. 16. 1983, Amsterdam: Elsevier.
86. Cardew, P.T., et al., *A Study of Some Parameters in Catalyst Preparation and their Influence on Catalyst Performance*, in *Studies in Surface Science and Catalysis*, P.G.P.A.J. B. Delmon and G. Poncelet, Editors. 1987, Elsevier. 15-27.
87. Perego, C. and P. Villa, *Catalyst preparation methods.* Catalysis Today, 1997. 34(3-4):281-305.
88. LePage, J.F., *Handbook of Heterogeneous Catalysis*, ed. H.K. G. Ertl, J. Weitkamp. Vol. 1. 1997, New York/Weinheim: Wiley/VCH.
89. Richardson, J.T., *Principles of Catalyst Development*. 1989, New York: Plenum Press.
90. *Catalyst Handbook*. 2 ed, ed. M.V. Twigg. 1989, London: Wolfe.
91. Che, M., O. Clause, and C. Marcilly, *Handbook of Heterogeneous Catalysis*, ed. G. Ertl, H. Knözinger, and J. Weitkamp. Vol. 1. 1997, New York/Weinheim: Wiley/VCH. 191.
92. Knözinger, H. and E. Taglauer, *Handbook of Heterogeneous Catalysis*, ed. G. Ertl, H.J. Knözinger, and J. Weitkamp. Vol. 1. 1997, New York/Weinheim: Wiley/VCH.
93. Geus, J.W. and J. Van Dillen, *Handbook of Heterogeneous Catalysis*, ed. H.K. G. Ertl, J. Weitkamp. Vol. 1. 1997, New York/Weinheim: Wiley/VCH.
94. Campanati, M., G. Fornasari, and A. Vaccari, *Fundamentals in the preparation of heterogeneous catalysts.* Catalysis Today, 2003. 77(4):299-314.
95. Bhatia, S., *Zeolite Catalysts: Principles and Applications*. 1990, Florida: CRC Press.
96. Nijhuis, T.A., et al., *Preparation of monolithic catalysts.* Catalysis Reviews, 2001. 43(4):345-380.
97. Schwarz, J.A., C. Contescu, and A. Contescu, *Methods for Preparation of Catalytic Materials.* Chemical Reviews, 1995. 95(3):477-510.
98. Wachs, I.E., *Catalyst Preparation: Science and Engineering By John R. Regalbuto.* AIChE Journal, 2009. 55(1):284-284.
99. Nair, G.S., et al., *Glycerol utilization: solvent-free acetalisation over niobia catalysts.* Catalysis Science & Technology, 2012. 2(6):1173-1179.
100. Lee, Y.Y., et al., *The effect of PO4 to Nb2O5 catalyst on the dehydration of glycerol.* Catalysis Today, 2014. 232(0):114-118.
101. Celdeira, P.A., et al., *Sulfonated niobia and pillared clay as catalysts in etherification reaction of glycerol.* Applied Catalysis A: General, 2014. 478:98-105.

102. Trejda, M., et al., *Development of niobium containing acidic catalysts for glycerol esterification.* Catalysis Today, 2012. 187(1):129-134.

103. Rodrigues, R., et al., *Effect of niobia and alumina as support for Pt catalysts in the hydrogenolysis of glycerol.* Chemical Engineering Journal, 2012. 198-199:457-467.

104. Souza, J., et al., *Production of compounds to be used as fuel additive: Glycerol conversion using Nb-doped MgAl mixed oxide.* Catalysis Today, 2013. 213:65-72.

105. Liu, R., et al., *Highly efficient production of acrylic acid by sequential dehydration and oxidation of glycerol.* Industrial and Engineering Chemistry Research, 2014. 53(21):8667-8674.

106. Oliveira, L.C.A., et al., *Modified niobia as a bifunctional catalyst for simultaneous dehydration and oxidation of glycerol.* Applied Catalysis B: Environmental, 2012. 117–118(0):29-35.

107. Lauriol-Garbey, P., et al., *Acid–base properties of niobium-zirconium mixed oxide catalysts for glycerol dehydration by calorimetric and catalytic investigation.* Applied Catalysis B: Environmental, 2011. 106(1–2):94-102.

108. Nair, G.S., et al., *Glycerol utilization: Solvent-free acetalisation over niobia catalysts.* Catalysis Science and Technology, 2012. 2(6):1173-1179.

109. Nowak, I. and M. Ziolek, *Niobium Compounds: Preparation, Characterization, and Application in Heterogeneous Catalysis.* Chem Rev, 1999. 99(12):3603-3624.

110. *21 - Titanium, Zirconium and Hafnium*, in *Chemistry of the Elements (Second Edition)*, N.N. Greenwood and A. Earnshaw, Editors. 1997, Butterworth-Heinemann: Oxford. 954-975.

111. Ziolek, M., *Niobium-containing catalysts—the state of the art.* Catalysis Today, 2003. 78(1–4):47-64.

112. Tanabe, K., *Catalytic application of niobium compounds.* Catalysis Today, 2003. 78(1–4):65-77.

113. Tanabe, K. and S. Okazaki, *Various reactions catalyzed by niobium compounds and materials.* Applied Catalysis A: General, 1995. 133(2):191-218.

114. Neves, I.C., et al., *The effect of acidity behaviour of Y zeolites on the catalytic degradation of polyethylene.* European Polymer Journal, 2006. 42(7):1541-1547.

115. Sing, K.S.W. and J. Rouquerol. Handbook of Heterogeneous Catalysis, ed. H.K. G.Ertl, J. Weitkamp. Vol. 2. 1997, Weinheim: Wiley-VCH.

116. Brunauer, S., P.H. Emmett, and E. Teller, *Adsorption of Gases in Multimolecular Layers.* Journal of the American Chemical Society, 1938. 60(2):309-319.

117. Lippens, B.C. and J.H. de Boer, *Studies on pore systems in catalysts: V. The t method.* Journal of Catalysis, 1965. 4(3):319-323.
118. de Boer, J.H., et al., *Thet-curve of multimolecular N2-adsorption.* Journal of Colloid And Interface Science, 1966. 21(4):405-414.
119. Manning, T.J. and W.R. Grow, *Inductively Coupled Plasma - Atomic Emission Spectrometry*. The Chemical Educator ed. M. Schimpf. Vol. 2. 1997, New York: Springer-Verlag.
120. Hou, X. and B.T. Jones, *Inductively Coupled Plasma/Optical Emission Spectrometry*. Encyclopedia of Analytical Chemistry, ed. R.A. Meyers. 2000, Chichester: John Wiley & Sons Ltd.
121. Stuart, B.H., *Introduction*, in *Infrared Spectroscopy: Fundamentals and Applications*. 2005, John Wiley & Sons, Ltd. 1-13.
122. Li, C. and Z. Wu, *Microporous Materials Characterized by Vibrational Spectroscopies*, in *Handbook of Zeolite Science and Technology*, K.A.C. S.M. Auerbach, P.K. Dutta, Editor. 2004, Basel, Marcel Dekker, Inc.: New York.
123. Fonseca, A.M. and I.C. Neves, *Study of silver species stabilized in different microporous zeolites.* Microporous and Mesoporous Materials 2013. 181:83-87.
124. Jentys, A. and J.A. Lercher, *Techniques of zeolite characterization*, in *Studies in Surface Science and Catalysis*, E.M.F. H. van Bekkum, P.A. Jacobs and J.C. Jansen, Editor. 2001, Elsevier: Amsterdam. 345-386.
125. Shriver, D. and P. Atkins, *Inorganic Chemistry*. 4th ed, ed. O.U. Press. 2006, Oxford.
126. Reimer, L., *Scanning Electron Microscopy: Physics of Image Formation and Microanalysis*. 1998: Springer.
127. Goldstein, J., *Scanning Electron Microscopy and X-ray Microanalysis: Third Edition*. 2003: Springer US.
128. Jeffery, G.H., J. Bassett, and J. Mendham, *Vogel's textbook of quantitative chemical analysis*. 5 ed. 1989, London Scientific & Technical: Longman.
129. Coats, A.W. and J.P. Redfern, *Thermogravimetric analysis. A review.* Analyst, 1963. 88(1053):906-924.
130. Haines P. J., Reading M., and W. F.W., *Differential thermal analysis and differential scanning calorimetry*. Handbook of Thermal Analysis and Calorimetry, ed. B. ME. 1998, Netherlands: Elsevier Science BV. 279–361.
131. Vuurman, M.A. and I.E. Wachs, *In situ Raman spectroscopy of alumina-supported metal oxide catalysts.* The Journal of Physical Chemistry, 1992. 96(12):5008-5016.

132. Bañares, M.A. and I.E. Wachs, *Raman Spectroscopy of Catalysts*, in *Encyclopedia of Analytical Chemistry*. 2006, John Wiley & Sons, Ltd.
133. Mestl, G., *In situ Raman spectroscopy — a valuable tool to understand operating catalysts.* Journal of Molecular Catalysis A: Chemical, 2000. 158(1):45-65.
134. Knops-Gerrits, P.-P., et al., *Raman spectroscopy on zeolites.* Microporous Materials, 1997. 8(1–2):3-17.
135. Scott, R.P.W., *Introduction to Analytical Gas Chromatography, Second Edition, Revised and Expanded*. 1997: Taylor & Francis.
136. Lopes, A.C., et al., *Enhancement of the Dielectric Constant and Thermal Properties of α-Poly(vinylidene fluoride)/Zeolite Nanocomposites.* The Journal of Physical Chemistry C, 2010. 114(34):14446-14452.
137. Machado, A.F.B., *Desenvolvimento de sistemas de libertação de fármacos baseados em nanoestruturas para o tratamento do cancro*, in *Dissertação de mestrado de Química Medicinal* 2013, Universidade do Minho.
138. Kolasinski, K.W., *Surface science*. 2 ed. 2008, England: Wiley.
139. Braga, V.S., et al., *Catalyst Materials Based on Nb2O5 Supported on SiO2−Al2O3: Preparation and Structural Characterization.* Chemistry of Materials, 2005. 17(3):690-695.
140. Barros, I.C.L., et al., *Effects of niobium addition on ZSM-5 studied by thermal and spectroscopy methods.* Microporous and Mesoporous Materials, 2008. 109(1–3):485-493.
141. Braga, V.S., et al., *Copper oxide and niobium pentoxide supported on silica-alumina: Synthesis, characterization, and application on diesel soot oxidation.* Journal of Catalysis, 2007. 247(1):68-77.
142. *Introduction to zeolite science and practice*. Studies in Surface Science and Catalysis, ed. J.C.J. H van Bekkum. E.M. Flanigen. Vol. 58. 1991, Amsterdam: Elsevier.
143. Lutz, W., C.H. Rüscher, and D. Heidemann, *Determination of the framework and non-framework [SiO2] and [AlO2] species of steamed and leached faujasite type zeolites: calibration of IR, NMR, and XRD data by chemical methods.* Microporous and Mesoporous Materials, 2002. 55(2):193-202.
144. Ghesti, G.F., et al., *Investigation of pyridine sorption in USY and Ce/USY zeolites by liquid phase microcalorimetry and thermogravimetry studies.* Microporous and Mesoporous Materials, 2007. 100(1–3):27-34.

145. Breck, D.W. and E.M. Flanigen. Molecular Sieves 1968, London: Society of Chemical Industry.
146. Neves, I.C., et al., *Catalytic degradation of polyethylene: An evaluation of the effect of dealuminated Y zeolites using thermal analysis.* Materials Chemistry and Physics, 2007. 104(1):5-9.
147. van Koningsveld, H., J.C. Jansen, and H. van Bekkum, *The monoclinic framework structure of zeolite H-ZSM-5. Comparison with the orthorhombic framework of as-synthesized ZSM-5.* Zeolites, 1990. 10(4):235-242.
148. McCusker, L.B. and C. Baerlocher. Studies in Surface Science and Catalysis, ed. J.C.a.H.v. Bekkum. Vol. 157. 2005: Elsevier.
149. Beauchet, R., et al., *Applied Catalysis B: Environmental*. Vol. 100. 2010.
150. van Santen, R.A. and G.J. Kramer, *Reactivity Theory of Zeolitic Broensted Acidic Sites.* Chemical Reviews, 1995. 95(3):637-660.
151. Nibou, D., et al., *Elaboration and characterization of solid materials of types zeolite NaA and faujasite NaY exchanged by zinc metallic ions.* Physics Procedia, 2009. 2(3):1433-1440.
152. Breck, D.W., *Zeolite molecular sieves: structure, chemistry, and use*. 1973: Wiley.
153. Figueiredo, H., *Reutilização Catalítica de Biossorventes Suportados em Zeólitos*. 2007, Universidade do Minho: Braga.
154. Mozgawa, W., *The influence of some heavy metals cations on the FTIR spectra of zeolites.* Journal of Molecular Structure, 2000. 555:299-304.
155. Mohamed, R.M., et al., *Influence of crystallization times on the synthesis of nanosized ZSM-5.* Materials Letters, 2005. 59(27):3441-3444.
156. Prakash, A.M. and L. Kevan, *Synthesis of niobium silicate molecular sieves of the MFI structure: Evidence for framework incorporation of the niobium ion.* Journal of the American Chemical Society, 1998. 120(50):13148-13155.
157. Nowak, I., *Textural and structural properties of niobium-containing micro-, meso- and macroporous molecular sieves.* Colloids and Surfaces A: Physicochemical and Engineering Aspects, 2004. 241(1–3):103-111.
158. Ziolek, M. and I. Nowak, *Characterization techniques employed in the study of niobium and tantalum-containing materials.* Catalysis Today, 2003. 78(1–4):543-553.
159. Corma, A. and H. Garcia, *Supramolecular Host-Guest Systems in Zeolites Prepared by Ship-in-a-Bottle Synthesis.* European Journal of Inorganic Chemistry, 2004. 2004(6):1143-1164.

160. McGuire, G.E., G.K. Schweitzer, and T.A. Carlson, *Inorganic Chemistry* 1973. 12(10):2450-2453.

161. Vicente, G., et al., *Acetalisation of bio-glycerol with acetone to produce solketal over sulfonic mesostructured silicas.* Green Chemistry, 2010. 12(5):899-907.

162. Kojima, S., *Anomalous behaviour of the O-H stretching vibrational mode in the liquid-glass transition of glycerol.* Journal of Molecular Structure, 1993. 294(0):193-195.

163. Mudalige, A. and J.E. Pemberton, *Raman spectroscopy of glycerol/D2O solutions.* Vibrational Spectroscopy, 2007. 45(1):27-35.

164. Mendelovici, E., R.L. Frost, and T. Kloprogge, *Cryogenic Raman spectroscopy of glycerol.* Journal of Raman Spectroscopy, 2000. 31(12):1121-1126.

165. Krishnan, K., *The Raman spectra of organic compounds.* Proceedings of the Indian Academy of Sciences - Section A, 1961. 53(3):151-167.

166. Frost, R.L., et al., *Rehydration of Potassium Acetate-Intercalated Kaolinite at 298 K.* Langmuir, 2000. 16(12):5402-5408.

167. Stuart, A.V. and G.B.B.M. Sutherland, *Effect of Hydrogen Bonding on the Deformation Frequencies of the Hydroxyl Group in Alcohols.* The Journal of Chemical Physics, 1956. 24(3):559-570.

168. Shimanouchi, T., *Tables of Molecular Vibrational Frequencies*. 1972: National Bureau of Standards.

169. Dellepiane, G. and J. Overend, *Vibrational spectra and assignment of acetone, ααα acetone-d3 and acetone-d6.* Spectrochimica Acta, 1966. 22(4):593-614.